

Dissertation zur Erlangung des Doktorgrades  
der Fakultät für Chemie und Pharmazie  
der Ludwig-Maximilians-Universität München

**Towards Genetic Dissection of Neural Crest  
Specification and Cartilage Differentiation  
in Zebrafish (*Danio rerio*)**

**Michael Lang**

aus

Münster-Hiltrup

**2003**

## Erklärung

Diese Dissertation wurde im Sinne von § 13 Abs. 3 bzw. 4 der Promotionsordnung vom 29. Januar 1998 von Prof. Dr. R. Grosschedl betreut.

## Ehrenwörtliche Versicherung

Diese Dissertation wurde selbständig, ohne unerlaubte Hilfe erarbeitet.

München, am 12. September 2003

.....  
(Michael Lang)

Dissertation eingereicht am 12. September 2003

1. Gutachter Prof. Dr. R. Grosschedl

2. Gutachter Prof. Dr. F. Eckardt-Schupp

Mündliche Prüfung am 19. Dezember 2003

**How does newness come into the world? How is it born?  
Of what fusions, translations, conjoinings is it made?  
How does it survive, extreme and dangerous as it is?**

Salman Rushdie (1988)

---

# Table Of Contents

<b>1</b>	<b>Commonly used abbreviations</b>	<b>5</b>
<b>2</b>	<b>Introduction</b>	<b>8</b>
<b>2.1</b>	<b>Zebrafish as a model organism</b>	<b>8</b>
2.1.1	A genetic approach to the study of zebrafish embryonic development	8
2.1.2	The vertebrate craniofacial skeleton	10
2.1.2.1	The vertebrate pharyngeal arches	10
2.1.2.2	The zebrafish craniofacial skeleton	11
<b>2.2</b>	<b>The Neural Crest</b>	<b>13</b>
2.2.1	Neural crest induction	13
2.2.2	Neural crest specification: Progressive fate restriction	13
2.2.3	Neural crest migration and the organization of cranial neural crest streams	16
2.2.4	Neural crest differentiation and derivatives	18
2.2.5	Hindbrain patterning and pharyngeal arch specification	19
2.2.6	Pharyngeal arch patterning	21
<b>2.3</b>	<b>Cartilage development</b>	<b>23</b>
2.3.1	Chondrogenesis	23
2.3.2	The extracellular matrix	24
2.3.3	Proteoglycans	24
<b>2.4</b>	<b>Strategies for the molecular dissection of neural crest derivative development in zebrafish</b>	<b>27</b>
2.4.1	Morphological and molecular analyses of ENU-induced zebrafish mutations	27
2.4.2	Genetic mapping of ENU-induced mutations	27
2.4.3	Gene identification by candidate and positional cloning approaches	31
<b>3</b>	<b>Aims of the thesis</b>	<b>32</b>
<b>4</b>	<b>Materials and Methods</b>	<b>33</b>
<b>4.1</b>	<b>Materials</b>	<b>33</b>
4.1.1	Chemicals	33
4.1.2	Radionucleotides	34
4.1.3	Buffers and Solutions	35
4.1.4	Oligonucleotides	36
4.1.5	Enzymes	38
4.1.6	Kits	38
4.1.7	Vectors	38
4.1.8	Biological Materials	39
4.1.8.1	Zebrafish strains	39
4.1.8.2	Bacterial strains	39
4.1.9	Equipment	40
<b>4.2</b>	<b>Methods</b>	<b>41</b>
4.2.1	Genetic mapping	41
4.2.1.1	Genomic DNA Preparation	41
4.2.1.2	Total Genome Scan by genotyping with microsatellite markers	41
4.2.1.3	PCR	42
4.2.1.4	Agarose gel electrophoresis	42
4.2.1.5	Single-stranded conformation polymorphism (SSCP) analysis	43
4.2.1.6	Overgo Probing of High-Density BAC and PAC Filters	44
4.2.2	Molecular biology and cloning	47
4.2.2.1	RNA Isolation	47
4.2.2.2	RT-PCR	48
4.2.2.3	Restriction digest of DNA	48
4.2.2.4	Ligation	49
4.2.2.5	Transformation	49
4.2.2.6	Synthesis of digoxigenin-labeled riboprobes for <i>in situ</i> hybridization	50

4.2.2.7	Capped mRNA synthesis (in vitro transcription)	51
4.2.3	Morphology and histology	52
4.2.3.1	Alcian Blue staining	52
4.2.3.2	Ultramicrotomy and histological staining	52
4.2.4	Molecular analysis of gene expression	54
4.2.4.1	Whole-mount <i>in situ</i> hybridization	54
4.2.4.2	Whole-mount immunohistochemistry	56
4.2.5	Functional assays	59
4.2.5.1	Microinjection of morpholino antisense oligonucleotides	59
4.2.5.2	Microinjection of capped mRNA	59
4.2.6	World Wide Web infrastructure	60
<b>5</b>	<b>Results</b>	<b>61</b>
<b>5.1</b>	<b>Analysis of the <i>brak</i> (<i>brk</i><sup>m452</sup>) mutation</b>	<b>61</b>
5.1.1	The <i>brak</i> <sup>m452</sup> mutation causes craniofacial defects and diminished melanophore pigmentation	61
5.1.2	The <i>brak</i> <sup>m452</sup> mutation maps to linkage group 14	63
<b>5.2</b>	<b>Analysis of the <i>mother superior</i> (<i>mos</i><sup>m188</sup>) mutation</b>	<b>65</b>
5.2.1	Craniofacial cartilage elements are lost in <i>mos</i> <sup>m188</sup> mutant embryos	65
5.2.2	Iridophores but not melanophores are greatly reduced in <i>mos</i> <sup>m188</sup> mutant embryos	67
5.2.3	The <i>mos</i> <sup>m188</sup> mutation leads to the development of supernumerary neuromast organs	68
5.2.4	Dorsal root ganglia and the enteric nervous system are greatly reduced in the absence of <i>mos</i> <sup>m188</sup> gene function	69
5.2.5	Migratory cranial neural crest cells and pharyngeal arch primordia display severely reduced expression of <i>dlx</i> genes in <i>mos</i> <sup>m188</sup> mutant embryos	70
5.2.6	Normal patterning of hindbrain rhombomeres in <i>mos</i> <sup>m188</sup> mutant embryos	72
5.2.7	The mutation in the <i>mos</i> <sup>m188</sup> locus leads to downregulation of key genes in neural crest progenitor cells	74
5.2.8	<i>foxD3</i> , a key regulator of neural crest specification, is not expressed in neural crest progenitor cells of <i>mos</i> <sup>m188</sup> mutant embryos	76
5.2.9	<i>foxD3</i> transcripts are maternally deposited	78
5.2.10	Genetic mapping of the <i>mos</i> <sup>m188</sup> locus	80
5.2.11	Knockdown of <i>foxD3</i> function phenocopies many aspects of the <i>mos</i> <sup>m188</sup> mutation	82
<b>5.3</b>	<b>Analysis of the cartilage differentiation mutations <i>round</i> (<i>rnd</i><sup>m211, m641, m713, m715</sup>) and <i>crusher</i> (<i>cru</i><sup>m299</sup>)</b>	<b>85</b>
5.3.1	Comparative phenotypic characterization of the <i>round</i> <sup>m211</sup> and <i>crusher</i> <sup>m299</sup> mutations	85
5.3.2	Comparative histological characterization of the <i>round</i> <sup>m211</sup> and <i>crusher</i> <sup>m299</sup> mutations	88
5.3.3	Mapping of the <i>round</i> <sup>m211, m641, m715</sup> and <i>crusher</i> <sup>m299</sup> mutations	95
5.3.3.1	The <i>round</i> <sup>m211, m641, m715</sup> mutation maps to linkage group 21	95
5.3.3.2	Mapping of the <i>crusher</i> <sup>m299</sup> mutation	98
5.3.3.2.1	Genetic mapping of the <i>crusher</i> <sup>m299</sup> mutation to linkage group 17	98
5.3.3.2.2	Physical mapping of the <i>crusher</i> <sup>m299</sup> mutation	99
5.3.3.2.3	The <i>sec23a</i> gene is likely to be disrupted by the <i>crusher</i> <sup>m299</sup> mutation	100
<b>6</b>	<b>Discussion</b>	<b>103</b>
<b>6.1</b>	<b>Zebrafish mutations as models for genetic disorders affecting neural crest and craniofacial development</b>	<b>103</b>
<b>6.2</b>	<b>Mutations affecting cartilage differentiation: <i>round</i><sup>m211, m641, m713, m715</sup> and <i>crusher</i><sup>m299</sup></b>	<b>104</b>
<b>6.3</b>	<b>Genetic mapping and cloning of the <i>round</i><sup>m211, m641, m715</sup> and <i>crusher</i><sup>m299</sup> mutations</b>	<b>106</b>
<b>6.4</b>	<b>The role of the <i>mother superior</i><sup>m188</sup> gene in neural crest development</b>	<b>108</b>
<b>6.5</b>	<b>The role of the <i>foxD3</i> gene in neural crest development</b>	<b>111</b>
<b>7</b>	<b>Summary</b>	<b>114</b>
<b>8</b>	<b>Bibliography</b>	<b>115</b>
<b>9</b>	<b>Acknowledgements</b>	<b>123</b>
<b>10</b>	<b>Curriculum Vitae</b>	<b>124</b>

# 1 Commonly used abbreviations

A	Adenine
AB	AB zebrafish wild-type line
AP	Alkaline phosphatase
APS	Ammonium peroxodisulfate
BAC	Bacterial artificial chromosome
bp	Base pairs
BCIP	5-Bromo-4-chloro-3-indolyl-phosphate
BMP	Bone morphogenetic protein
BSA	Bovine serum albumine
C	Cytosine
cDNA	Complementary DNA
DASPEI	2-(4-Dimethylaminostyryl)-N-ethyl pyridinium iodide
DDSH	Dyssegmental dysplasia Silverman-Handmaker type
DEPC	Diethylpyrocarbonate
dH <sub>2</sub> O	Distilled H <sub>2</sub> O
DMF	N,N-Dimethyl formamide
DMSO	Dimethyl sulfoxide
DNA	Desoxyribonucleic acid
DNase	Desoxyribonuclease
(d)dNTP	(Di)Desoxyribonucleoside triphosphate
dpf	Days post fertilization
ECM	Extracellular matrix
EDTA	Ethylenediamine tetraacetic acid
ENU	1-Ethyl-1-nitrosourea
ER	Endoplasmic reticulum
EST	Expressed sequence tag
G	Guanine
HEPES	N-2-Hydroxyethylpiperazine-N'-2-ethanesulfonic acid
HK	Hong Kong zebrafish wild-type line
hpf	Hours post fertilization
HRP	Horse radish peroxidase
IN	India zebrafish wild-type line

Commonly used abbreviations

---

ISH	<i>In situ</i> hybridization
kb	Kilo base pairs
LB	Luria-Bertani
LG	Linkage group
M	Molar
Mb	Mega base pairs
mRNA	Messenger RNA
NBT	Nitro blue tetrazolium
NGS	Normal goat serum
OD	Optical density
OLB	Oligo labeling buffer
ORF	Open reading frame
PAC	P1-derived artificial chromosome
PCR	Polymerase chain reaction
PEG	Polyethylene glycol
PFA	Paraformaldehyde
PTU	1-Phenyl-2-thio-urea
RFLP	Restriction fragment length polymorphism
RNA	Ribonucleic acid
RNase	Ribonuclease
rpm	Revolutions per minute
RT	Reverse transcription/reverse transcriptase
SDS	Sodium dodecyl sulfate
SNP	Single nucleotide polymorphism
SSC	Standard saline citrate
SSCP	Single strand conformation polymorphism
SSLP	Simple sequence length polymorphism
STS	Sequence tagged site
T	Thymine
TAE	Tris-Acetate-EDTA
Taq	<i>Thermus aquaticus</i>
TBE	Tris-Borate-EDTA
TE	Tris-EDTA
TEMED	N, N, N', N'-Tetramethylethylenediamine

Commonly used abbreviations

---

TL	Tübingen long fin zebrafish wild-type line
Tris	Tris-(hydroxymethyl)-aminomethane
U	Unit
UTR	Untranslated region
v/v	Volume per volume
WIK	WIK zebrafish wild-type line
Wnt	Gene family, named according to the <i>Drosophila</i> segment polarity gene <i>wingless</i> and to its vertebrate ortholog, <i>int-1</i> , a mouse protooncogene
WT	Wild-type
w/v	Weight per volume



## 2 Introduction

### 2.1 Zebrafish as a model organism

The zebrafish (*Danio rerio*) is a fresh water teleost combining developmental and genetic characteristics rendering it a unique vertebrate model system. Following external fertilization the embryos remain largely transparent throughout development. Embryogenesis proceeds rapidly with the heart starting to beat before 24 hours post fertilization (hpf) and the embryos hatching at about 48 hpf. The developing embryos are easily amenable to experimental analyses including cell lineage tracing, whole mount stainings, cell transplantations etc. With a genome size suitable to genetic analysis (1700Mb, 25 chromosomes), a short generation time of three months, thousands of progeny available from a single breeding pair and low maintenance costs, the zebrafish is an ideal vertebrate for phenotype-driven large scale mutagenesis screens (Mullins et al. 1994).

#### 2.1.1 A genetic approach to the study of zebrafish embryonic development

In 1996, two large scale ENU mutagenesis screens for mutations affecting early development in zebrafish were carried out, one at the Max-Planck-Institute for Developmental Biology in Tübingen and one at Harvard Medical School (Cardiovascular Research Center, CVRC) in Boston. Over 2000 mutations have been recovered and described that affect development of the brain, head skeleton, blood, heart, somites, muscles, skin, pigmentation, sensory organs, gut, liver and fin (Driever et al. 1996; Haffter et al. 1996). ENU (1-Ethyl-1-nitrosourea) is a potent ethylating agent that has been found to be an effective mutagen in the mouse (Russell et al. 1979). ENU induces DNA point mutations with a high frequency in male mouse germ cells. Based on the experience with ENU in the mouse field, the two zebrafish mutagenesis screens in Boston and Tübingen adopted a treatment protocol aimed at mutagenizing pre-meiotic spermatogonia. ENU can transfer its ethyl group and thus produce alkylation at base oxygen atoms, such as the O<sup>4</sup> and O<sup>2</sup> positions of thymine and the O<sup>6</sup> position of guanine (Favor 1999; Shibuya and Morimoto 1993). Molecular genetic data obtained from ENU-induced mutants in

various species suggest that ENU produces all types of base substitutions, transitions and transversions.

In the Tübingen and Boston screens, 109 and 48 mutations affecting craniofacial development have been isolated, respectively. As confirmed by complementation analysis, the 109 Tübingen mutations correspond to mutations in 26 genetic loci (Piotrowski et al. 1996; Schilling et al. 1996) and the 48 Boston mutations correspond to mutations in 34 distinct genetic loci (Neuhauss et al. 1996). Complementation analysis reveals whether two mutations (with similar phenotypes) affect the same genetic locus. If crosses between two heterozygotes for different mutations give rise to 25% of mutant progeny, this indicates that the two recessive mutations do not complement each other and thus they represent two alleles of the same genetic locus. For example, from the Boston collection of craniofacial mutations, 4 independent mutant alleles of the *round* locus were recovered. If crosses between two heterozygotes for different mutations do not result in mutant progeny (i.e. if they complement each other), the mutations are in two different genetic loci. The 34 affected genetic loci from the Boston screen have been assorted to groups based on their phenotype. Group I comprises mutations affecting the layout of the pharyngeal skeleton. Group II comprises mutations affecting cartilage differentiation and morphogenesis whereas group III includes mutations affecting the spatial arrangement of pharyngeal skeletal elements. In addition there are four mutations that could not be grouped into the above categories and were classified as other mutations affecting pharyngeal development. The ENU-induced craniofacial mutations are inherited in a recessive Mendelian mode and lead to embryonic lethality in homozygous embryos. During my Ph.D. thesis project I studied four zebrafish craniofacial mutations from the Boston screen.

## **2.1.2 The vertebrate craniofacial skeleton**

### **2.1.2.1 The vertebrate pharyngeal arches**

One of the fundamental vertebrate characteristics is the acquisition of a muscularised pharynx supported by skeletal elements originally serving the dual functions of feeding and respiration.

I will use the term vertebrates throughout this thesis in the traditional meaning, thus including the Myxini (hagfish). The hagfish, however, lack a vertebral column or vertebral elements, but they possess a cranium (skull). For this reason, recent phylogenetic classification has created a group named craniates to encompass vertebrates plus hagfish (Shimeld and Holland 2000). The taxon name vertebrates will be used in this thesis synonymously to the new taxon name craniates.

The pharynx arises from the pharyngeal arches on either side of the head of vertebrate embryos. The development of the pharyngeal arches is complex involving a number of embryonic cell types of different germ layer origin. Each arch comprises an outer layer of ectoderm, an inner covering of endoderm and a core, the mesenchyme of which is derived from both neural crest and mesoderm (Noden 1988). The different embryonic cell populations of the arches generate distinct components of the pharynx. The ectoderm produces the epidermis and the sensory neurons of the arch-associated cranial ganglia, while the endoderm gives rise to the epithelial cells lining the pharynx. The mesoderm gives rise to the musculature and the endothelial cells of the arch arteries, whereas the neural crest generates the skeletal and connective tissues (Couly et al. 1993). The contributions of the different embryonic cell populations to the pharyngeal arches are highly coordinated ensuring both the appropriate temporal and spatial formation of the arch components and the generation of appropriate arch identities (Graham and Smith 2001).

The vertebrate head comprises seven pharyngeal arches. In all vertebrates the first (anteriormost) arch forms the jaw, while the second one forms the hyoid apparatus supporting the jaw. The more posterior arches either develop gills in fish and juvenile amphibians or contribute to the throat in adult amphibians and the amniote tetrapods (reptiles, birds and mammals).

All pharyngeal arch cartilages are derived from cranial neural crest cells. In contrast, the vertebrate neurocranium has a bipartite origin as was shown by fate mapping studies in birds, amphibians and in lamprey: The anterior neurocranium (trabeculae and ethmoid plate) is a derivative of cranial neural crest cells whereas the posterior parachordal and otic capsule cartilage elements are derived from the paraxial mesoderm (Chibon 1967; Langille and Hall 1986; Le Lievre 1978).

### **2.1.2.2 The zebrafish craniofacial skeleton**

The zebrafish embryonic craniofacial skeleton is fully developed by 5 dpf. The two anteriormost pharyngeal arches are the mandibular arch giving rise to the jaw and the hyoid arch forming the associated supportive apparatus (Kimmel et al. 1998; Kimmel et al. 2001). These rostral pharyngeal arches are always distinctive from the more posterior arches 3-7, collectively termed branchial arches (Figure 1). The ventral cartilage of the mandibular arch (Meckel's cartilage) and the ventral element of the hyoid arch (ceratohyal) are large supportive structures of the lower jaw beneath the oral cavity. The corresponding dorsal elements are the palatoquadrate of the first arch and the hyosymplectic (also called hyomandibular) of the second arch. The next four pharyngeal arches, branchial arches 1-4 (corresponding to pharyngeal arches 3-6), are bearing gills. A gill slit forms posterior to the hyoid arch and between each of the branchial arches, making five gill slits in total. The rudiments of gill filaments develop late in the hatching period as buds along the posterior walls of the four branchial arches facing the slits. The last arch of the pharyngeal series (branchial arch 5 or pharyngeal arch 7) does not develop gills. There is also no gill slit behind it. However, in the fashion of all the other branchial arches it does make a linear cartilage element termed ceratobranchial (Figure 1). Pharyngeal teeth develop in association with this 7th pharyngeal arch ceratobranchial cartilage. A complex set of craniofacial muscles accompanies the pharyngeal arch cartilages.

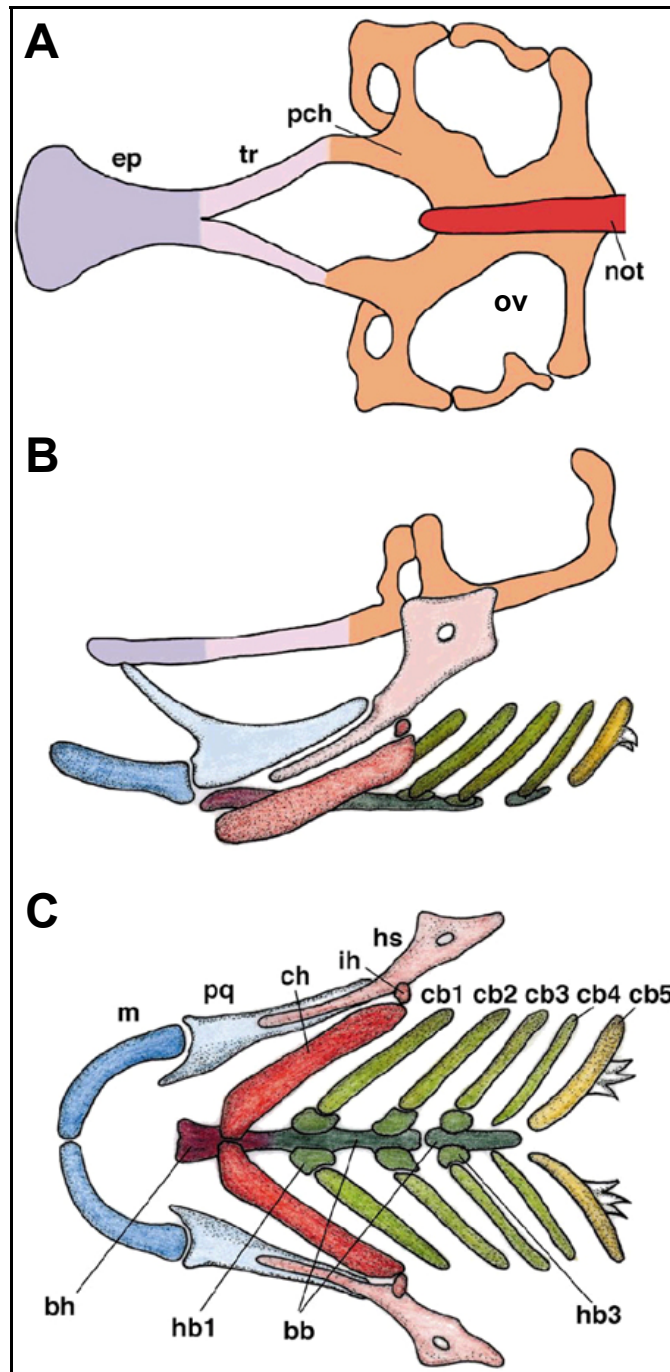


**Figure 1.** Schematic representation of the 5 dpf zebrafish embryonic craniofacial skeleton (Kimmel et al. 2001). Anterior is to the left. The skeletal elements are color-coded. (A) The neurocranial cartilages and the notochord from the dorsal aspect. (B) The neurocranium and the pharyngeal skeleton in lateral view. (C) The pharyngeal skeleton in ventral view.

Abbreviations: bb, basibranchial; bh, basihyal; cb, ceratobranchial; ch, ceratohyal; ep, ethmoid plate; hb, hypobranchial; hs, hyosymplectic; ih, interhyal; m, Meckel's cartilage; not, notochord; ov, otic vesicle; pch, parachordal; pq, palatoquadrate; tr, trabecula.

## 2.2 The Neural Crest

Neural crest cells are vertebrate-specific pluripotent embryonic cells that give rise to a diverse set of derivatives. The skeletal elements and connective tissue of the craniofacial skeleton are generated entirely from neural crest cells. Neural crest cell development involves the steps of induction, specification, epithelial to mesenchymal transition/delamination, migration and differentiation.

### 2.2.1 Neural crest induction

Neural crest cells are ectodermal cells arising at the boundary between the neural plate and non-neural ectoderm. The mechanisms of neural crest cell induction are only beginning to be unraveled and here I will shortly outline the basics of a current model of neural crest induction (Knecht and Bronner-Fraser 2002). A dorso-ventral gradient of bone morphogenetic proteins (BMPs) is established, with non-neuroectoderm forming in regions with high BMP concentrations, neural plate forming in regions with low BMP concentrations and neural crest forming in regions with intermediate BMP concentrations. Wnt signaling might also be necessary for the neural crest induction process. (The *Wnt* genes encode a large family of secreted growth factors that have been identified in animals from hydra to humans.) Within the domain of intermediate BMP signaling, the ectodermal cells are competent to form either neural crest cells or Rohon-Beard neurons. These are primary sensory neurons located in the dorsal neural tube. The final cell fate decision is subsequently accomplished via Delta-Notch signaling (Cornell and Eisen 2000). As soon as some cells in the area of intermediate BMP signaling begin to differentiate as Rohon-Beard neurons, they inhibit adjacent cells to also differentiate to Rohon-Beard neurons (by activating Notch), thus promoting these neighbors to become neural crest cells.

### 2.2.2 Neural crest specification: Progressive fate restriction

The questions of when and how neural crest cells adopt a specific fate are an area of active research. The concepts of competence, fate specification and fate commitment are very important in this context. Competence for a given developmental fate is defined as the ability to adopt that fate. A cell is defined as being specified to a fate if it adopts this fate when isolated from the embryo and

cultured in a neutral medium, i.e. in the absence of other signals. Fate specification is accompanied by changes in gene expression, cell behavior or even by the initiation of overt differentiation. In contrast, a cell is defined as being committed to a particular fate when it maintains that fate even in a new environment, i.e. in the presence of other signals. Cell lineage tracing and transplantation experiments in zebrafish indicate that neural crest cells become biased in their fate choices (=specified) prior to migration but are not committed to these choices (Schilling and Kimmel 1994; Schilling et al. 2001). They are still competent to respond to signals from the environment through which they migrate.

Studies of pigment cell development have contributed the most to the current understanding of neural crest specification and suggest a model of progressive fate restriction. There are three types of neural crest-derived pigment cell types in zebrafish, namely black melanophores (producing melanin), yellow xanthophores (containing pteridine pigments and carotenoids) and iridescent, metallic silvery iridophores (containing crystalline purine deposits). One gene playing a pivotal role in pigment cell development is *sox10*. This gene has been found to be required for the specification of all non-ectomesenchymal neural crest fates such as pigment fates (melanophores, iridophores and xanthophores) and neural fates (neurons and glia cells). In the *colourless (cls)* mutant lacking functional Sox10 protein these neural crest derivatives are absent while ectomesenchymal derivatives are unaffected (Dutton et al. 2001; Kelsh and Eisen 2000). Following the emergence of this non-ectomesenchymal progenitor cells, high levels of Wnt signaling molecules secreted from dorsal neural keel cells are being utilized to promote pigment cell specification at the expense of neuron and glia formation. Another important gene in the specification process is *mitfa*, a zebrafish microphthalmia-associated transcription factor (MITF) homologue. This gene is disrupted in the *nacre* mutation (*nac*), which is causing a lack of melanoblasts (unpigmented melanophore precursors) and melanophores (Lister et al. 1999). The *nac/mitfa* gene is essential for melanophore lineage specification but is expressed in melanoblasts as well as in xanthoblasts. This indicates that at this stage the pigment cell progenitors are not fully committed to either the melanophore or the xanthophore lineage. A third gene involved is a zebrafish *c-kit* homologue which corresponds to the *sparse (spa)* pigmentation mutation (Parichy et al. 1999). *spa/kit* expression overlaps with but appears later than

*nacl/mitfa* expression. *spa/kit* has been shown to be required specifically for melanoblast migration and survival. A fourth gene crucial in melanophore specification is *dct*. This gene encodes the melanogenic enzyme dopachrome tautomerase and is expressed in migrating late melanoblasts and in melanophores (Kelsh et al. 2000). *dct* is also expressed in the retinal pigmented epithelium (RPE) and thus it is an early marker for all melanin-synthesizing cells, both neural crest-derived and neuroectoderm-derived. The following is a hierarchy of gene function in melanophore specification and differentiation:

***cls/sox10* → *nacl/mitfa* → *spa/kit* → *dct***

This pathway exemplifies the concept of progressive fate restriction of neural crest cells. First, a non-ectomesenchymal progenitor arises from a pluripotent neural crest progenitor. Subsequently a pigment cell progenitor is induced by high levels of Wnt signaling. The next progenitor has lost the competence to generate iridophores but still has the potential to generate either melanophores or xanthophores. The final fate restriction step is the limitation to one single cell fate: melanophore.

Following their specification neural crest cells undergo an epithelial to mesenchymal transition and delaminate from the dorsolateral edge of the neural tube. Epithelial to mesenchymal transition requires the repression of members of the E-cadherin family of cell adhesion molecules by members of the Snail family of zinc finger transcription factors (Cano et al. 2000). Moreover, the GTP-binding protein rhoB, which is induced by BMP signalling, has been shown to be essential for the epithelial to mesenchymal transition and delamination of premigratory neural crest cells (Liu, J. P. and Jessell 1998).



### **2.2.3 Neural crest migration and the organization of cranial neural crest streams**

Although neural crest cells are pluripotent, differences exist between cells that are generated from different anteroposterior levels: Trunk neural crest cells and cranial neural crest cells differ from each other with respect to specification, migration pathways and, consequently, potential fates (see also Table 1; chapter 2.2.4).

Trunk neural crest cells migrate from the neural tube to their destinations along one of two pathways. The lateral pathway is a route between the somites and the epidermis and the medial pathway runs between the somites and the notochord. Neural crest cells that migrate on the lateral pathway form pigment cells exclusively whereas cells that migrate on the medial pathway give rise to either pigment cells or neural derivatives.

The cranial neural crest that populates the pharyngeal arches arises from the level of the hindbrain, which is undergoing segmentation during the period of neural crest production (Lumsden et al. 1991; Tosney 1982). The hindbrain (or rhombencephalon) is subdividing into eight units, termed rhombomeres r1-r8 (Lumsden and Keynes 1989). Cranial neural crest cells migrate in three streams: The crest for the first pharyngeal arch arises from the r2 level, the crest for the second arch from the r4 level (preotic stream) and the crest for the branchial arches from the level of r6 and r7 (postotic stream; Figure 2). Separating these regions of crest production are the two rhombomeres r3 and r5 that are depleted in neural crest production. The segregation of the crest into these three pharyngeal crest streams has been shown to be significant for the accurate transfer of positional information from the neural tube to the pharyngeal arches.

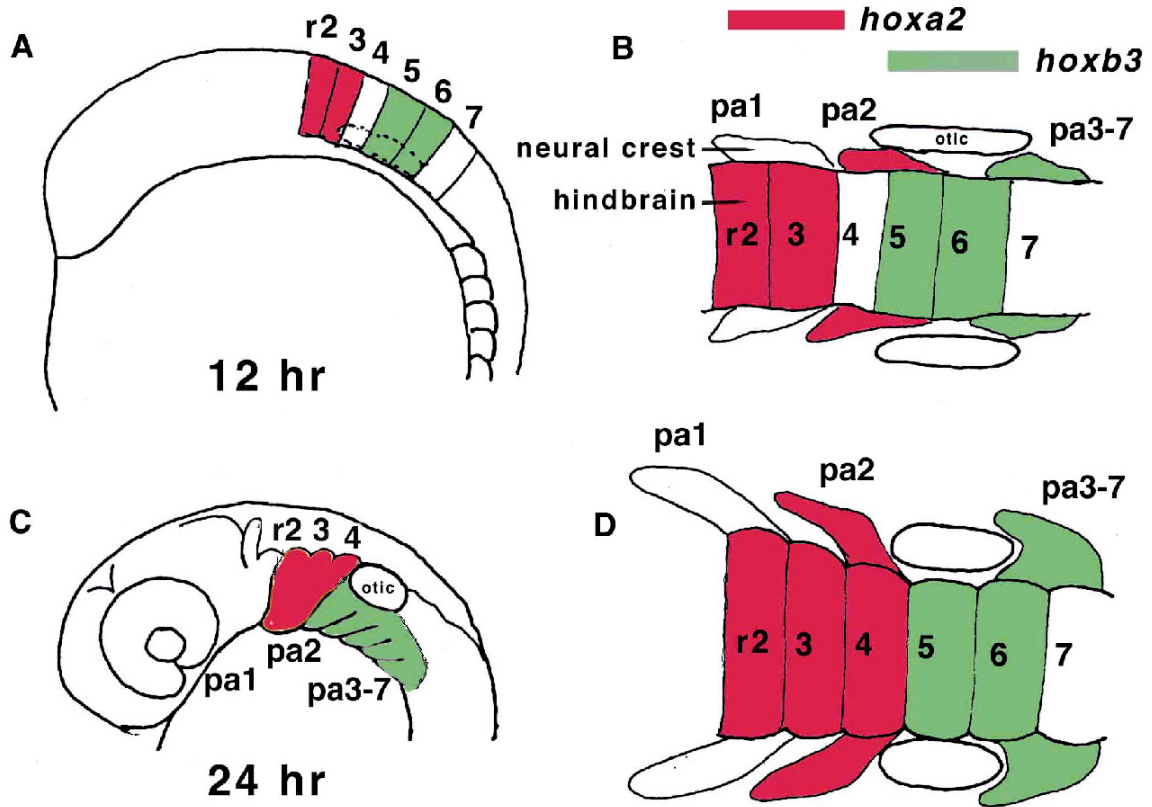


**Figure 2.** Hindbrain patterning, cranial neural crest stream organization and *hox* gene expression in embryonic zebrafish (Schilling et al. 2001). (A,C) Lateral views. (B,D) Dorsal views. (A,B) 12 hpf embryo. (C,D) 24 hpf embryo. Abbreviations: otic, otic vesicle; pa1-pa7, pharyngeal arches 1-7; r1-r7, rhombomeres 1-7.

In the chick there is only little neural crest production at the levels of the rhombomeres 3 and 5. Instead, these territories are associated with elevated levels of cell death (Graham et al. 1993). The rhombencephalic neural crest cell death in r3 and r5 is under the interactive control of the flanking even-numbered rhombomeres. If either of these flanking segments are removed, the cell death program is ceased and r3+r5 produce a large amount of neural crest cells (Graham et al. 1993). Two key components of this apoptosis program are the gene encoding the signaling molecule Bmp4 and the homeobox gene *msx2*. Both of these are expressed in the apoptotic foci of r3 and r5 and are dependent for their expression upon signals from the neighboring segments. The association between Bmp4 and *Msx2* and morphogenetic cell death seems to be widespread since they are also involved in the establishment of foci of apoptosis in the interdigital regions during digit formation (Zou and Niswander 1996). Additionally, it has been shown that some neural crest cells from the levels of the rhombomeres 3 and 5 escape apoptotic elimination and migrate rostrally and caudally to join the streams arising from the even-numbered

segments. The third (postotic) neural crest stream originates and migrates from the posterior hindbrain level as a single cluster and is only separated into each of the 5 branchial arches (Figure 2C) when it comes into contact with the associated pharyngeal pouches (Kuratani 1997). This segregation of the most posterior stream does not involve apoptotic cell death.

## 2.2.4 Neural crest differentiation and derivatives

Depending on their location of origin, cranial and trunk neural crest cells give rise to a wide variety of cell types (Table 1). In addition, it has recently been reported in zebrafish that both cranial and trunk neural crest also contribute to myocardial cells of the heart (Li, Y. X. et al. 2003; Sato and Yost 2003).

**Table 1.** Neural crest (NC) derivatives in zebrafish.

Neural crest derivatives	Cranial NC	Trunk NC
Ectomesenchymal fates		
Craniofacial skeleton + connective tissue	+	-
Fin mesenchyme	-	+
Non-ectomesenchymal fates		
Pigment		
Melanophore	+	+
Iridophore	+	+
Xanthophore	+	+
Neural		
Cranial ganglia	+	-
Dorsal root ganglia	-	+
Sympathetic neuron	-	+
Glia of the PNS (peripheral nervous system)	+	+

The cranial sensory ganglia consist of sensory neurons and glial cells. The majority of sensory neurons in these ganglia is derived from cranial ectodermal placodes but a substantial number of sensory neurons as well as all the glial cells are formed from cranial neural crest (Baker and Bronner-Fraser 2001).

### 2.2.5 Hindbrain patterning and pharyngeal arch specification

The segmental organization of the hindbrain is critical for the subsequent specification of cranial neural crest streams. Two gene families have been found to be essential for accurate hindbrain patterning. First, the Eph family of receptor tyrosine kinases and their ligands, the ephrins, have been shown to play pivotal roles in the establishment of segmental boundaries in the hindbrain. EphB4a is expressed in rhombomeres 5+6, whereas its ligand, ephrin-B2a, is expressed in r4+r7. The gene *valentino* (*val*; zebrafish orthologue to the mouse *Kreisler* gene) is expressed in r5+r6 (Moens et al. 1998) and is essential in setting up the complementary expression domains of EphB4a and ephrinB2a (Cooke et al. 2001). In *val* mutants this complementary expression pattern is lost, giving rise to a so-called rhombomere rX between r4 and r7, which displays a mixed identity (Moens et al. 1996). Interestingly, repulsive interactions between Eph receptors and ephrin ligands have also been found to be required for the separation of cranial neural crest streams.

Secondly, the prominent hindbrain and neural crest expression of *Hox* genes suggested that these genes might be involved in patterning of the hindbrain and in specifying anteroposterior neural crest cell identity (McGinnis and Krumlauf 1992). It has even been proposed that there is a transfer of *Hox* gene expression from the hindbrain to the neural crest, which could be read in the form of a code and by that means direct the development of the pharyngeal arches (Hunt et al. 1991). It is now clear that *Hox* genes play a pivotal role in the regional specification of the hindbrain and the arches, but that there is no simple transference of positional information from the hindbrain to the neural crest in the form of a *Hox* code. For example, molecular analyses have identified independent regulatory elements controlling *Hox* gene expression in the hindbrain and in the neural crest (Prince, V. and Lumsden 1994). *Hoxa2* is expressed in the hindbrain rostrally up to the r1/r2 boundary and in cranial neural crest cells that migrate into the second branchial arch. In r3 and r5 *Hoxa2* expression is directly regulated by the zinc finger transcription factor *Krox-20*. In contrast, *Hoxa2* expression in prospective second branchial arch neural crest cells is tightly controlled by a cranial neural crest enhancer that is activated by AP-2 $\alpha$  family members (Maconochie et al. 1999). Mutation or deletion of these AP-2 $\alpha$  sites in the *Hoxa2* enhancer abolishes *Hoxa2* expression in cranial neural crest cells but does

not affect hindbrain expression. This demonstrates that at the molecular level *Hoxa2* is independently regulated in rhombomeres and in neural crest cells.

Gain-of-function and loss-of-function experiments in mouse, frog and zebrafish emphasize the importance of *Hox* genes in the specification of the first and second pharyngeal arches. In contrast to the rest of the rhombomeres, rhombomere 1 is devoid of *Hox* gene expression. Likewise, there is no *Hox* expression in neural crest cells emanating from rhombomere 2 to populate the first arch (Prince, V. E. et al. 1998). The targeted inactivation of *Hoxa2* in mice results in a homeotic transformation of neural crest-derived second arch elements into mirror image duplications of first arch elements (Gendron-Maguire et al. 1993). However, only the mesenchymal and not the neurogenic derivatives of the second branchial arch are transformed in *Hoxa2*-null mutant mice. This suggests that *Hoxa2* is essential for proper patterning of neural crest-derived ectomesenchymal second arch structures. Ectopic expression of *Hoxa2* in the first arch in *Xenopus* embryos results in a converse phenotype (Pasqualetti et al. 2000). *Hoxa2* overexpression leads to a homeotic transformation of first arch structures into second arch elements. The duplicated elements are fused to the original elements in a manner similar to that seen in the *Hoxa2* knockout mice. This result confirms the role of *Hoxa2* as a selector gene specifying second arch fate.

Zebrafish as well as the mouse have just two members of *Hox* paralogue group 2: *Hoxa2* and *Hoxb2*. The effect of the mouse *Hoxa2* knockout suggests, that this gene is solely responsible for second arch specification. However, in the zebrafish only a simultaneous morpholino-mediated gene knockdown of both *hoxa2* and *hoxb2* results in a homeotic transformation comparable to the mouse null mutant phenotype (Hunter and Prince 2002). Knockdown of either of these two genes alone fails to have any effect. This shows that there is a high redundancy of *hoxa2* and *hoxb2* in governing second arch specification and patterning in zebrafish. In compliance with this function, ectopic expression of either of the two paralogue group 2 genes in the first pharyngeal arch (normally devoid of any *Hox* gene expression) leads to a shift from first to second arch identity.

## 2.2.6 Pharyngeal arch patterning

The formation and regional patterning of the pharyngeal arches depend largely on the inductive properties of the endoderm. The endoderm has been shown to be required for the development of chondrogenic neural crest cells in the zebrafish (David et al. 2002). Studies in amphibia have implicated the endoderm in directing neural crest cells towards a chondrogenic fate, while it has been shown in chick that this tissue is the inducer of the epibranchial placodes (Begbie et al. 1999). These are focal thickenings of ectoderm giving rise to sensory neurons of the cranial ganglia. The epibranchial placodes are induced by the secretion of Bmp7 from the underlying endoderm.

To determine whether neural crest is required for arch formation and patterning, neural crest ablation experiments were carried out. Interestingly, in the absence of the neural crest the pharyngeal arches form and are properly regionalized (Veitch et al. 1999). In normal arches Bmp7 is expressed at the posterior endodermal margin, Fgf8 is expressed in the anterior endoderm and the overlying ectoderm, whereas Pax1 is expressed in the most proximal endoderm of the pharyngeal pouches. These expression patterns are established correctly in pharyngeal arches that lack neural crest cells. These and additional results demonstrated that the pharyngeal arches are not dependent upon the neural crest for their formation, for their early regionalization or even for their sense of identity. Therefore, normal arch morphogenesis must result from an integration of neural crest-dependent and endoderm-dependent patterning mechanisms.

The fact that many aspects of pharyngeal arch formation and patterning are not dependent upon the neural crest reflects the evolutionary history of the arches. Pharyngeal segmentation is characteristic of the entire phylum chordata, encompassing urochordates, cephalochordates and vertebrates. However, neural crest or more specifically neural crest-derived ectomesenchyme that forms the skeletal and connective tissues of the arches is an exclusively vertebrate characteristic. Studies on the expression patterns of the *AmphiPax1/9* and *AmphiPax2/5/8* genes in *Amphioxus*, the nearest extant relative of the vertebrates, have demonstrated that not only does this animal possess pharyngeal pouches but

that these pouches also exhibit regionalization (Holland and Holland 1996). Thus, the mechanism for pharyngeal segmentation and regionalization seems to have predated the emergence of the neural crest in evolution.

## 2.3 Cartilage development

Cartilage cells (chondrocytes) have different origins depending on the different embryonic locations in which they arise. In the branchial arches and head cartilages, these cells are derived from cranial neural crest cells; in sclerotomes, which generate vertebrae and ribs, the cells are derived from the paraxial mesoderm, whereas limb cartilage chondrocytes are derived from the lateral mesoderm.

### 2.3.1 Chondrogenesis

Chondrogenesis (cartilage formation) involves the steps of condensation, differentiation, morphogenesis and growth. When chondrogenic cranial neural crest cells have completed their migration, they start to form precartilage mesenchymal condensations in the pharyngeal arches. Uncondensed chondroprogenitors produce an extracellular matrix (ECM) rich in collagen type I, hyaluronan, tenascin and fibronectin (DeLise et al. 2000; Pizette and Niswander 2000). Upon aggregation into prechondrogenic condensations, the chondroprogenitors start to express and produce ECM components specific for the chondrogenic lineage, e.g. collagen type II, collagen types IX and XI, Gla protein, aggrecan, and link protein, while the expression of collagen type I is turned off (Hall and Miyake 2000). Condensation is hallmarked by changes in cell adhesion and cytoskeletal architecture: The restricted temporal and spatial expression patterns of N-cadherin, fibronectin, syndecans, tenascins, thrombospondins, neural cell adhesion molecule, focal adhesion kinase and paxillin in chondrogenic condensations have been reported (Knudson and Knudson 2001; Shum and Nuckolls 2002). The condensed prechondrogenic mesenchyme subsequently differentiates into chondrocytes: The cells deposit cartilage matrix components into their extracellular matrix and acquire a characteristic rounded chondrocyte morphology. Cartilage differentiation is accompanied by cartilage morphogenesis. The chondrocytes undergo rearrangements resulting in stereotypically arranged stacks of chondrocytes (stack-of-coin arrangement). It is at this morphogenesis stage that the shape of the skeletal elements is established. The final step in chondrogenesis is growth of the cartilage elements by chondrocyte divisions. The skeletal elements grow isometrically, i.e. the shape of the elements is preserved (Kimmel et al. 1998).



### **2.3.2 The extracellular matrix**

The extracellular matrix (ECM) is a mixture of macromolecules synthesized by many cell types, especially connective tissue cells, and deposited in the extracellular milieu. The majority of ECM components is transported to the extracellular space via the classical ER-Golgi-dependent secretory pathway. Through a multiplicity of interactions the matrix macromolecules form complexes, aggregates and large composites. In skeletal tissues the volume occupied by the ECM far exceeds the volume of the cells that produce this matrix (Knudson and Knudson 2001). This leads to complications in the ability of some skeletal cells to remodel and repair the extensive volume of extracellular matrix. Bone cells accomplish this by having a separate cell type, the osteoclast, which is responsible for bone matrix resorption. Cartilage cells both synthesize and remodel their matrix. The majority of cartilage matrix remodeling occurs in the pericellular environment. The nature of the ECM in a skeletal tissue defines the material properties of that tissue. Collagens are the major structural fibrous proteins of the ECM. Cartilage collagens (collagens II, IX and XI) provide the structural framework of bone and cartilage and are responsible for the biomechanical properties such as resistance to pressure, torsion or tension. The next most abundant extracellular matrix components in the skeleton are proteoglycans.

### **2.3.3 Proteoglycans**

Proteoglycans are a family of macromolecules displaying a high degree of structural diversity and complex biosynthetic pathways (Schwartz 2000). Proteoglycan molecules have a core protein and at least one covalently attached glycosaminoglycan chain. The glycosaminoglycan molecules are long unbranched polysaccharides containing a repeating disaccharide unit. The disaccharide units are normally sulfated and usually contain either of two modified amino sugars - N-acetylgalactosamine (GalNAc) or N-acetylglucosamine (GlcNAc) - and a uronic acid such as glucuronate or iduronate. Chondroitin sulfate is the most common glycosaminoglycan chain. Other chains include dermatan sulfate, keratan sulfate, heparan sulfate and heparin. The majority of glycosaminoglycans in the body are linked to core proteins, forming proteoglycans. The linkage of glycosaminoglycans to the protein core involves a specific trisaccharide composed of two galactose residues

and a xylulose residue (GAG-GalGalXyl-O-CH<sub>2</sub>-protein). The trisaccharide linker is coupled to the protein core through an O-glycosidic bond to a serine residue in the protein. Some forms of keratan sulfates are linked to the protein core through an N-asparaginyl bond. The protein cores of proteoglycans are rich in serine and threonine residues, which allows multiple glycosaminoglycan attachments. Both the addition of sulfate groups and glycosylations take place in the Golgi complex prior to secretion to the ECM. One glycosaminoglycan, hyaluronan, does not contain any sulfate, is synthesized at the cell surface and is not attached to a core protein. It is, however, a component of non-covalently formed complexes with proteoglycans such as aggrecan. Aggrecan contains about a 100 chondroitin sulfate chains and a smaller number of keratan sulfate chains. Some small proteoglycans contain repeating leucine-rich motifs and are present in many connective tissues. These include molecules like decorin, biglycan and fibromodulin. Decorin and fibromodulin have been shown to bind to collagen fibrils (Knudson and Knudson 2001). Other small proteoglycans contain heparan sulfate side chains and associate with the plasma membranes on cells. Among these, the syndecans contain a membrane-spanning domain while glypicans are membrane-associated through a glycosylphosphatidylinositol (GPI) anchor at the C-terminus of the protein (Lander and Selleck 2000).

A zebrafish glypican controlling cell polarity during gastrulation movements has been shown to be disrupted by the *knypek* mutation (Topczewski et al. 2001). Most notably, given the structural diversity of proteoglycans, their complex biosynthesis and their importance in the function of the ECM, they are prime candidate molecules for zebrafish mutations with impaired cartilage differentiation. The zebrafish *jekyll* mutation that causes a similar reduction of the pharyngeal skeleton as the *crusher*<sup>m299</sup> and *round*<sup>m211, m641, m713, m715</sup> mutations has been shown to interfere with glycosaminoglycan biosynthesis (Walsh and Stainier 2001).

The importance of proteoglycans in skeletal development will be exemplarily illustrated by the consequences of deficiencies in perlecan biosynthesis. Perlecan is a large heparan sulfate proteoglycan present in all basement membranes and in some other tissues such as cartilage. Mice lacking the perlecan gene (*Hspg2*) develop a severe chondrodysplasia (Arikawa-Hirasawa et al. 1999) and show

extensive similarity to the human lethal autosomal recessive disorder dyssegmental dysplasia, Silverman-Handmaker type (DDSH). Recently, it has been shown that DDSH also results from null mutations in the perlecan gene *HSPG2* (Arikawa-Hirasawa et al. 2001). Cartilage of *Hspg2* null mice shows a severe disorganization of the stacked columnar structures of chondrocytes and defective bone homeostasis. The cartilage matrix contains reduced amounts of disorganized collagen fibrils and glycosaminoglycans, suggesting that perlecan indeed is a crucial matrix component. Moreover, chondrocyte proliferation is reduced. Short, irregular chondrocyte stacks and cartilage degeneration are also seen in DDSH cartilage, likely due to a destabilization of the ECM structure caused by the absence of a normal composition of proteoglycans. Importantly, DDSH perlecan molecules are unstable and fail to be secreted from the cells into the ECM.

In addition to their biomechanical properties, heparan sulfate proteoglycans interact with ECM proteins, growth factors and receptors, and their absence from the matrix may impair growth factor action. Specifically, perlecan has been implicated in cellular signaling processes governing cell growth and differentiation.

## **2.4 Strategies for the molecular dissection of neural crest derivative development in zebrafish**

### **2.4.1 Morphological and molecular analyses of ENU-induced zebrafish mutations**

Following the initial isolation of the zebrafish ENU-induced mutations only very limited morphological analysis has been performed (Neuhauss et al. 1996). To analyze the phenotypes caused by ENU-induced mutations in greater detail, I have conducted extensive morphological, histological and molecular analyses. The cartilaginous craniofacial skeleton of mutant embryos was visualized by staining of extracellular matrix components with the Alcian Blue dye. The Alcian Blue stained skeletons were dissected, allowing inspection of the morphogenesis of single craniofacial cartilage elements. I performed histological analysis of mutant and wild-type embryos at identical planes on ultra thin plastic sections stained with the Toluidine Blue dye. This has led to a detailed description of the phenotype at the cellular level. Gene expression analysis is a valuable tool to pinpoint the function of mutated genes. I have performed whole mount *in situ* hybridizations with digoxigenin-labeled riboprobes to determine which genetic pathways are affected by the mutated genes. Where available, I used antibodies in whole mount immunohistochemistry assays to characterize the development of various cranial neural crest derivatives. Moreover, I used microinjection of modified antisense oligonucleotides (morpholinos) into wild-type embryos, a powerful loss-of-function assay (Nasevicius and Ekker 2000). The injected antisense oligonucleotide binds to the mRNA of the targeted gene and thereby blocks its translation. The injection of a morpholino against a gene which is known to be disrupted by a mutation (or against a downstream target of this gene) allows to generate a phenocopy of the mutant phenotype in wild-type embryos.

### **2.4.2 Genetic mapping of ENU-induced mutations**

ENU-induced mutations are not marked by specific molecular tags and require genetic linkage analysis and positional and/or candidate cloning strategies to identify the causative gene. The genetic mapping of ENU-induced mutations can be established via bulked segregant analysis (Michelmore et al. 1991) and a total

genome scan using a microsatellite genetic linkage map (Knapik et al. 1996; Knapik et al. 1998; Shimoda et al. 1999). First the heterozygous fish carrying the ENU-induced mutation in the AB strain background are crossed to highly polymorphic IN (India), HK (Hong Kong), WIK (from Calcutta in India) or TL (Tübingen long fin) strains. Tübingen long fin is a line that harbors a dominant mutation for long fins (*longfin*) and a recessive mutation *leopard* (*leo*, former name *tup*) that causes the striping pattern to dissolve into isolated spots. The F1 hybrid generation is screened for the F1 heterozygotes which are subsequently used to generate the embryos of the F2 generation (Figure 3A). The F1 heterozygotes are genetically polymorphic and the recombinations (cross-overs) taking place between the location of the mutation and certain microsatellite markers can be scored in the meioses of both the male and the female F1 heterozygotes. The distance between a mutation and a genetic marker is proportional to the number of recombination events occurring between them. The smaller the distance between a mutated locus and a microsatellite marker, the less likely it is that a cross-over will take place between them in the germline of the F1 heterozygotes. This principle of linkage analysis provides the basis for the genome scan and the subsequent genetic fine mapping.

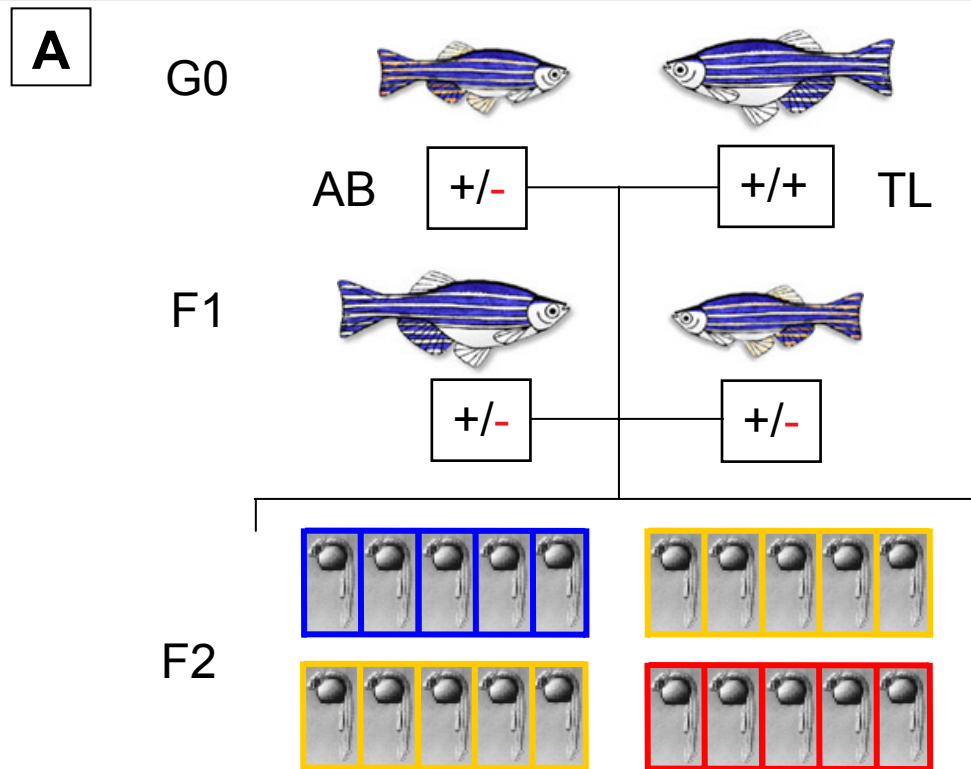
Based on the normal Mendelian segregation of an autosomal recessive mutation, the F2 progeny is expected to consist of 25% homozygous wild-type embryos, 50% heterozygous wild-type embryos and 25% homozygous mutant embryos. The homozygous and heterozygous wild-type embryos cannot be distinguished phenotypically. For the genome scan, approximately equal amounts of DNA from 10 F2 homozygous mutant embryos or from 10 F2 wild-type embryos are pooled and these mutant and wild-type DNA pools are genotyped with SSLP (simple sequence length polymorphism) markers which are spaced approximately evenly across the whole zebrafish genome (25 linkage groups). The SSLP markers are microsatellites which normally consist of TA, CA or GT dinucleotide repeats. The length of these repeats differs between the zebrafish strains used, thereby offering the possibility to use them as polymorphic genetic markers. In the case of a close linkage between a polymorphic SSLP marker and the mutation, two bands will be generated on the wild-type DNA pool and only one band will be generated on the mutant DNA pool in a PCR assay. One of the two wild-type bands is more intense because both homozygous and heterozygous wild-type embryos contribute to the DNA pool and to

the amplification products. The mutant DNA pool yields only one amplification product unless there has been a recombination event between the mutation and the SSLP marker. In this case there are two bands, but the intensity of the bands should be reciprocal compared to that described for the wild-type DNA pool.

Candidate linked markers are subsequently tested on single F2 embryos for confirmation or exclusion of linkage (Figure 3B). In the case of a confirmed linkage, the mapping is refined by testing higher numbers of embryos with more markers from the chromosomal region of interest. The goal is to lose recombinants on both sides of the mutation and to find the closest flanking markers.

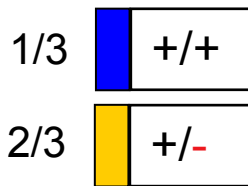
Scorable recombination events (cross-overs) in F2 intercrosses take place in the meioses of both F1 heterozygotes (male and female). Genotyping of the resulting F2 embryos reveals the number of recombination events that have occurred between the mutated locus and the tested microsatellite marker in any of the two parental meioses. One F2 embryo thus equals two parental meioses. Consequently, the number of meioses (male plus female meioses) which can be scored by genotyping a given number of F2 progeny is exactly twice as high as the number of the F2 progeny. The genetic distance in cM (centiMorgans) is calculated by dividing the number of recombinants for a given marker by the number of meioses tested with this marker and multiplying with one hundred (1 chromosome = 1 Morgan or 100 centiMorgans). Example: A genotyping experiment yields 12 recombinations between a linked microsatellite marker and a mutation in 250 F2 embryos (=500 meioses). The genetic distance between the marker and the mutation is calculated as follows:

$$12 / 500 \times 100 = 2.4\text{cM}$$



For the Genome scan pool:

10 F2 WT embryos



10 F2 mutant embryos

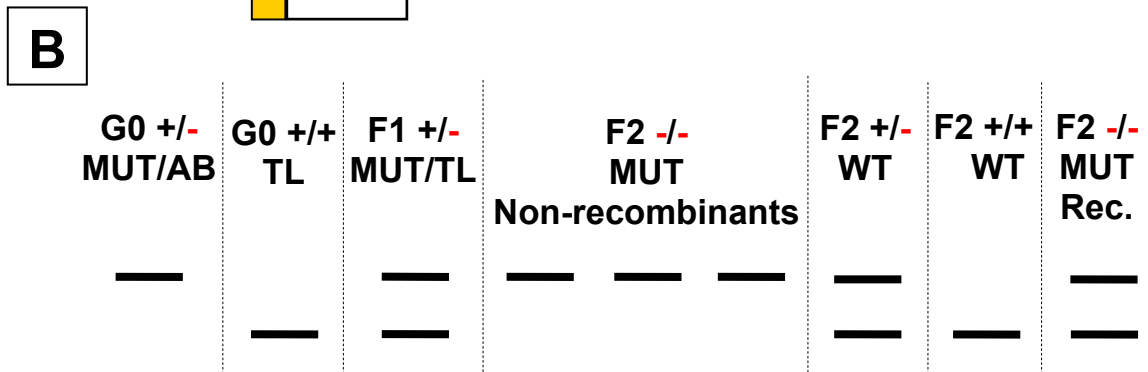
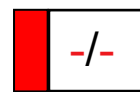


**Figure 3.** Breeding and mapping strategy. (A) F2 intercross breeding scheme. A heterozygote carrier of an ENU-induced mutation is crossed to the polymorphic TL line (G0 generation). The F1 heterozygote fish are crossed to each other to generate embryos of the F2 generation for genetic mapping (genome scan and subsequent fine mapping). Recombinations (cross-overs) occur in the meioses of both F1 heterozygote animals (male and female). One third of the F2 wild-type embryos are homozygotes (blue) and two thirds of the F2 wild-type embryos are heterozygotes (yellow). All F2 mutant embryos are homozygous for the mutated locus (red). (B) Segregation of a linked microsatellite marker. The upper allele is the mutant allele in the AB genetic background. The lower allele is the TL allele (in the polymorphic TL genetic background). F1 heterozygotes have both the mutant and the TL alleles. In F2 non-recombinants the mutation and the marker are linked (indicated by the presence of the mutant allele only). In F2 recombinants a cross-over has occurred between the mutation and the marker (indicated by the presence of both marker alleles).

### **2.4.3 Gene identification by candidate and positional cloning approaches**

The chromosomal localization of the mutation provides a starting point for a search for potential candidate genes in this region and in the syntenic regions of other species. Human, mouse and *Fugu rubripes* genome sequences are available and the Zebrafish Genome Sequencing Project is being conducted at the Sanger Centre (Cambridge, UK), providing valuable sequencing data to probe for suitable candidate genes. Potential candidate genes can be tested for linkage by SSCP (single strand conformation polymorphism) analysis on the recombinant F2 mapcross embryos and in case of a positive result (loss of all recombinants) the mutant allele is sequenced in search of a mutation site. If the critical minimal region does not contain a good candidate gene, physical mapping and positional cloning have to be performed. The closest SSLP markers are used to assemble a YAC (insert size: up to 2 Mb) contig spanning the region. Smaller genomic clones such as BAC (insert size: up to 300 kb), PAC (insert size: 130-150 kb) and cosmid (insert size: 30-50 kb) clones are assembled in the process of physical fine mapping. One possibility to determine which of the genomic clones obtained from a library screen contain the gene of interest and which ones do not is to inject the DNA clones into mutant embryos and select the one(s) which cause(s) a partial or complete rescue of the phenotype. Testing subcloned fragments of the positive genomic clone is a good strategy to identify the gene of interest. An alternative method is to screen cDNA libraries with BACs, PACs or cosmids and to sequence the positive cDNAs. Shot-gun sequencing of BAC and PAC clones and software based prediction of ORFs (open reading frames) in these clones can also be adopted.



### 3 Aims of the thesis

The neural crest is one of the major innovations of the vertebrate evolutionary lineage. The spectrum of neural crest derivatives is highly conserved within the vertebrate sublineages. The goal of this thesis project is to contribute to a better understanding of the genetic pathways governing neural crest specification and differentiation of a neural crest derivative, the craniofacial cartilage. To achieve this, four ENU-induced mutations affecting craniofacial development in the zebrafish will be characterized at the molecular and functional level. These mutations are inherited in a recessive Mendelian mode and lead to embryonic lethality in homozygous embryos. The *brak* (*brk*<sup>m452</sup>) mutation combines defects in craniofacial cartilage morphogenesis and in melanophore pigmentation. The *round* (*rnd*<sup>m211</sup>, *rnd*<sup>m641</sup>, *rnd*<sup>m713</sup> and *rnd*<sup>m715</sup>) and *crusher* (*cru*<sup>m299</sup>) mutations affect cartilage differentiation and morphogenesis. The *mother superior* (*mos*<sup>m188</sup>) mutation was identified based on the absence of branchial arch cartilage elements in the *mos*<sup>m188</sup> homozygous embryos. Phenotypic analysis of the mutations affecting cartilage differentiation will include whole-mount skeletal stainings and histological analyses and aims at revealing specific defects in cartilage morphogenesis and chondrocyte morphology. I will perform a detailed analysis of the *mos*<sup>m188</sup> mutant phenotype including characterization of all affected neural crest derivatives. Additionally, I will focus on the analysis of the development of the ectodermal placodal derivatives. The experiments aiming at a complete characterization of the complex *mos*<sup>m188</sup> mutant phenotype will include vital dye stainings, fluorescence microscopy and immunohistochemistry. In order to determine the spatial and temporal requirements for *mos*<sup>m188</sup> gene function as well as to establish its position in genetic pathways regulating neural crest cell development, I will perform *in situ* hybridizations with riboprobes for key genes involved in neural crest development. Molecular characterization of the four ENU-induced mutations will include genetic mapping of the mutated loci to small genetic intervals, and if possible positional candidate cloning will be initiated. The integration of all available data on zebrafish mutations affecting neural crest and craniofacial development is likely to provide a deeper insight into the underlying genetic and developmental pathways and will ultimately contribute to a better understanding of the etiology of some diseases from the large group of human congenital craniofacial syndromes.

---

## 4 Materials and Methods

### 4.1 Materials

#### 4.1.1 Chemicals

Acetic acid	Merck
Acrylamide (30% with 0.8% Bisacrylamide)	Roth
Agar	Difco
Agarose	Biozym
Agarose (NuSieve)	Biowhittaker
Alcian blue	Sigma
APS (Ammonium peroxodisulfate)	Merck
Ampicillin	Sigma
Boric acid	Sigma
Bromophenol Blue	Sigma
BSA (Bovine serum albumine)	Sigma
Calcium chloride (dihydrate)	Sigma
Chloroform	Merck
DASPEI (2-(4-Dimethylaminostyryl)-N-ethyl pyridinium iodide)	Sigma
DEPC (Diethylpyrocarbonate)	Aldrich
DMF (N,N-Dimethyl formamide)	Sigma
DMSO (Dimethyl sulfoxide)	Sigma
dNTPs	Roche
EDTA (Ethylenediamine tetraacetic acid)	Sigma
Ethanol	Merck
Ethidium bromide	Sigma
Eukitt	Fluka
Formamide	Fluka
Glycerol	Sigma
Heparin	Sigma
HEPES (N-2-Hydroxyethylpiperazine-N'-2-ethanesulfonic acid)	Sigma
Hydrochloric acid	Merck
Hydrogen peroxide	Sigma
Isopropanol	Merck

Kanamycin	Sigma
Magnesium chloride	Sigma
$\beta$ -mercaptoethanol	Sigma
Methanol	Merck
Methylene blue	Sigma
Mineral oil	Sigma
PFA (Paraformaldehyde)	Sigma
Phenol	Biosolve
Potassium acetate	Sigma
Potassium chloride	Sigma
Potassium hydroxide	Sigma
PTU (1-Phenyl-2-thio-urea)	Sigma
SDS (Sodium dodecyl sulfate)	Sigma
Sodium acetate	Sigma
Sodium chloride	Sigma
Sodium citrate	Sigma
Sodium dihydrogen phosphate	Sigma
Sodium hydrogen phosphate	Sigma
Sodium phosphate	Sigma
TEMED (N, N, N', N'-Tetramethylethylenediamine)	Sigma
Toluidine blue	Sigma
Tris	Sigma
Triton X-100	Sigma
Tween-20	Merck

#### 4.1.2 Radionucleotides

$[\alpha\text{-}^{32}\text{P}]\text{dATP}$	Amersham
$[\alpha\text{-}^{32}\text{P}]\text{dCTP}$	Amersham

### 4.1.3 Buffers and Solutions

- DEPC-H<sub>2</sub>O 0.1% (v/v) DEPC in dH<sub>2</sub>O
- Ethidium bromide stock solution 10 mg Ethidium bromide/ml dH<sub>2</sub>O
- 1x PBS buffer (pH 7.5)
  - 140 mM NaCl
  - 8.1 mM Na<sub>2</sub>HPO<sub>4</sub>
  - 1.5 mM KH<sub>2</sub>PO<sub>4</sub>
  - 2.5 mM KCl
- 1x PBT buffer 0.1% Tween-20 in PBS
- 20x SSC (pH 7.0) buffer
  - 300 mM Sodium citrate
  - 3 M NaCl
- 1x TE buffer (pH 8.0)
  - 10 mM Tris-HCl, pH 8.0
  - 1 mM EDTA
- 10x TBE buffer
  - 1.4 M Tris-HCl, pH 8.3 – 8.7
  - 45 mM Boric acid
  - 25 mM EDTA
- 1x Lysis buffer
  - 10 mM Tris pH 8.0
  - 50 mM KCl
  - 0.3% Tween-20

#### 4.1.4 Oligonucleotides

The sequence data of all microsatellite markers (SSLP markers = Z markers) are available on the MGH / CVRC Zebrafish Server (<http://zebrafish.mgh.harvard.edu/>). The critical Z markers used in genotyping and sequencing are listed below (except standard sequencing primers). All oligonucleotides have been synthesized by the company MWG Biotech (Ebersberg) and sequencing was performed by the companies Sequiserve (Vaterstetten) and MWG Biotech (Ebersberg).

**Table 2:** Sequences of SSLP (Z) markers used for genetic mapping.

Name	Forward primer (5'→3')	Reverse primer (5'→3')
Z11574 (LG 21)	GGC TAC ACA TGC AGT GAT GC	AGT GAT CAG GAG ATG ACC CG
Z1251 (LG 21)	AGA CGA GTG GAG CAG ACC AC	AGC ACT GCT CAG AGC AAA CA
Z22852 (LG 21)	CGG TAC TGG GCT GCT CTT AC	CCG TTC CTT CTG GCA AAT AA
Z67493 (LG 21)	CAA AAA CAC TCA GAA AAA GCA CA	ATG GAT GGT GTA TGT GCG AG
Z6295 (LG 21)	TCA CAG CAG GTT AGT CAC GTG	GTG AGA TCT CTA TCG TCA TGC A
Z22083 (LG 17)	GCA CAT TGT AGC TCG CTC TG	CTC AGA CCA CCA CCT GTC CT
Z22674 (LG 17)	AAA GTC TTT AGG CCT TTT ACA ATG A	CGT TCC CAG ATG CTT TCA AT
Z48508 (LG 17)	CCA GCA CTC AGC ATT TTT CA	GCC ATT TGC GCC ATA ATA AT
Z19625 (LG 17)	TCA GCT GTC GAC AAG TCT GG	AGA TCA AGT CCA GCG ACG TT
Z24082 (LG 17)	TCC CCA CAA TTC ACA ATA ACA A	GCC ACC TCC ATT GTG TCT TT
Z9831 (LG 17)	GAA TCC CTG TGC CAG TTG TT	TCA GGT GTC TTA GGA AAA TTG TT
Z43267 (LG 14)	CAA AGG GTG CAA AGT GCA TT	AGC AAA AGT GCT GGT GAT CA
Z6847 (LG 14)	GGC CAA TTA ATG TGC TGA TG	AAG CCA AAC CAT AGT GTG CC
Z9017 (LG 14)	GGG GAC TGA GTC ATT TTC CA	GGC CCA AAG AAC CCA GAT AT
Z22094 (LG 14)	GCA AAC TGA GGC TGA GCT CT	AAG CCG TCC ATC TTG GTA TG
Z53938 (LG 14)	CAT CAA CTT TTA TCC CGC GT	TTC ATG CAC AAA GAG CCT TG
Z68788 (LG 14)	TTC CCG TTA TTG ACT TTG CC	AGC AAC TGG GCA GTG GAT AT
Z30429 (LG 14)	TTA GAC GCA GTG GGT AGG CT	TTA ATT CTG TGG CGC ATC AA
Z21080 (LG 14)	AAT GCT AGT GCA TAG TAG TTC ATGA	CGT CTT GAG GAG TTT CTG CC

Additional - mostly gene-specific - oligonucleotides which have been used are listed in Table 3.

**Table 3:** Sequences of additional oligonucleotides.

Name	Forward primer (5'→3')	Reverse primer (5'→3')
foxD3-1F/9R	GAC CGA CCT GCA TTT ATA GCC	TCT GGT CCC TGA GAA TGT CC
foxD3-9F/12R	CCA TAA CTT GTC GCT CAA CG	TCC AGT GCT GCC TAT AGT TCG
foxD3-3F/7R	CGG TCG TCA ACT GAT CTT ACC	GGT CCA GTA GTT GCC TTT GC
foxD3-4F/4R	AGG ACA GTG ACT GCG AAA GC	ACT CGC AGA TTC CAC TGA GC
foxD3 1st round	TCG ATT GTT TGA GAT GAA CTG G	GAC GAA CAG AGG CGA TGT TAC
foxD3 2nd round	ACC GAC CTG CAT TTA TAG CC	TCG ATA TCC ACA TCG TCA GC
oep 1st round	GTG AAA GTT GGG GTT TCT GG	GCG TTC ATC GTA TTC ACA GC
oep 2nd round	GGA AAA CCA AAG CAA TAC GC	GCA GAA ACT TCC CAA AAT GC
msxa intron	GCA TCA TAA ATC AAG ATG ATC G	AGC TGA GCA GTG GTG AAA GG
sec23a	CAC GAG CTG GGC TGT GAA GG	CAT TAC GAA TCA TAC GCT CC
Z19625 overgo L	TCAGCTGTCGACAAGTCTGGCAGT	CTGAGTGCTTTACGATACTGCCAG
Z19625 overgo R	CAACCTCACGTGACATTTTGAACG	AGATCAAGTCCAGCGACGTTCAAA

The first four *foxD3* oligonucleotide pairs were used for sequencing and RFLP analysis of the *foxD3* gene:

- **foxD3-1F/9R** spans the region from nucleotide 122 to nucleotide 806 of the *foxD3* gene.
- **foxD3-9F/12R** spans the region from nucleotide 631 to nucleotide 1393 of the *foxD3* gene.
- **foxD3-3F/7R** spans the region from nucleotide 145 to nucleotide 709 of the *foxD3* gene.
- **foxD3-4F/4R** spans the region from nucleotide 306 to nucleotide 569 of the *foxD3* gene.

**foxD3 1st round** and **foxD3 2nd round** (nested) primers were used in the RT-PCR analysis of maternal *foxD3* deposition.

**oep 1st round** and **oep 2nd round** (nested) primers were used as controls in the RT-PCR analysis of maternal *foxD3* deposition. The oep primers are in exon 3 and exon 4 of the *oep* gene, thus spanning the third intron.

**msxa intron** amplifies a polymorphic intron-containing region of the *msxa* gene and was used for genetic mapping of the *msxa* gene relative to the *brak*<sup>m452</sup> mutation.

**sec23a** primers have been used in RT-PCR reactions on wild-type and *crusher*<sup>m299</sup> mutant RNA and amplify a 2 kb *sec23a* cDNA product. **sec23a** primers have been subsequently used for sequencing of this *sec23a* 2 kb RT-PCR product.

**Z19625 overgo L** and **Z19625 overgo R** are designed from the „left“ and from the „right“ non-repetitive regions of the SSLP marker Z19625 and were used for screening a PAC and a BAC library in the course of the fine mapping of the *crusher*<sup>m299</sup> mutation.

### 4.1.5 Enzymes

Various restriction endonucleases produced by MBI Fermentas and by New England Biolabs have been used. The table below contains other enzymes which have been used and which are not included in any of the kits listed further below.

**Table 4:** Enzymes used in the thesis projects.

Name	Concentration [U/ $\mu$ l]	Manufacturer
<i>Taq</i> DNA polymerase	5	Roche
Klenow fragment	2	Boehringer
T4 DNA ligase	400	New England Biolabs

### 4.1.6 Kits

Plasmid Mini Kit	Qiagen
Plasmid Maxi Kit	Qiagen
QIAquick PCR Purification Kit	Qiagen
QIAquick Gel Extraction Kit	Qiagen
QIAquick Nucleotide Removal Kit	Qiagen
SuperScript One-Step RT-PCR kit	Invitrogen
Dig RNA Labeling Kit	Roche
mMESSAGE mMACHINE transcription kit	Ambion
VECTASTAIN ABC Kit	Vector Laboratories
JB-4 Embedding Kit	Polysciences

### 4.1.7 Vectors

Table 5 contains the vectors which were used in the thesis projects.

**Table 5:** Plasmid vectors which were used in the cloning of DNA fragments.

Name	Size [bp]	Resistance	Manufacturer
pBluescript II SK (+)	2961	Ampicillin	Stratagene
pGem-T Easy	3018	Ampicillin	Promega
pCR2.1-TOPO	3931	Ampicillin+Kanamycin	Invitrogen

## 4.1.8 Biological Materials

### 4.1.8.1 Zebrafish strains

Zebrafish (*Danio rerio*) stocks were maintained under standard laboratory conditions (Westerfield, M., 1994: The Zebrafish book. A guide for the laboratory use of zebrafish. University of Oregon Press, Eugene).

The following wild-type zebrafish strains were used:

- AB line from the laboratory of George Streisinger
- HK (Hong Kong) line from the laboratory of Mark Fishman
- IN (India) line from the laboratory of Wolfgang Driever
- TL (Tübingen long fin) line from the laboratory of Christiane Nüsslein-Volhard
- WIK line from the laboratory of Pascal Haffter

The following ENU-induced craniofacial mutations isolated in the Boston screen were used (the independent mutant alleles are in parentheses):

- *mother superior* (*mos*<sup>m188</sup>)
- *brak* (*brk*<sup>m452</sup>)
- *round* (*rnd*<sup>m211</sup>, *rnd*<sup>m641</sup>, *rnd*<sup>m713</sup> and *rnd*<sup>m715</sup>)
- *crusher* (*cru*<sup>m299</sup>)

Embryos were incubated at 28.5°C and staged in hours (hpf) or days (dpf) post-fertilization. Where necessary, embryos were raised in 0.2 mM PTU (1-Phenyl-2-thiourea) to inhibit pigment formation. Embryos were fixed with 4% PFA (Paraformaldehyde) overnight at 4°C at the required developmental stages.

### 4.1.8.2 Bacterial strains

- *E.coli* DH5α
- *E.coli* DH10B
- *E.coli* XL1 blue



### 4.1.9 Equipment

Centrifuge	5415	Eppendorf
Centrifuge	Universal 32R	Hettich
Centrifuge	4-15C	Sigma/Qiagen
Waterbath	Ecoline E100	Lauda
Gel chamber	Mini-Sub Cell GT	BioRad
Gel chamber	Sub Cell GT	BioRad
Gel chamber	Gator A3-1	Owl
Power supply	PowerPac 300	BioRad
Power supply	PowerPac 3000	BioRad
Transilluminator	TFX-35M	Vilber Lourmat
Thermal cycler	Robocycler 96	Stratagene
Thermal cycler	PTC-100	MJResearch
Spectrophotometer	DU 530	Beckman
Hybridization oven	7601	GFL
Platform shaker	Polymax 1040	Heidolph
Incubator	BK-600	Heraeus Instruments
Stereo microscope	Stemi 2000-C	Zeiss
Stereo microscope	Stemi SV 11	Zeiss
Upright microscope	Axioplan 2	Zeiss
Slide camera system	MC80DX+Databack D4	Zeiss
Digital video camera	DEI-750	Optronics
Microinjector	Femtojet	Eppendorf

## 4.2 Methods

### 4.2.1 Genetic mapping

Unless otherwise noted, genetic mapping methods were performed as previously described (Birren, B. et al., 1999. *Genome Analysis: A Laboratory Manual*. Cold Spring Harbor Laboratory Press, Cold Spring Harbor, NY).

#### 4.2.1.1 Genomic DNA Preparation

Zebrafish embryos (5dpf) were pipetted into the wells of a 96-well plate. Each well thus contained 15  $\mu$ l of egg water plus one embryo. The plates were then frozen and stored or the DNA isolation was initiated immediately. The first step was the addition of 50  $\mu$ l lysis buffer (10 mM Tris pH 8.0, 50 mM KCl, 0.3% Tween-20) to each well. The plate was subsequently closed and boiled in a water bath for 10 min, followed by a 10 min cooling period on ice. Then 5  $\mu$ l of proteinase K (10 mg/ml stock) were added to each well. Alternatively the proteinase K stock solution was diluted 1:10 in lysis buffer, and 50  $\mu$ l of this solution were added to each well. The proteinase K digestion lasted overnight at 55°C. The next day the plate was boiled again in a waterbath for 10 min, followed by 10 min cooling on ice. The last step was the addition of 200  $\mu$ l 0.1x TE (pH 8.0) to each well, yielding DNA stock solution which was ready for genotyping by PCR (5  $\mu$ l stock DNA per PCR reaction).

#### 4.2.1.2 Total Genome Scan by genotyping with microsatellite markers

Approximately equal amounts of DNA from 10 mutant embryos (200  $\mu$ l DNA per embryo) as well as from 10 wild-type embryos (200  $\mu$ l DNA per embryo) were pooled. This resulted in one pool of mutant embryo DNA (2 ml) and one pool of wild-type embryo DNA (2 ml). 150  $\mu$ l of each DNA pool were aliquoted into each well of two rows of a 96-well plate (first row: mutant DNA, second row: wild-type DNA). Genotyping by PCR was performed with 144 primer pairs (microsatellite markers = SSLP markers) evenly spaced across all of the 25 zebrafish linkage groups and with the wild-type and mutant DNA pools. Each mutant pool, or bulk, contains individuals that are identical for the particular genomic region of the mutation site but arbitrary at

all unlinked regions. Thus, this method (bulked segregant analysis) takes advantage of the linkage of certain microsatellite markers to the mutated locus and of the arbitrary segregation of the unlinked microsatellite markers (Michelmore et al. 1991).

#### 4.2.1.3 PCR

Below is a typical PCR (Polymerase Chain Reaction) reaction mastermix setup with a total volume of 15  $\mu$ l.

**Table 6:** PCR reaction assembly.

<b>Component</b>	<b>Volume (1 reaction)</b>	<b>Volume (110 reactions)</b>
Distilled water	12.61 $\mu$ l	1387 $\mu$ l
10x Reaction buffer	2 $\mu$ l	220 $\mu$ l
Each dNTP (100 mM)	0.04 $\mu$ l	4.4 $\mu$ l
Forward primer (100 pmol/ $\mu$ l)	0.064 $\mu$ l	7 $\mu$ l
Reverse primer (100 pmol/ $\mu$ l)	0.064 $\mu$ l	7 $\mu$ l
Taq polymerase	0.1 $\mu$ l	11 $\mu$ l
<b>Total volume</b>	<b>15 <math>\mu</math>l</b>	<b>1650 <math>\mu</math>l</b>

15  $\mu$ l of the mastermix were added to 5  $\mu$ l of embryonic stock DNA. PCR was usually performed in 96-well format under the following conditions:

3'	96°C	initial denaturation
40 cycles of:	45'' 96°C	denaturation
	45'' 55°C	primer annealing
	45'' 72°C	elongation (1' per kb)
3'	72°C	final extension
$\infty$	4°C	storage temperature

#### 4.2.1.4 Agarose gel electrophoresis

Agarose gels of 0.7%-1% were used for large DNA fragments (e.g. plasmids) whereas the PCR and RT-PCR products (usually smaller than 1 kb) have been resolved in 2%-3% agarose gels. DNA was visualized by adding 5  $\mu$ l ethidium bromide (10  $\mu$ g/ $\mu$ l) to 100 ml of agarose gel solution. For PCR and RT-PCR products a 100 bp ladder (Invitrogen) was used as a size marker.

#### 4.2.1.5 Single-stranded conformation polymorphism (SSCP) analysis

SSCP analysis is the method of choice for the detection of DNA polymorphisms in high resolution gene mapping. MDE Gel Solution (BioWhittaker Molecular Applications) is a polyacrylamide-like matrix that has a high sensitivity to DNA conformational differences. The denatured single DNA strands are separated in this matrix on the basis of both size and conformation. With this technique the probability of detecting any sequence difference is approximately 80% ( $\pm 5\%$ ).

A standard sequencing gel setup was used to resolve PCR products. The glass plates were assembled and sealed using spacers of 0.4 mm thickness. 100 ml of 0.5x MDE Gel Solution were prepared as follows.

**Table 7:** Preparation of 0.5x MDE Gel Solution.

<b>Component</b>	<b>Volume</b>
MDE Gel Solution (2x)	25 ml
10x TBE Buffer	6 ml
Deionized water	fill to 100 ml
TEMED	40 $\mu$ l
10% APS	400 $\mu$ l
<b>Total volume</b>	<b>100 ml</b>

TEMED and APS were added just before the gel was poured. The gel solution was poured between the glass plates and a sharktooth comb was inserted in an inverted position. The gel was allowed to polymerize for at least 60 minutes. The comb was removed and the gel cassette was mounted onto the sequencing apparatus, where both anodal and cathodal chambers were filled with 0.6x TBE running buffer.

The PCR was performed with radioactively labeled  $^{32}\text{P}$ -dCTP\*. After thermal cycling, 1  $\mu$ l of the PCR reaction was added to 9  $\mu$ l of stop solution (95% formamide; 10 mM NaOH; 0.25% bromophenol blue and 0.25% xylene cyanol), heat denatured at 94°C for 3 minutes and subsequently placed in an ice water bath. The top of the gel was rinsed thoroughly with running buffer and the sharktooth comb was re-inserted such that the teeth were just touching the gel. 3  $\mu$ l of the sample were loaded and the gel was run for 14 hours at 8 watts.

The next day the gel was transferred onto Whatman chromatography paper 3 MM Chr (Whatman), covered with plastic wrap and exposed to X-Ray film X-OMAT DS (Kodak) for 16 hours at -80°C.

#### 4.2.1.6 Overgo Probing of High-Density BAC and PAC Filters

(developed by John D. McPherson; Washington University, St. Louis, Missouri)

##### Principle:

A unique repeat-free 40 bp region of DNA sequence is selected. From this sequence two 24mer oligonucleotides are designed in opposite orientations having a complementary 8 bp overlap in their respective 3' ends. After these two overlapping oligos (overgos) have annealed to each other the single-stranded overhangs (16 bases) are filled in with  $^{32}\text{P}$  labeled dATP and dCTP. Subsequently, filter hybridizations with either single labeled overgos or with pools of up to 40 labeled overgos are performed (Figure 4). This method allows for very specific low background library screens with a large number of probes.

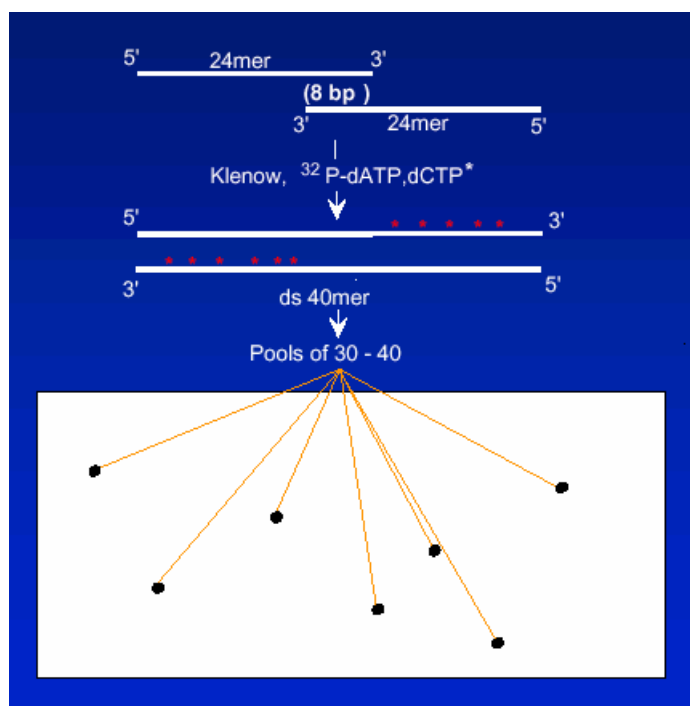


**Figure 4.** Design and labeling of overlapping oligonucleotides (overgos) for filter hybridizations. Two 24mer oligonucleotides are allowed to anneal to each other via their complementary 8 bp overlapping sequences in their respective 3' ends. The single-stranded overhangs (16 bases) are filled in with  $^{32}\text{P}$ -dATP\* and  $^{32}\text{P}$ -dCTP\*. Filter hybridizations can be performed with single overgos or with pools of up to 40 overgos.

Overgo labeling:

The stock solution (10 pmol/ $\mu$ l) of the mixed oligos was heated at 80°C for 5 min. Then the overgos were incubated at 37°C for 10 min and subsequently stored on ice. Below is the setup for the labeling reaction (total reaction volume: 10  $\mu$ l).

**Table 8:** Reaction assembly for the labeling of overlapping oligonucleotides.

<b>Component</b>	<b>Volume</b>
Annealed oligonucleotides (10 pmol/ $\mu$ l each)	1 $\mu$ l
BSA (2 mg/ml)	0.5 $\mu$ l
OLB (-A,-C,-N6) reaction buffer	2 $\mu$ l
<sup>32</sup> P-dATP*	0.5 $\mu$ l
<sup>32</sup> P-dCTP*	0.5 $\mu$ l
distilled water	4.5 $\mu$ l
Klenow fragment (2 U/ $\mu$ l)	1 $\mu$ l
<b>Total volume</b>	<b>10 <math>\mu</math>l</b>

The reaction was allowed to occur for 1 hour at room temperature. Unincorporated nucleotides were removed using Sephadex G50 columns.

Preparation of the modified oligo labeling buffer OLB (-A,-C,-N6): It does not contain dATP, dCTP nor random hexameric nucleotides, which are contained in a “normal” oligo labeling buffer in a random primer labeling reaction. The buffer was prepared from the solutions A, B and C in the following proportions: A:B:C = 1:2.5:1.5.

## Solution O:

- 1.25 M Tris-HCl, pH 8.0
- 125 mM MgCl<sub>2</sub>

## Solution A:

- 1 ml solution O
- 18  $\mu$ l  $\beta$ -mercaptoethanol
- 5  $\mu$ l 0.1 M dTTP
- 5  $\mu$ l 0.1 M dGTP

Solution B:

- 2 M HEPES-NaOH, pH 6.6

Solution C:

- 3 mM Tris-HCl, pH 7.4
- 0.2 mM EDTA

Hybridizations:

Hybridization solution:

- 1% BSA (Fraction V, Sigma)
- 1 mM EDTA
- 7% SDS
- 0.5 M sodium phosphate

50 ml of prewarmed (60°C) hybridization solution were added to each 30 cm x 4 cm hybridization bottle. The filters were prewet with warmed 2x SSC (60°C) and then each filter was rolled and inserted into a bottle. The bottles were rotated to allow the filters to unroll slowly and not to trap air bubbles. Filters were prehybridized for 4 hours in hybridization solution without overgos.

After prehybridization 10 ml of the hybridization solution was removed from each bottle and combined. The labeled overgos were denatured at 90°C for 10 minutes and then added to the removed hybridization solution. Following mixing by pipetting, 10 ml of this probe containing hybridization solution was added back to each bottle. The probes were allowed to hybridize to their targets at 60°C overnight in the hybridization oven.

Washing:

The hybridization solution was removed and the bottle filled to two-thirds of its volume with room temperature 4x SSC, 0.1% SDS. The bottle was returned to the oven and rotated for 30 min. The filters were then transferred to a larger tub on a rotary platform and washed as follows:

- 2L 1.5x SSC, 0.1% SDS at 58°C for 30 min
- 2L 0.75x SSC, 0.1% SDS at 58°C for 30 min

Autoradiography:

The filters were sealed in plastic bags and exposed to X-Ray film X-OMAT DS (Kodak) for 16 hours at -80°C.

## **4.2.2 Molecular biology and cloning**

Unless otherwise noted, molecular biology and cloning methods were performed as previously described (Sambrook, J. and Russell, D.W., 2001. *Molecular Cloning: A Laboratory Manual*. 3rd Edition, Cold Spring Harbor Laboratory Press, Cold Spring Harbor, NY).

### **4.2.2.1 RNA Isolation**

Total RNA was isolated using the commercially available phenol-based TRIZOL kit (Invitrogen). All centrifugation steps were carried out at 4°C. 50 zebrafish embryos (4-5 dpf) to 150 zebrafish embryos (0-3 hpf) were homogenized manually in 1 ml of TRIZOL solution using a 20-gauge needle and a syringe. Following a 5 min incubation at room temperature, 200 µl of chloroform per 1 ml TRIZOL were added. After vortexing for 15 seconds and incubating for 3 min at room temperature, the sample was centrifuged at 12000 rpm for 15 min. The aqueous upper phase was transferred to a new tube. Following the addition of 500 µl isopropanol per 1 ml TRIZOL, mixing and a 10 min incubation at room temperature a centrifugation step at 12000 rpm was carried out for 10 min to pellet the RNA. The pellet (precipitated RNA) was subsequently washed with 1 ml 70% ethanol per 1 ml of TRIZOL initially added. A centrifugation step at 7000 rpm for 5 min was followed by the removal of all ethanol and gentle air-drying of the RNA pellet. The RNA was subsequently dissolved in DEPC treated distilled water.



#### 4.2.2.2 RT-PCR

RT-PCR (reverse transcription and subsequent PCR) has been performed using the SuperScript One-Step RT-PCR kit (Invitrogen). Table 9 shows a typical RT-PCR reaction setup with a total volume of 50  $\mu$ l.

**Table 9:** RT-PCR reaction assembly.

Component	Volume
DEPC treated water	20 $\mu$ l
2x Reaction Mix	25 $\mu$ l
Template RNA	2 $\mu$ l
Forward primer (10 pmol/ $\mu$ l)	1 $\mu$ l
Reverse primer (10 pmol/ $\mu$ l)	1 $\mu$ l
RT/Taq polymerase mix	1 $\mu$ l
<b>Total volume</b>	<b>50 <math>\mu</math>l</b>

The RT-PCRs were performed in 8-well format under the following cycling conditions:

30'	50°C	cDNA synthesis
2'	94°C	initial denaturation
35 cycles of:	30'' 94°C	denaturation
	30'' 55°C	primer annealing
	45'' 72°C	elongation (1' per kb)
5'	72°C	final extension
$\infty$	4°C	storage temperature

#### 4.2.2.3 Restriction digest of DNA

Type II restriction endonucleases recognize and cut specific palindromic sequences in DNA. They are therefore used in the linearization of circular plasmids, in cloning of DNA fragments into vectors, in defining RFLPs between two DNA sequences, which in other respects are very similar etc. As a general guideline 1 unit of restriction enzyme should be used for each  $\mu$ g of DNA in a 1 hour digest. The choice of the buffer as well as the reaction temperature depend on the specific restriction endonuclease. The digest can be either purified for following experiments or directly analyzed by gel electrophoresis.

#### 4.2.2.4 Ligation

One type of ligation is between DNA fragments (e.g. vector and insert) that have been cut with the same restriction endonucleases. This reaction is catalyzed by T4 DNA ligase. Another class of vectors has single 3' deoxythymidine (T) overhangs which allow efficient cloning of PCR products which have complementary single 3' deoxyadenosine (A) overhangs. pGem-T Easy (Promega) is an example of such a vector which still requires T4 DNA ligase for the ligation to occur. The pCR2.1-TOPO vector (Invitrogen) on the other hand uses a T4 DNA ligase independent mechanism of ligation. Like the pGem-T Easy vector it has 3' T overhangs which complement the 3' A overhangs of the PCR product. Additionally topoisomerase I is coupled to the ends of the linearized vector. Topoisomerase I has ligation activity and thus enables the "activated" vector to integrate PCR products. A typical reaction assembly (total volume: 10  $\mu$ l) for the ligation of a PCR insert into the pGem-T Easy Vector is shown below.

**Table 10:** Ligation reaction assembly.

<b>Component</b>	<b>Volume</b>
PCR product (10 ng/ $\mu$ l)	3 $\mu$ l
2x T4 DNA ligase buffer	5 $\mu$ l
pGem-T Easy Vector (50 ng/ $\mu$ l)	1 $\mu$ l
T4 DNA ligase (3 Weiss units/ $\mu$ l)	1 $\mu$ l
<b>Total volume</b>	<b>10 <math>\mu</math>l</b>

Depending on the type of ligase and kit used the reactions were carried out for one hour at room temperature or overnight at 16°C.

#### 4.2.2.5 Transformation

Heat-shock transformation was used to deliver the ligation products into competent *E.coli* bacteria. *E.coli* DH5 $\alpha$  cells were treated with CaCl<sub>2</sub> and MgCl<sub>2</sub> and thus rendered competent to DNA uptake. Plasmid DNA was transformed into *E.coli* cells by incubation of the entire ligation reaction with 300  $\mu$ l of competent bacteria for 1 hour on ice, followed by a 45 seconds heat shock at 42°C (waterbath). Subsequently

the cells were cooled on ice. After the addition of 1 ml of prewarmed (37°C) LB medium (without antibiotic) they were allowed to recover and divide for 1 hour (37°C) in the shaker. 100-200 µl of the cell suspension was then plated on a selective plate and incubated overnight at 37°C.

#### 4.2.2.6 Synthesis of digoxigenin-labeled riboprobes for *in situ* hybridization

The plasmid template for the probe synthesis was linearized first. For this, 10 µg of plasmid DNA were cut with the appropriate restriction enzyme in 100 µl total volume for 3 hours. For DNA purification purposes, the digest was then subjected to chloroform extraction and ethanol precipitation. The linearized DNA pellet was dissolved in 20 µl DEPC-H<sub>2</sub>O.

The antisense RNA probe synthesis was done using the Dig RNA Labeling Kit (Roche). The reaction assembly (total volume: 20 µl) was as follows:

**Table 11:** Reaction assembly for the synthesis of digoxigenin-labeled riboprobes.

Component	Volume
DEPC-H <sub>2</sub> O	11 µl
10x transcription buffer	2 µl
10x NTP labeling mix containing Dig-UTP	2 µl
linearized plasmid	2 µl
RNase inhibitor	1 µl
RNA polymerase (T3, T7 or SP6)	2 µl
<b>Total volume</b>	<b>20 µl</b>

The reaction was incubated for 2 hours at 37°C. After the addition of 2 µl (40 units) of DNaseI the reaction was incubated for another 30 minutes at 37°C. Afterwards, the RNA was precipitated with 2.5 µl 4M LiCl and 75 µl ethanol. The pellet was spun down and redissolved initially in 100 µl DEPC-H<sub>2</sub>O. The quantity of the RNA probe was determined spectrophotometrically, and following this, the concentration has been adjusted to 100 ng/µl.

#### 4.2.2.7 Capped mRNA synthesis (in vitro transcription)

For rescue experiments it is crucial to inject capped mRNA in order to protect the injected RNA from being instantaneously degraded by endogenous RNases. Capped transcripts were produced with the mMESSAGE mMACHINE transcription kit from Ambion (Table 12).

**Table 12:** Reaction assembly for capped mRNA synthesis.

<b>Component</b>	<b>Volume</b>
Nuclease-free water	5 $\mu$ l
2x NTP/cap analog	10 $\mu$ l
10x Reaction Buffer	2 $\mu$ l
Linearized plasmid DNA (1 $\mu$ g/ $\mu$ l)	1 $\mu$ l
Enzyme mix (containing SP6, T3 or T7 RNA polymerase)	2 $\mu$ l
<b>Total volume</b>	<b>20 <math>\mu</math>l</b>

After mixing of all the components the reaction was allowed to proceed for 2 hours at 37°C. The RNA was purified by phenol:chloroform extraction and subsequent isopropanol precipitation. The yield of the transcription reaction and the integrity of the mRNA were tested by spectrophotometry and gel electrophoresis, respectively.

## 4.2.3 Morphology and histology

### 4.2.3.1 Alcian Blue staining

Alcian Blue staining has been used to visualize the cartilaginous skeleton of zebrafish embryos. The Alcian Blue dye binds to sugar moieties of proteoglycans in the cartilage extracellular matrix. The fish were fixed in 4% PFA overnight at 4°C and then washed twice for 10 min in PBS. Subsequently they were bleach treated as follows: 1.5 ml of 10% H<sub>2</sub>O<sub>2</sub> and two drops of 2 M KOH were added to the tube, the tube was closed and the solutions were mixed. Afterwards the tube was opened and the embryos were bleached for 1 hour. Following two short washes with PBS, the bleached embryos were incubated in the Alcian Blue staining solution overnight.

Alcian Blue staining solution:     0.1% Alcian Blue  
  70% ethanol  
  1% HCl

The next day the embryos were washed once in acidic ethanol (70% ethanol, 5% HCl), followed by an overnight destaining step in fresh acidic ethanol. The following day the embryos were dehydrated in 85% and 100% ethanol for 15 min each and subsequently transferred to 80% glycerol in which they are stored at 4°C.

### 4.2.3.2 Ultramicrotomy and histological staining

All histological sections of 5 dpf zebrafish embryos were prepared in plastic resin medium. The embedding was performed using the JB-4 embedding kit from Polysciences. The JB-4 infiltration solution was prepared by dissolving 0.45 g of the catalyst in 50 ml JB-4 solution A overnight. The embryos were fixed in 4% PFA, rinsed in PBS and subsequently dehydrated (each step for 30 min): 25% EtOH - 50% EtOH - 70% EtOH - 85% EtOH - 95% EtOH - 95% EtOH. Then the embryos were incubated in the infiltration solution, the solution was changed two more times and the embryos were infiltrated overnight at 4°C. The embryos were placed in plastic molds (Polysciences) with very little liquid. The embedding solution was prepared by mixing 1 ml of infiltration solution with 40 µl of solution B. The molds were filled to the

top with the embedding solution and subsequently covered with parafilm. This is because anaerobic conditions are needed for JB-4 polymerization. Polymerization is complete after one hour but usually the parafilm was not removed until the next day. The JB-4 plastic resin blocks were removed from the molds and trimmed for ultramicrotomy.

Sections were made using a Reichert OmU3 microtome. 5  $\mu\text{m}$  sections were cut with self-manufactured dry glass knives, collected with fine forceps and transferred to a drop of water on a heated adhesive-coated slide (Superfrost Plus, Fisher). The sections were air-dried, stained with the metachromatic dye Toluidine Blue and mounted using Eukitt as a mounting medium. Certain basic dyes, such as Toluidine Blue and Methylene Blue, stain nucleic acids blue (the orthochromatic color), but sulfated polysaccharides purple (the metachromatic color). When dye molecules bound to sulfate groups are stacked closely together, the dye experiences a color shift from blue to purple. Thus, a metachromatic reaction often indicates the presence of numerous closely packed sulfate groups.

## 4.2.4 Molecular analysis of gene expression

### 4.2.4.1 Whole-mount *in situ* hybridization

This method was used to detect the spatio-temporal expression patterns of genes involved in neural crest specification and differentiation. Zebrafish embryos are transparent until the melanophores start to produce melanin around 26 hpf. We incubated developing embryos in 0.2 mM PTU (1-Phenyl-2-thio-urea) starting at 8-10 hpf in order to prevent melanin synthesis and thus maintain optical clarity of the embryos.

Staged embryos were fixed in 4% PFA (paraformaldehyde) overnight at 4°C. They were dechorionated and rinsed in PBT (PBS with 0.1% Tween-20) several times. The duration of the following permeabilization step with proteinase K varied depending on the age of the embryos:

<tail bud	no digestion
0-2 somites	10 µg/ml prot. K, 2 min.
4-10 somites	10 µg/ml prot. K, 3.5 min.
10-20 somites	10 µg/ml prot. K, 5 min.
24 hpf	10 µg/ml prot. K, 10 min.
48 hpf	10 µg/ml prot. K., 30 min.
> 48 hpf	50 µg/ml prot. K, 1 hour

Following 2 quick washes with PBT, the embryos were refixed with 4% PFA for at least 20 minutes. After rinsing 5 times in PBT, the embryos were prehybridized for at least one hour in hybridization mix at 70°C in a waterbath.

Hybridization mix: (hybe mix)	65% formamide	32.5 ml 100% stock
	5x SSC	12.5 ml 20x SSC stock
	50 µg/ml heparin	86 µl of 29 mg/ml
	0.5 mg/ml yeast tRNA	25 mg powder
	0.1% Tween-20	250 µl 20% stock
	9.2 mM citric acid, pH 6.0	920 µl 0.5 M stock
		<u>3.8 ml H<sub>2</sub>O</u>
		50 ml total

For hybridization, the embryos were incubated in 250 µl of new hybridization mix containing 500 ng of digoxigenin-labeled riboprobe. The hybridization step was

performed overnight at 70°C in a waterbath. The following day the embryos were rinsed as follows:

10 min. 70°C in 75% hybe mix + 25% 2x SSC  
 10 min. 70°C in 50% hybe mix + 50% 2x SSC  
 10 min. 70°C in 25% hybe mix + 75% 2x SSC  
 10 min. 70°C in 100% 2x SSC  
 30 min. 70°C in 0.05x SSC  
 30 min. 70°C in 0.05x SSC

5 min. room temperature in 75% 0.05x SSC + 25% PBT  
 5 min. room temperature in 50% 0.05x SSC + 50% PBT  
 5 min. room temperature in 25% 0.05x SSC + 75% PBT  
 5 min. room temperature in 100% PBT

Afterwards the embryos were incubated in the blocking solution PBT/NGS/BSA for at least one hour at room temperature. PBT/NGS/BSA is PBT containing 2% NGS (normal goat serum) and 2 mg/ml BSA (bovine serum albumin).

The anti dig-AP (alkaline phosphatase) antibody (Boehringer Mannheim) was pre-adsorbed before usage. For this purpose it was diluted 1/100 in PBT/NGS/BSA and incubated overnight at 4°C in a tube containing zebrafish embryos. The antibody binding step with the pre-adsorbed anti dig-AP antibody (diluted 1:50 in PBT/NGS/BSA) was performed overnight at 4°C.

Embryos were rinsed at room temperature 5 times in PBT for 5 min each and 3 times in NTMT for 15 min each.

NTMT:	100 mM Tris-HCl pH 9.5	5 ml 1M stock
	50 mM MgCl <sub>2</sub>	2.5 ml 1M stock
	100 mM NaCl	1 ml 5M stock
	0.1% Tween-20	<u>250 µl 20% stock</u>
		+ dH <sub>2</sub> O to 50 ml total volume

The alkaline phosphatase staining was developed at room temperature in freshly prepared NTMT/NBT/BCIP solution in the dark.

NTMT/NBT/BCIP:	10 ml NTMT	
	225 µg/ml NBT	22.5 µl (100 mg/ml in 70% DMF)
	175 µg/ml BCIP	35 µl (50 mg/ml in 100% DMF)



The reaction was monitored under the stereo microscope until adequate staining was visible (routinely 30 min to 2 hours, depending on individual probes and the stage of the embryos). The embryos were rinsed four times in PBT, fixed in 4% PFA, rinsed again 2 times in PBT and then rinsed in PBT + 5 mM EDTA for 20 min. After the washes, the embryos were transferred to 80% glycerol/20% PBT to clear and they were stored at 4°C.

#### **4.2.4.2 Whole-mount immunohistochemistry**

To monitor protein expression in whole mount embryos, I performed immunohistochemistry using the mouse monoclonal antibody anti-Hu 16A11 (anti-human neuronal protein HuC/HuD) from Molecular Probes.

##### Solutions:

###### PTD:

- PBS
- 0.3% Triton X-100
- 1% DMSO

###### PTDBN:

- PTD
- 2 mg/ml BSA (bovine serum albumin)
- 2% NGS (normal goat serum)

The zebrafish embryos were fixed overnight in 4% PFA, rinsed in PBT and then dehydrated in a methanol/PBTseries:

15 min 25% MeOH / 75% PBT

15 min 50% MeOH / 50% PBT

15 min 75% MeOH / 25% PBT

15 min 100% MeOH

The embryos were stored overnight at -20°C in 100% methanol. This step contributes to the permeabilization of the embryos.

The rehydration series has been done in reverse order to the above dehydration series:

15 min 75% MeOH / 25% PBT

15 min 50% MeOH / 50% PBT

15 min 25% MeOH / 75% PBT

15 min 100% PBT

Subsequently, the embryos were bleached with 1 ml 10% H<sub>2</sub>O<sub>2</sub> + 1 drop of 2 M KOH in an open tube for 40 min. Following three 5 min washes with PBT, the embryos were permeabilized by incubation in 0.1 mg/ml proteinase K solution for 10 min at room temperature. After two washes with PBT for 1 min each, the embryos were refixed with 4% PFA for 20 min. Following five 5 min washes in PBT, 2 quick washes in distilled water and 2 rinsing steps in acetone, the embryos were frozen in acetone at -20°C for 1 hour. This step enhances the permeabilization effects achieved by the methanol and proteinase K treatments. Then two quick washing steps with distilled water and five washing steps with PTD for 5 min each were performed. After this the embryos were transferred to 24 well plates and incubated in the blocking solution PTDBN (freshly prepared) for at least 1 hour. The primary antibody, mouse anti-Hu, was diluted (1:20) in PTDBN. The embryos were incubated in this solution overnight at 4°C.

The following day, after five washes with PTD for 10 min each, the secondary antibody (anti-mouse IgG diluted 1:200 in PTDBN) was applied to the embryos. Following a 1 hour incubation at room temperature, five washes in PTD for 10 min each had to be performed. In the meantime the ABC complex (Vectastain kit) was prepared: This was done by mixing 20 µl solution A (avidin) with 1 ml PTDBN, then adding 20 µl solution B (biotinylated-HRP) and mixing again. The ABC complex was prepared at least 30 min before usage. The incubation in the ABC complex was for 1 hour at room temperature. Five 10 min washes in PTD preceded the staining procedure, which was performed as follows using the Vectastain kit:

Two drops (100 µl) of buffer stock solution were mixed with 5 ml distilled water. Four drops (200 µl) of DAB (diaminobenzidine) stock solution were added, followed by mixing. The embryos were preincubated in one half of the above solution for 10 min in the dark. One drop (50 µl) of H<sub>2</sub>O<sub>2</sub> solution was mixed with the remaining solution. The DAB preincubation solution was removed and replaced with the H<sub>2</sub>O<sub>2</sub> containing

staining solution. The developing reaction was allowed to occur in the dark till adequate staining was achieved (routinely 1 - 40 min). Subsequently the staining reaction was stopped by rinsing the embryos in distilled water for at least 20 min. The embryos were transferred to PBT and finally to the mounting medium 80% glycerol/20% PBT. The embryos were stored in this medium at 4°C.

## 4.2.5 Functional assays

### 4.2.5.1 Microinjection of morpholino antisense oligonucleotides

Morpholinos are modified antisense oligonucleotides that are designed to block translation by pairing with the translation start site in the 5' untranslated region (Nasevicius and Ekker 2000). Alternatively they can be designed to block RNA splicing. Microinjection was used to deliver 1 nanoliter of morpholino antisense oligonucleotide solution into the cytoplasm of 1-4 cell stage zebrafish embryos. The embryos were placed into the wells of prepared agarose (1%) dishes and oriented in order to facilitate microinjection. Microinjection was performed using a Femtojet microinjector from Eppendorf and a stereo microscope Stemi SV 11 from Zeiss. Morpholinos were purchased from GeneTools (Philomath, USA). Two anti-*foxD3* morpholinos have been used: MO-1 is targeted against the first 25 coding bases (starting with the [ATG](#)) and MO-2 is targeted against the 25 bases immediately upstream of the ATG (last 25 bases of the 5'UTR).

Sequence MO-1: 5'-CACTGGTGCCTCCAGACAGGGT[CAT](#)-3'

Sequence MO-2: 5'-CACCGCGCACTTTGCTGCTGGAGCA-3'

The effective doses were determined to be 2 to 6 nanograms in single morpholino injections and 4 nanograms of each morpholino in co-injection experiments. For control injections, a morpholino which is derived from the sequence of MO-1 but incorporates four mismatch bases (4bp mismatch morpholino) was used.

### 4.2.5.2 Microinjection of capped mRNA

Rescue experiments aimed at the restoration of the wild-type phenotype in homozygous *mos*<sup>m188</sup> mutant embryos by providing the embryos with wild-type *foxD3* transcripts. Heterozygous *mos*<sup>m188</sup> fish were crossed and 50 picograms of capped full-length *foxD3* mRNA were injected into the cytoplasm of 1-4 cell stage zebrafish embryos from these matings. The number of injected fish was larger than in the morpholino injection experiments because only 25% of the injected embryos were homozygous *mos*<sup>m188</sup> mutants. Hence, a partial or complete rescue of the mutant phenotype resulting from the injection of *foxD3* capped mRNA can only be assessed based on the phenotype of this quarter of homozygous *mos*<sup>m188</sup> embryos.

## 4.2.6 World Wide Web infrastructure

I used the following websites and webtools to aid genetic mapping and gene identification experiments.

The Zebrafish Information Network (ZFIN) Homepage

<http://zfish.uoregon.edu/>

MGH / CVRC Zebrafish Server (Searchable Zebrafish Microsatellite Map)

<http://zebrafish.mgh.harvard.edu/>

Washington University - Zebrafish Genome Resources EST Project Homepage

[http://www.genetics.wustl.edu/fish\\_lab/frank/cgi-bin/fish/](http://www.genetics.wustl.edu/fish_lab/frank/cgi-bin/fish/)

The Sanger Institute: Danio Rerio Sequencing Project

[http://www.sanger.ac.uk/Projects/D\\_rerio/](http://www.sanger.ac.uk/Projects/D_rerio/)

Entrez Nucleotide: Database of nucleotide sequences

<http://www.ncbi.nlm.nih.gov:80/entrez/query.fcgi?db=Nucleotide>

NCBI BLAST Home Page: Sequence similarity search programs

<http://www.ncbi.nlm.nih.gov/blast/>

Maps of Human-Mouse Homology (Human-Mouse conserved synteny maps)

<http://www.ncbi.nlm.nih.gov/Homology/>

Entrez Genome view (Searchable maps of the human genome)

[http://www.ncbi.nlm.nih.gov/mapview/map\\_search.cgi](http://www.ncbi.nlm.nih.gov/mapview/map_search.cgi)

RZPD Resource Center: Service Center and Repository for Genomics + Proteomics

<http://www.rzpd.de/>

Simple radiation hybrid mapping in zebrafish using the LN54 panel

<http://mgchd1.nichd.nih.gov:8000/zfrh/beta.cgi>

Primer3 Input primer design program

[http://www-genome.wi.mit.edu/cgi-bin/primer/primer3\\_www.cgi](http://www-genome.wi.mit.edu/cgi-bin/primer/primer3_www.cgi)

## 5 Results

### 5.1 Analysis of the *brak* (*brk*<sup>m452</sup>) mutation

#### 5.1.1 The *brak*<sup>m452</sup> mutation causes craniofacial defects and diminished melanophore pigmentation

The *brak*<sup>m452</sup> mutation was isolated during the ENU mutagenesis screen based on its phenotype including both craniofacial and pigmentation defects. Homozygous *brak*<sup>m452</sup> embryos display a strong reduction of melanophore pigmentation in the whole body at 3 dpf (Figure 5). The embryonic zebrafish pigment pattern encompasses four melanophores stripes, the dorsal, the lateral, the ventral and the yolk sac stripe (Figure 5). The dorsal, the ventral and the yolk sac stripe also contain iridophores which are intermingled with the melanophores, while xanthophores are located along the entire dorsal surface of the embryo. The melanophore deficit in *brak*<sup>m452</sup> mutant embryos affects both neural crest-derived melanophores and neuroectoderm-derived melanophores in the retinal pigmented epithelium of the eye. In *brak*<sup>m452</sup> mutant embryos the lateral melanophore stripe is completely absent whereas the other melanophore stripes are present but contain reduced numbers of melanophores (Figure 5). Iridophore and xanthophore pigmentation seem to be normal in *brak*<sup>m452</sup> mutant embryos.

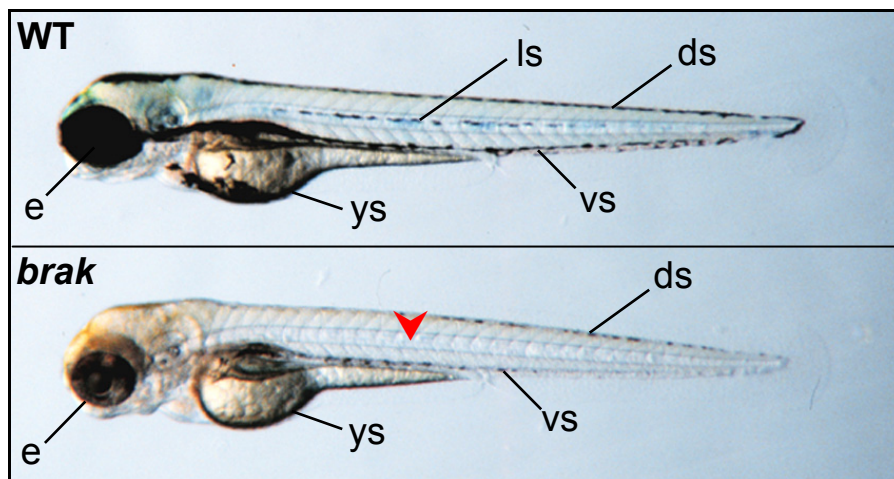


**Figure 5.** Lateral views of 3 dpf wild-type (WT) and homozygous *brak*<sup>m452</sup> mutant embryos. Both body and eye (e) melanophore pigmentation are reduced in *brak*<sup>m452</sup> mutant embryos. Homozygous *brak*<sup>m452</sup> mutants lack the lateral melanophore stripe (ls; arrowhead), whereas the dorsal stripe (ds), the ventral stripe (vs) and the yolk sac stripe (ys) are present but greatly reduced.

The *brak*<sup>m452</sup> mutation causes a bending of individual cartilage elements of the head skeleton. I have performed Alcian Blue analyses on 5 dpf *brak*<sup>m452</sup> mutants, revealing that the deformation of the cartilages is seen most frequently in the neurocranial ethmoid plate and in the ventral elements of the first arch (Meckel's cartilage) and the second arch (ceratohyal). The cartilage elements of the branchial arches are not affected (Figure 6C,D).

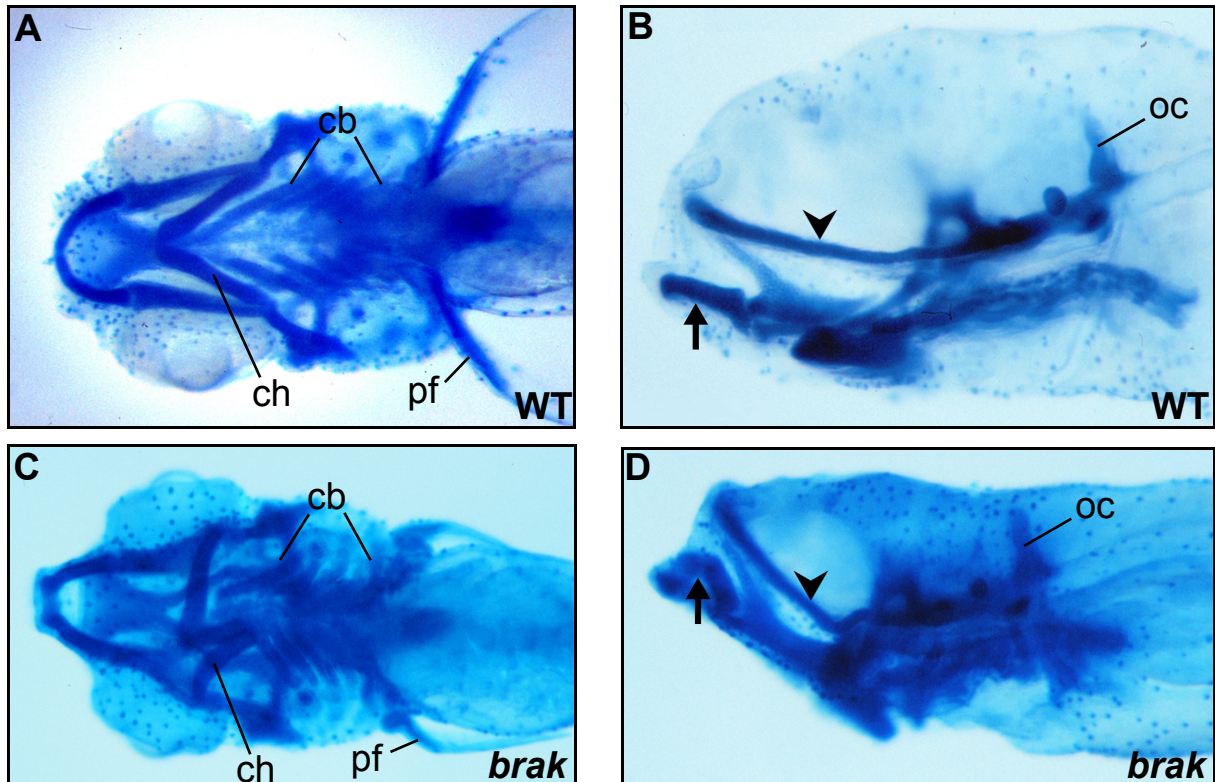


**Figure 6.** Craniofacial skeleton of 5 dpf wild-type (A,B) and homozygous *brak*<sup>m452</sup> embryos (C,D) stained with Alcian Blue. (A,C) Ventral views. (B,D) Lateral views. The ceratohyal (ch) is severely malformed in homozygous *brak*<sup>m452</sup> embryos (C) when compared to wild-type embryos (A). Both Meckel's cartilage (arrow) and the ethmoid plate (arrowhead) are bent in a way characteristic for the *brak*<sup>m452</sup> mutation (D). cb, ceratobranchials; oc, otic capsule; pf, pectoral fin.

### 5.1.2 The *brk*<sup>m452</sup> mutation maps to linkage group 14

The total genome scan for the *brk*<sup>m452</sup> mutation indicated possible linkage to the marker Z21080 on LG 14. This result was confirmed by genotyping single embryos and showed that the marker Z21080 is located 9.4cM from the *brk*<sup>m452</sup> locus. A substantial amount of the genetic mapping work was performed by undergraduate students under my supervision. Following detailed mapping with all available SSLP markers we have established that the *brk*<sup>m452</sup> mutation maps in close proximity to the centromere. The critical interval is flanked by the centromeric marker Z6874 and the marker Z9017 (Figure 7). The *brk*<sup>m452</sup> mutation is closely linked to the marker Z9017; the distance is 0.14cM (or one recombination event in 704 meioses).

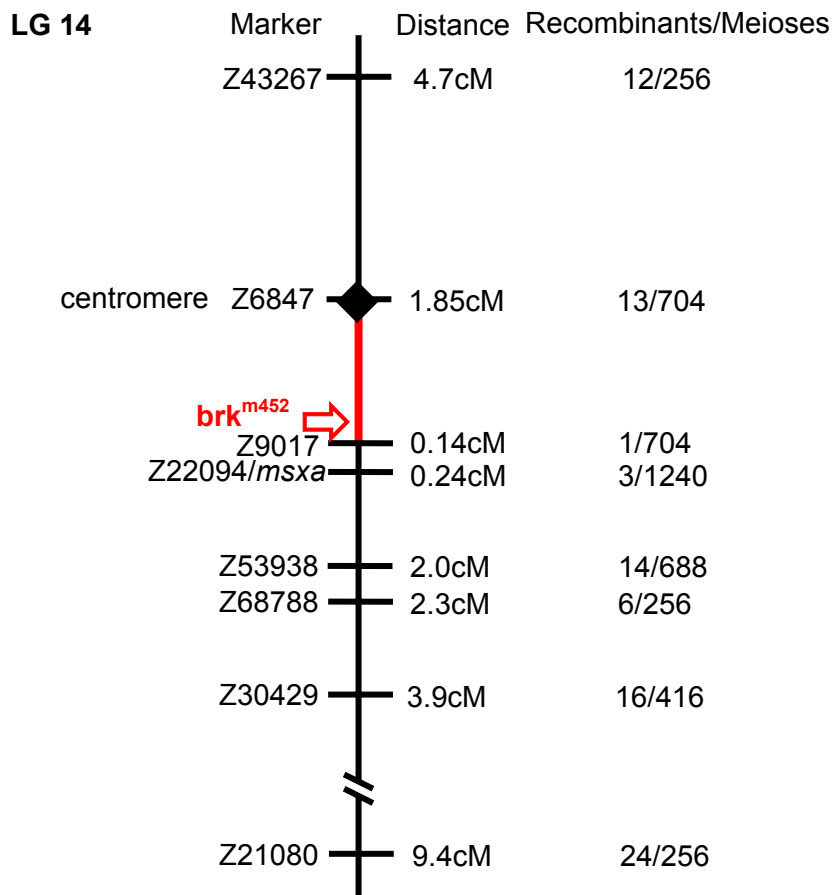


**Figure 7.** Genetic map of the *brk*<sup>m452</sup> mutation on LG 14. The arrow indicates the map position of the *brk*<sup>m452</sup> locus. The number of recombinants, the number of meioses tested and the resulting genetic distance from the mutated locus are indicated for each genetic marker.



There is considerable synteny between the zebrafish genomic region on LG 14 where the *brak*<sup>m452</sup> mutation was mapped and the human genomic region 5q31–q35 (Liu, T. X. et al. 2002). We analysed all the zebrafish ESTs in the critical interval and we determined that they all have orthologues on human chromosome 5q31–q35. On the contrary, there is no single syntenic region in the mouse genome. Mouse chromosomes 11, 13 and 18 all contain regions that correspond to the zebrafish *brak*<sup>m452</sup> genetic interval. The zebrafish *msxa* gene, which had been mapped to LG 14, appeared to be a good candidate gene for the *brak*<sup>m452</sup> mutation. The human orthologue MSX2 resides at 5q34-q35 and it has been shown to be involved in the etiology of Boston-type craniosynostosis (Ma et al. 1996). This prompted me to determine the precise position of *msxa* on LG 14. By genetic mapping I placed the *msxa* gene close to the marker Z22094 with three recombinations separating the gene and the *brak*<sup>m452</sup> locus (Figure 7). Therefore, I could exclude it as a candidate gene for the *brak*<sup>m452</sup> mutation. The current size of the *brak*<sup>m452</sup> genetic interval remains at 1.99cM and further mapping will be needed to narrow the critical interval and to test additional candidate genes suggested by the human syntenic region.

## 5.2 Analysis of the *mother superior* ( $mos^{m188}$ ) mutation

### 5.2.1 Craniofacial cartilage elements are lost in $mos^{m188}$ mutant embryos

The *mother superior* ( $mos^{m188}$ ) mutation was isolated during the ENU mutagenesis screen based on its very characteristic phenotype of a smaller head and a gaping jaw accompanied by a loss of jaw elements posterior to the Meckel's cartilage. This results in a large chasm between Meckel's cartilage and the heart that displays mild pericardial edema (Figure 8A,B). Additionally, the  $mos^{m188}$  mutant embryos are slightly shorter and the eyes are smaller. The melanophore pigmentation is present in  $mos^{m188}$  mutants but it appears to be somewhat reduced. The mutation is embryonic lethal and  $mos^{m188}$  mutant embryos die between 5 and 7 dpf because of a failure to inflate the swim bladder.

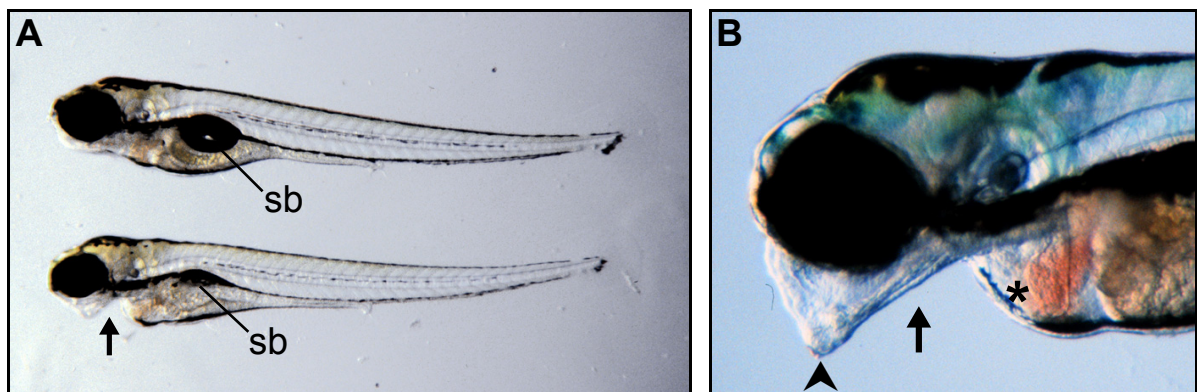


**Figure 8.** Phenotype of  $mos^{m188}$  mutant embryos at 5 dpf. (A) Lateral view of live wild-type (WT, above) and  $mos^{m188}$  mutant embryos (below). (B) Higher magnification of the head of a live  $mos^{m188}$  mutant embryo. The Meckel's cartilage is pointing ventrally (arrowhead, B) and the posterior branchial arches are absent (arrow in A,B). The heart exhibits mild pericardial edema (asterisk, B) and the swim bladder (sb) does not inflate in the  $mos^{m188}$  mutant embryos (A).

Previously published Alcian Blue analysis of cartilage elements revealed that the  $mos^{m188}$  mutant embryos form a normal neurocranium including the ethmoid plate (Neuhauss et al. 1996). On the contrary, the neural crest derived craniofacial skeleton is greatly reduced and only the first pharyngeal arch derived cartilages were observed. I have performed extensive analysis of Alcian blue stained head skeletons and found that the first arch cartilage elements (Meckel's cartilage and palatoquadrate) are always present in  $mos^{m188}$  mutant embryos (Figure 9). The Meckel's cartilage appears to be a little shorter and ventrally displaced contributing to

a gaping jaw appearance. The lack of the branchial arches 1-4 (or pharyngeal arches 3-6) might be causing the displacement of the Meckel's cartilage. The palatoquadrate is often fused to the ventral part of the hyosymplectic (Figure 9B), whereas the dorsal part of the hyosymplectic is missing in most mutant embryos. Also the other second arch derived cartilages, ceratohyal and interhyal, are absent in most cases (Figure 9B,C). Interestingly, I have found that although the majority of the branchial arch cartilages (ceratobranchials, basibranchials and hypobranchials) are missing, some small cartilage condensations can be seen at the location of the ceratobranchials (Figure 9D). Also, the 7th pharyngeal arch (5th branchial arch) cartilages are present in many *mos*<sup>m188</sup> mutant embryos. They are shorter, thinner and abnormally bent but they are built by normally stacked chondrocytes (Figure 9D).

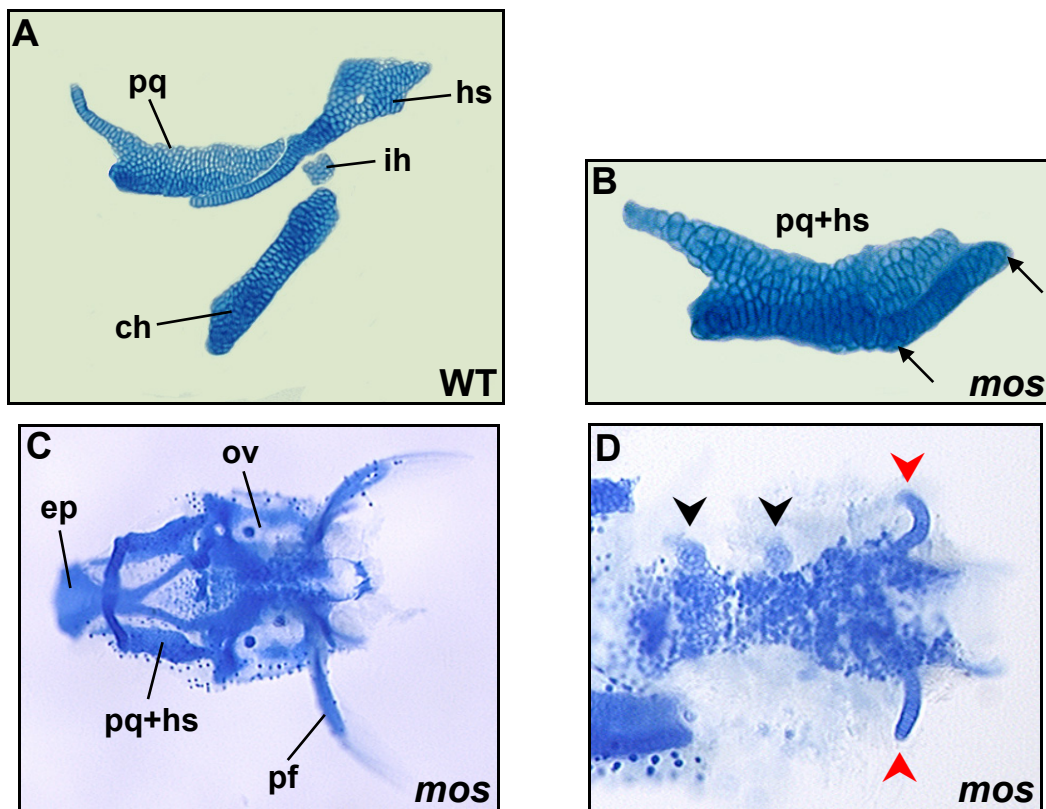


**Figure 9.** Cartilage preparation of the Alcian Blue stained craniofacial skeleton of 5 dpf wild-type (A) and homozygous *mos*<sup>m188</sup> embryos (B-D). (A) Flat mount dissected cartilages of the first and the second pharyngeal arches in wild-type (WT) embryos. The Meckel's cartilage is perpendicular to the plane of the picture and is not included in A and B. (B) The *mos*<sup>m188</sup> mutant embryo lacks the ceratohyal and interhyal cartilage elements. The palatoquadrate is slightly shortened and fused to the ventral portion of the hyosymplectic (arrows). (C) Whole mount preparation of the *mos*<sup>m188</sup> mutant head skeleton shows complete neurocranium and ventrally positioned visceral skeleton. The eyes have been removed. (D) Higher magnification of dissected branchial arches in the *mos*<sup>m188</sup> mutant embryo from (C). Unilateral anterior branchial arch cartilage condensations (black arrowheads) and symmetrical ceratobranchial elements of the last branchial arch (red arrowheads) are present. Abbreviations: ch, ceratohyal; ep, ethmoid plate; ih, interhyal; hs, hyosymplectic; ov, otic vesicle; pf, pectoral fin; pq, palatoquadrate.

### 5.2.2 Iridophores but not melanophores are greatly reduced in *mos*<sup>m188</sup> mutant embryos

An additional phenotype observed in *mos*<sup>m188</sup> mutant embryos is a delay of melanophore pigmentation and a substantial reduction in autofluorescent iridophores. The melanophores of the dorsal stripe situated most posteriorly in the trunk normally migrate caudally, around the tip of the tail and then a small distance rostrally, now being at the same dorsoventral level as the melanophores of the ventral stripe but never reaching this far anteriorly. At 48 hpf the melanophores of the dorsal stripe normally have completed their migration around the tip of tail. In *mos*<sup>m188</sup> mutants, however, the migration of these melanophores lags behind, and by 48 hpf the cells have not reached and surrounded the tip of the tail. Also, at this early stage, a significant reduction in the number of iridophore cells in the *mos*<sup>m188</sup> mutants as compared to the wild-type embryos is apparent. The *mos*<sup>m188</sup> melanophore phenotype seems to represent in part a delay or slowdown of cell migration because at 4 dpf the *mos*<sup>m188</sup> melanophore pigmentation is only slightly reduced when compared to the wild-type pattern (Figure 8A). In contrast, the significant reduction in the number of iridophores in *mos*<sup>m188</sup> versus wild-type embryos persists till later stages (5 dpf) and this reduction affects iridophores at all anteroposterior and dorsoventral levels (Figure 10).

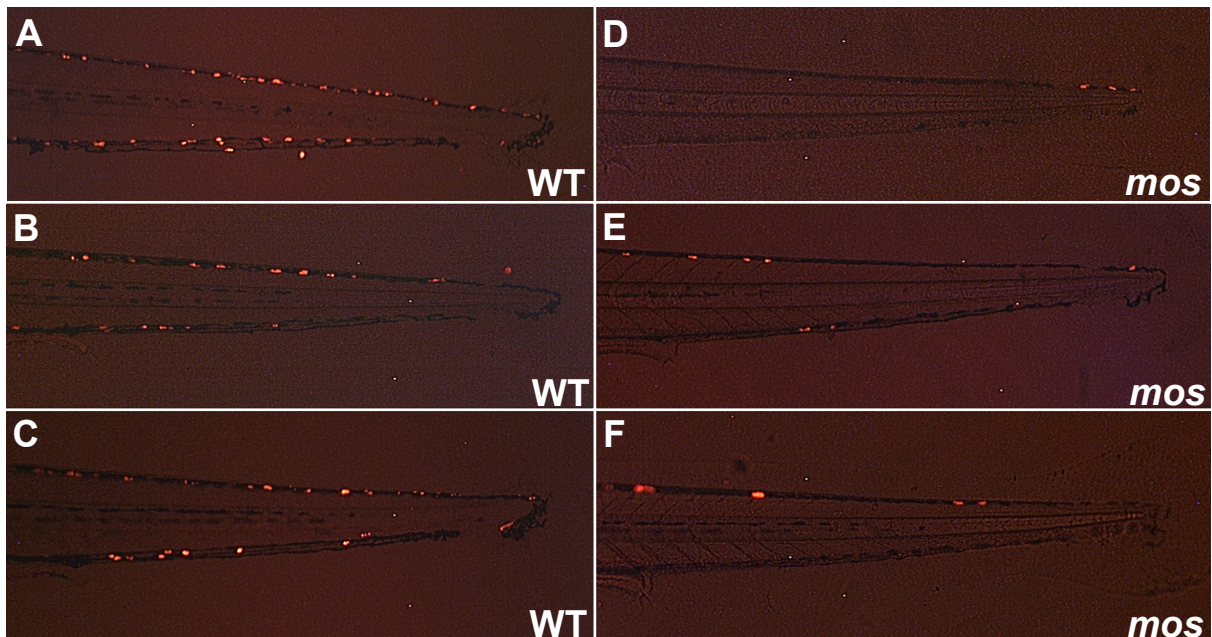


**Figure 10.** Iridophore patterns in 5 dpf wild-type (A-C) and homozygous *mos*<sup>m188</sup> (D-F) embryos. The number of iridophores in *mos*<sup>m188</sup> mutant embryos is greatly reduced when compared to wild-type embryos. Lateral views of representative embryos in the tail regions. Anterior is to the left.

### 5.2.3 The *mos*<sup>m188</sup> mutation leads to the development of supernumerary neuromast organs

Dorsolateral cranial ectodermal placodes give rise to a set of mechanosensory organs that allow fish to sense water movements and are critical for schooling behavior. One of the dorsolateral cranial ectodermal placodes, the posterior lateral line placode, differentiates into a posterior lateral line ganglion and a caudally migrating lateral line primordium, initially located posterior to the otic vesicle. This primordium begins to migrate along the horizontal myoseptum (the horizontal myoseptum divides the myotomes of the somites into dorsal and ventral halves) at about 20 hpf and deposits seven to eight patches of proneuromasts. Each proneuromast contains on average 24 cells and will differentiate within six hours of being deposited into functional mechanosensory sense organs termed neuromasts consisting of sensory hair cells and a ring of epithelial supporting cells (Gompel et al. 2001). The migration and differentiation of the embryonic neuromasts are completed at about 48 hpf. The neuromasts of the trunk and tail are innervated by sensory neurons of the posterior lateral line ganglion that is located at the posterior edge of the ear capsule. The posterior lateral line axons projecting from these sensory neurons are comigrating with the posterior lateral line primordium. The glial cells insulating this lateral line nerve have been shown to be of neural crest origin (Gilmour et al. 2002).

I analyzed the pattern of neuromasts in 4 dpf zebrafish embryos using DASPEI, a vital dye that is specifically up-taken by sensory hair cells. I observed that the number of neuromasts in the posterior lateral line is significantly increased in *mos*<sup>m188</sup> mutant embryos compared to wild-type embryos (Figure 11). In wild-type embryos the average number of neuromasts is 7.3 (n=10) while in the *mos*<sup>m188</sup> mutant embryos the average number of neuromasts is 13.9 (n=10). A t-test yielded an absolute t-value of 7.889 compared to a critical t-value of 2.878 (alpha level of significance  $\alpha = 0.01$ ; degrees of freedom: 18). Thus the observed differences in neuromast numbers are statistically significant. The variability within the *mos*<sup>m188</sup> group was very wide with neuromast numbers ranging between 10 and 18 (Figure 11B shows an example with 18 neuromast organs). It has to be noted that the number of sensory hair cells per neuromast was lower in many of the *mos*<sup>m188</sup> mutant embryos when compared to the wild-type ones.

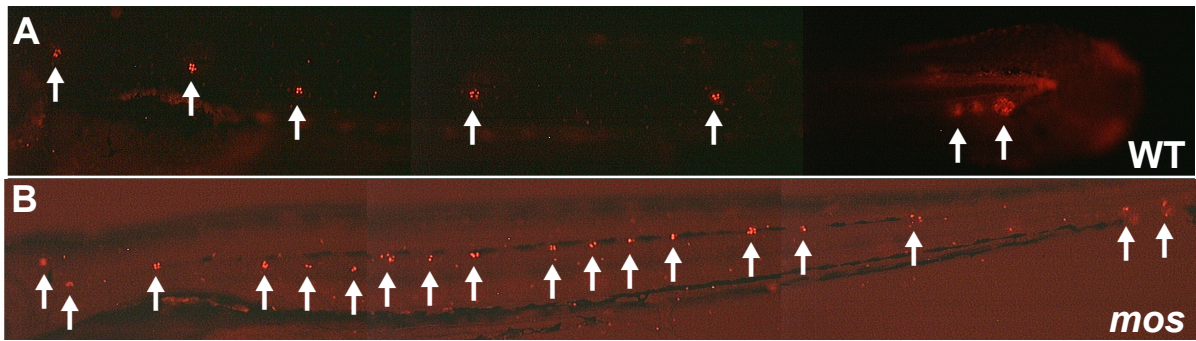


**Figure 11.** Neuromasts of the posterior lateral line system in 4 dpf zebrafish embryos visualized by using the vital dye DASPEI. (A) Wild-type embryo with seven neuromasts (arrows). (B) Homozygous *mos*<sup>m188</sup> embryo with 18 neuromasts (arrows). The dramatic increase in neuromast number coincides with a decrease in the number of sensory hair cells per individual neuromast. Lateral views. Anterior to the left.

#### 5.2.4 Dorsal root ganglia and the enteric nervous system are greatly reduced in the absence of *mos*<sup>m188</sup> gene function

Three major neural crest derivatives of the peripheral nervous system are dorsal root ganglia (DRGs), enteric neurons and cranial ganglia. Following neural crest migration and differentiation, the sensory neurons of the dorsal root ganglia are located bilaterally in every somite segment. The DRGs reside in positions adjacent and ventrolateral to the neural tube (Figure 12A). Each DRG initially consists of one to three neurons (48 hpf). These neurons continue to proliferate, resulting in three to five neurons per DRG at 4 dpf and 10-15 neurons per DRG by 14 dpf.

I used a monoclonal antibody against human neuronal protein HuC/HuD raised in mouse (Antibody 16A11, Molecular Probes) that specifically marks all neuronal cells in the zebrafish embryo. I found that in 4 dpf *mos*<sup>m188</sup> mutant embryos many DRGs are missing completely and the remaining ones contain reduced numbers of sensory neurons (Figure 12B). Occasionally I identified sensory neurons ectopically positioned at the level of the lateral neural tube or lateral to the notochord.

The same experiment revealed a severe deficit of neurons in the enteric nervous system of *mos*<sup>m188</sup> mutant embryos. Enteric neurons establish the local nervous system of the gastrointestinal tract. There are both sensory enteric neurons receiving information from sensory receptors in the mucosa and in smooth muscle, and enteric motor neurons acting directly on a large number of effector cells including smooth

muscle and secretory cells. In 4 dpf *mos*<sup>m188</sup> mutant embryos the enteric neurons are completely absent (Figure 12B). Interestingly, the development of the cranial sensory ganglia is not impaired in the *mos*<sup>m188</sup> mutant embryos (data not shown).

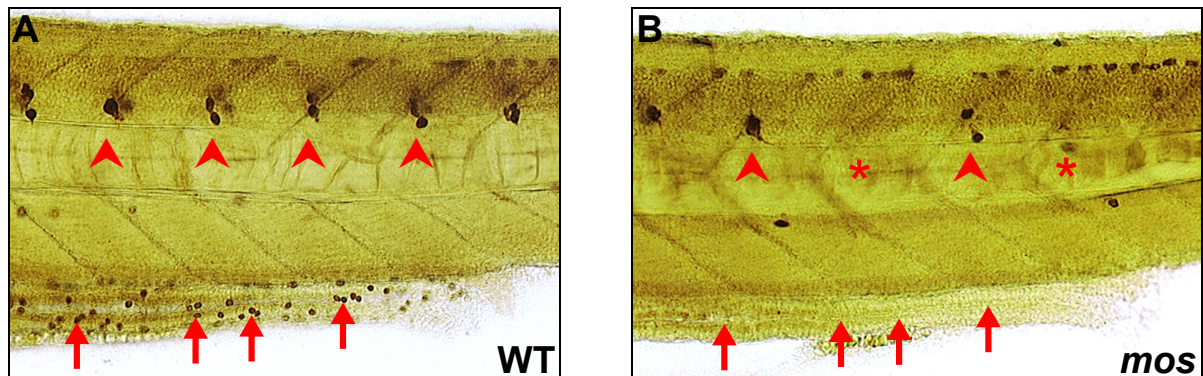


**Figure 12.** Peripheral nervous system in the trunk of 4 dpf zebrafish embryos stained by the pan-neuronal antibody anti-Hu. Lateral views of a 6 somite-wide region encompassing the posterior intestine and anus. (A) In wild-type embryos the dorsal root ganglia are evenly spaced at the level of the intersomitic boundaries (arrowheads) and the enteric neurons are located in the intestinal wall (arrows). (B) In homozygous *mos*<sup>m188</sup> embryos, the enteric nervous system is completely absent (arrows) and the development of dorsal root ganglia is substantially impaired. Some dorsal root ganglia are abolished (asterisks) whereas others are present but contain less neurons (arrowheads).

### 5.2.5 Migratory cranial neural crest cells and pharyngeal arch primordia display severely reduced expression of *dlx* genes in *mos*<sup>m188</sup> mutant embryos

Specific segmental loss of cartilage elements derived from the second (preotic) neural crest stream and from the third (postotic) neural crest stream prompted me to test the expression of neural crest specific gene markers. For this purpose I performed *in situ* hybridizations with *dlx2* and *dlx8*, members of the distal-less-related *dlx* homeobox gene family.

*dlx2* is expressed in a subset of premigratory cranial neural crest cells, in cranial neural crest cells migrating into the pharyngeal arches and subsequently in postmigratory craniofacial cartilage precursors in the pharyngeal arches (Akimenko et al. 1994). Additionally, *dlx2* is expressed in the ventral forebrain. I found that the number of *dlx2* expressing cranial migratory neural crest cells is strongly reduced in all streams at 19 hpf in *mos*<sup>m188</sup> mutant embryos (Figure 13B). The postotic stream of cranial neural crest cells is almost absent. In addition, the first two neural crest streams are fused together in *mos*<sup>m188</sup> mutant embryos, while *dlx2* expression in the forebrain is unaffected (Figure 13B). This phenotype persists at 24 hpf (Figure 13D).

*dlx8* is expressed in the pharyngeal arch primordia and in the pectoral fin buds during the second day of development. Consistent with the *dlx2* expression pattern, I found that the *dlx8* expression in *mos*<sup>m188</sup> mutant embryos is significantly diminished in the second arch primordium and is practically abolished in the most posterior branchial arch primordia at 36 hpf (Figure 13F).

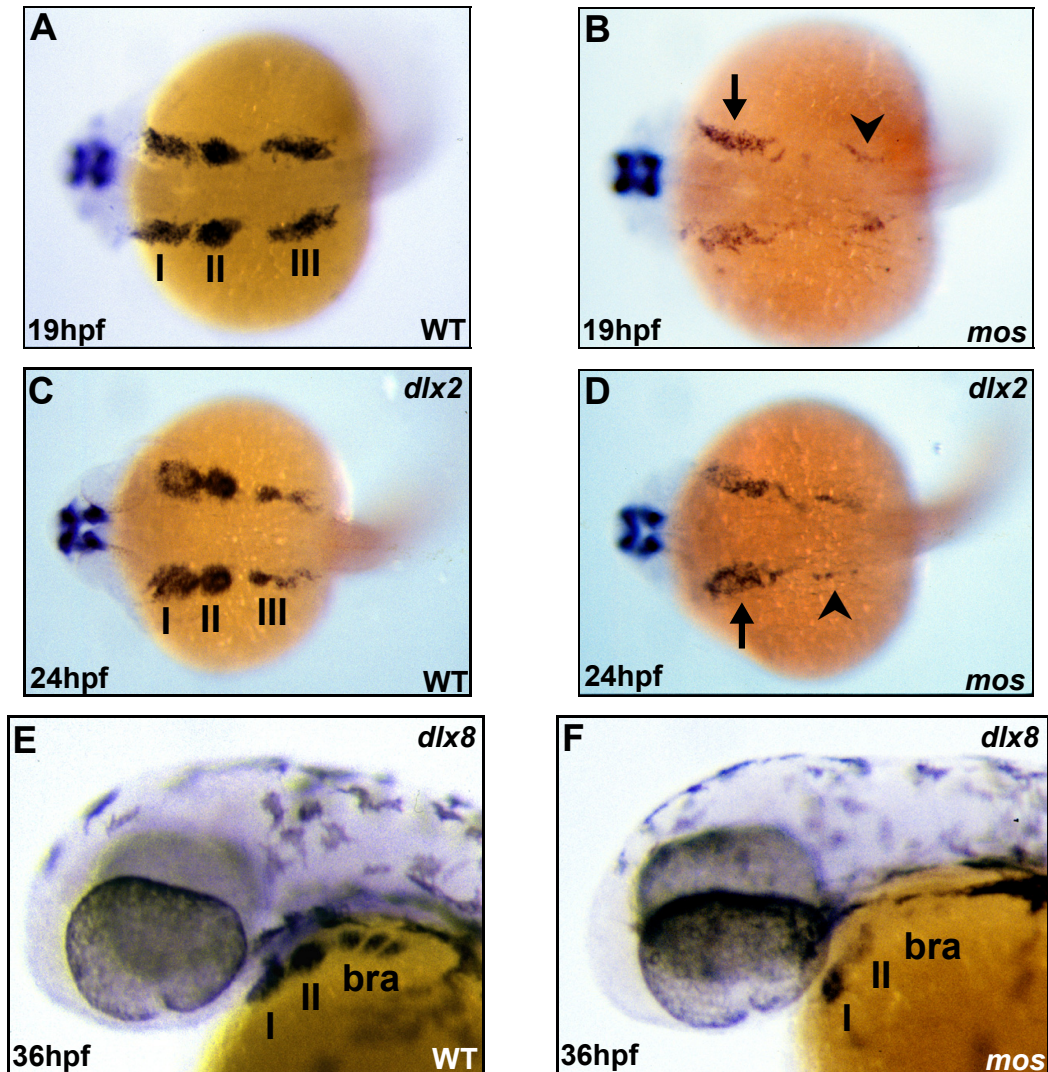


**Figure 13.** Migratory cranial neural crest cells and pharyngeal arch primordia express *dlx2* and *dlx8* genes. (A-D) *dlx2* expression in 19 hpf (A,B) and 24 hpf (C,D) zebrafish embryos. Dorsal views. Anterior to the left. In wild-type embryos (A,C) the migratory neural crest cells of the three cranial neural crest streams (I+II+III) express *dlx2*. The third (postotic) stream begins subdivision into distinct branchial arch primordia (C). In *mos*<sup>m188</sup> mutant embryos (B,D) the number of cranial migratory neural crest cells expressing *dlx2* is strongly reduced. The third neural crest stream is most severely affected (arrowhead). The anterior cranial neural crest streams are no longer separated but fuse in *mos*<sup>m188</sup> mutant embryos (arrow). (E,F) *dlx8* expression in pharyngeal arch primordia of 36 hpf wild-type (E) and homozygous *mos*<sup>m188</sup> (F) embryos. Lateral views. Anterior to the left. *dlx8* expression in homozygous *mos*<sup>m188</sup> embryos is lost in an anterior to posterior direction: Expression in pharyngeal arch primordium I is almost normal, expression in pharyngeal arch primordium II is strongly reduced and expression in the branchial arch primordia (bra) is almost completely lost.



### 5.2.6 Normal patterning of hindbrain rhombomeres in *mos*<sup>m188</sup> mutant embryos

To test if the deficit in formation of cranial neural crest streams is accompanied by hindbrain patterning defects, I analyzed the expression patterns of four genes, *valentino*, *krox-20*, *hoxa2* and *hoxb2*, that mark both of these structures.

The bZIP transcription factor *val* (*valentino*; zebrafish ortholog of the mouse gene *Kreisler*) is expressed in rhombomeres 5 and 6 and in postotic neural crest cells migrating out at the level of rhombomere 6. In *mos*<sup>m188</sup> mutant embryos the hindbrain expression of *val* in r5 and r6 is normal while there is no expression in the cells of the postotic neural crest stream at 15 hpf (Figure 14A,B). Similar results were obtained with the zinc-finger transcription factor gene *krox-20* (data not shown).

The *Hox* paralogue group 2 genes *hoxa2* and *hoxb2* are expressed in the hindbrain and in subsets of migrating neural crest cells in a partially overlapping fashion. *hoxa2* is expressed in rhombomeres 2 to 5 and in migrating neural crest cells of the two posterior (2nd and 3rd) streams (Figure 14C). *hoxb2* is expressed in rhombomeres 3 to 5, with a gradual decrease of the expression level from r3 to r5. In addition, *hoxb2* is expressed in migrating neural crest cells of the 2nd stream (Figure 14E). As observed for *val* and *krox-20* genes, I found that in *mos*<sup>m188</sup> mutant embryos migrating neural crest cells expressing either *hoxa2* or *hoxb2* are practically absent (Figure 14C-F) whereas the hindbrain expression domains of these genes are undisturbed at 22 hpf. These data indicate that the *mos*<sup>m188</sup> gene is required for neural crest cell development but has no effect on hindbrain patterning.

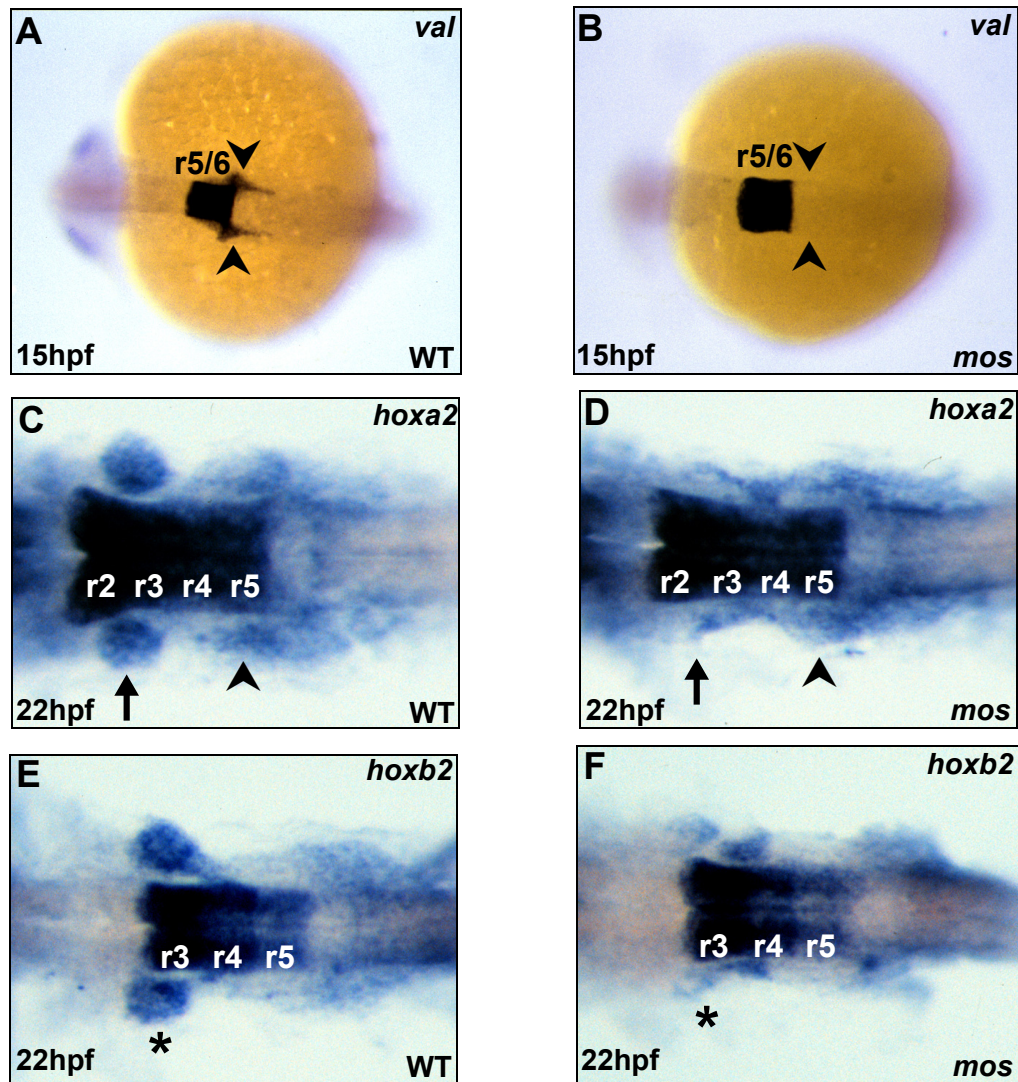


**Figure 14.** The zebrafish embryonic hindbrain and migratory cranial neural crest cells express *val*, *hoxa2* and *hoxb2*. (A,B) *val* expression in 15 hpf wild-type (A) and homozygous *mos*<sup>m188</sup> (B) embryos. The *mos*<sup>m188</sup> mutant embryos lack *val* expressing postotic migratory neural crest cells (arrowheads). *val* expression in the hindbrain (r5/r6, rhombomeres 5+6) is unaltered. (C,D) *hoxa2* expression in 22 hpf wild-type (C) and homozygous *mos*<sup>m188</sup> (D) embryos. In homozygous *mos*<sup>m188</sup> embryos there is a substantial reduction in the number of migratory neural crest cells expressing *hoxa2* in the two posterior neural crest streams (arrow: second stream; arrowhead: third stream). (E,F) *hoxb2* expression in 22 hpf wild-type (E) and homozygous *mos*<sup>m188</sup> (F) embryos. The number of migratory neural crest cells of the second stream expressing *hoxb2* is greatly diminished in *mos*<sup>m188</sup> mutant embryos (asterisk). *hoxa2* and *hoxb2* expression in the hindbrain (r2-r5, rhombomeres 2-5) is unaltered (C-F). Dorsal views. Anterior to the left.

### 5.2.7 The mutation in the *mos*<sup>m188</sup> locus leads to downregulation of key genes in neural crest progenitor cells

To determine when the *mos*<sup>m188</sup> locus function is required for the first time during neural crest development I have analyzed the expression of key genes in neural crest progenitors. Zebrafish *sox9b* is expressed in a dynamic spatio-temporal pattern in premigratory neural crest progenitors and is gradually downregulated as neural crest migration proceeds (Li, M. et al. 2002). Sox9b is a homologue of the human HMG (high mobility group domain) transcription factor Sox9 that was shown to be mutated in campomelic dysplasia patients (Foster et al. 1994; Wagner et al. 1994). I found that the expression of *sox9b* in *mos*<sup>m188</sup> mutant embryos is greatly reduced in cranial neural crest progenitor cells at 12 hpf, while the expression in the otic placode appeared to be unaffected (Figure 15B). This result provided the first indication that the *mos*<sup>m188</sup> locus is most likely regulating neural crest specification and is acting upstream of the *sox9b* gene.

To further confirm this finding I have analyzed the expression of *snail2*, one of the earliest markers expressed in neural crest progenitors. *snail2* encodes a zinc finger protein of the Snail family and is expressed in premigratory and early migratory neural crest cells starting at 11 hpf (Thisse et al. 1995). In wild-type embryos the neural crest progenitors started forming neural crest streams at 14 hpf (Figure 15C). In 14 hpf *mos*<sup>m188</sup> mutant embryos the expression of *snail2* is dramatically reduced to a thin layer of cells on the lateral sides of the neural tube (Figure 15D). Additionally, the anterior-posterior extent of the expression domain is shortened.

I have also tested the pan-neural crest marker *crestin*, a multi-copy retroelement, that very specifically labels all premigratory and migratory neural crest cells (Luo et al. 2001). In 14 hpf *mos*<sup>m188</sup> mutant embryos *crestin* expression is greatly reduced in premigratory trunk neural crest cells and completely abolished in premigratory cranial neural crest cells (Figure 15E,F).

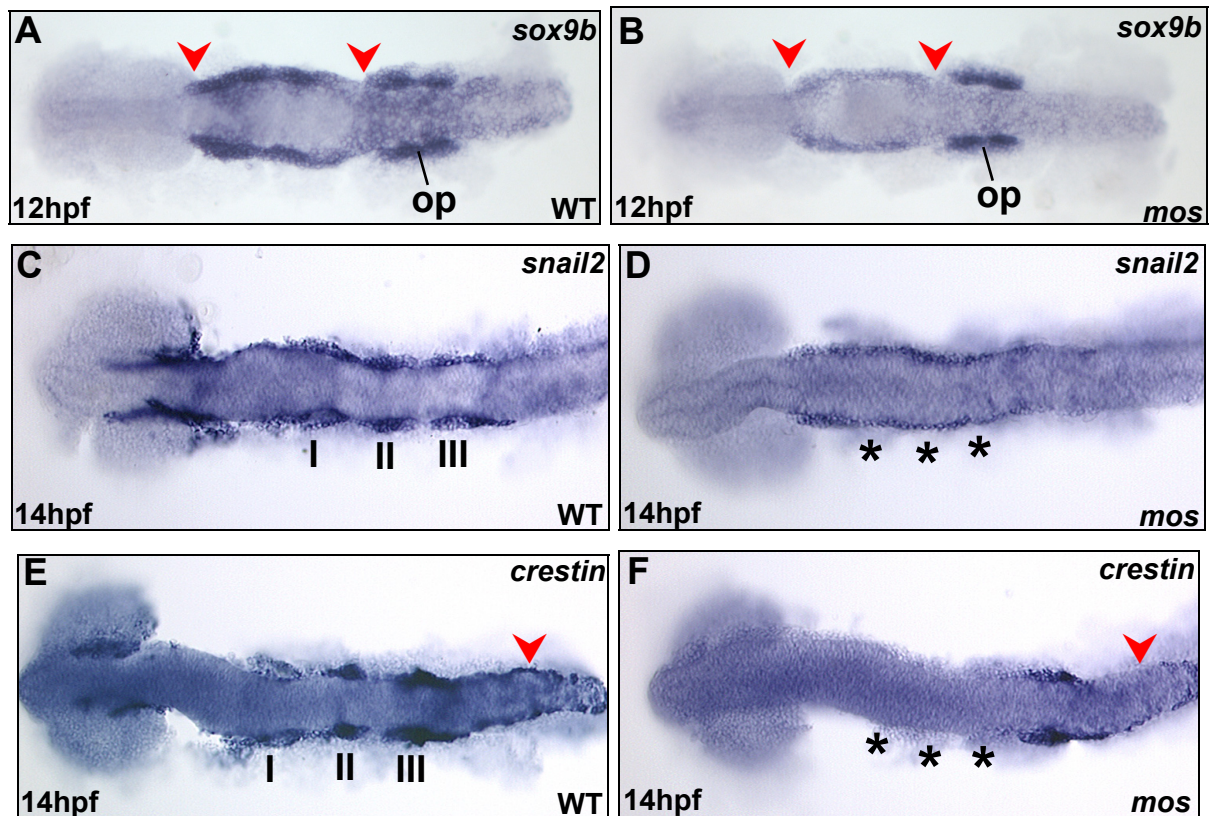


**Figure 15.** Cranial neural crest progenitors express *sox9b*, *snail2* and *crestin*. (A,B) *sox9b* expression in 12 hpf wild-type (A) and homozygous *mos*<sup>m188</sup> (B) embryos. In *mos*<sup>m188</sup> mutant embryos, *sox9b* expression in cranial premigratory neural crest cells (region between the arrowheads) is considerably reduced compared to wild-type embryos. *sox9b* expression in the otic placode (op) is unaltered. (C,D) *snail2* expression in 14 hpf wild-type (C) and homozygous *mos*<sup>m188</sup> (D) embryos. In *mos*<sup>m188</sup> mutant embryos the level of *snail2* expression is lower when compared to wild-type embryos and the three prospective cranial neural crest streams (I+II+III) do not form (asterisks). (E,F) *crestin* expression in 14 hpf wild-type (E) and homozygous *mos*<sup>m188</sup> (F) embryos. *crestin* expression in *mos*<sup>m188</sup> mutant embryos is completely abrogated in cranial neural crest progenitors (asterisks) and is reduced in trunk neural crest progenitors (arrowheads). I+II+III, wild-type premigratory neural crest cells of the three prospective cranial neural crest streams. Dorsal views. Anterior to the left.

Interestingly, the expression of the transcription factor *ap-2α/mob* (*mont blanc*) in premigratory and early migratory neural crest cells is unaffected in *mos*<sup>m188</sup> mutant embryos (Barrallo et al., *personal communication*). Similarly, the HMG-domain transcription factor *sox10/clis* is also normally expressed in *mos*<sup>m188</sup> mutant premigratory and migratory trunk neural crest (data not shown). Taken together these results suggest that the *mos*<sup>m188</sup> locus is regulating a subset of genes expressed in neural crest progenitors (*snail2*, *sox9b*), but it has no effect on other regulators like *ap-2α* and *sox10*. Expression of genes associated with neural crest induction like transcription factor gene *pax3* appears to be normal (data not shown).

---

I have found that the arrangement of the cranial sensory ganglia is not perturbed in *mos*<sup>m188</sup> mutant embryos at 4 dpf. To rule out any possible defects earlier in development, I have tested the two atonal-related bHLH transcription factors Neurogenin1 (Ngn1) and NeuroD. Both are expressed in all cranial neurogenic placodes which give rise to the placode-derived sensory neurons of the cranial ganglia (Andermann et al. 2002). The expression of *ngn1* and *neuroD* was found to be normal in *mos*<sup>m188</sup> mutant embryos (data not shown).

### **5.2.8 *foxD3*, a key regulator of neural crest specification, is not expressed in neural crest progenitor cells of *mos*<sup>m188</sup> mutant embryos**

*FoxD3* has been shown to be expressed in all premigratory neural crest cells of zebrafish, frog, chick and mouse and rapidly down-regulated at the onset of migration. In zebrafish, *foxD3* expression is seen at later stages specifically in neural crest-derived satellite glial cells and in Schwann cells. Besides the neural crest expression domain, *foxD3* is expressed in the floor plate, tail bud and somites of 14 hpf embryos (Figure 16E). Because of the genetic linkage (see chapter 5.2.10) and the tight correlation between the expression domains of *foxD3* and the *mos*<sup>m188</sup> mutant phenotype, I have studied *foxD3* as a potential candidate gene for the *mos*<sup>m188</sup> locus. Whole mount in situ hybridization revealed surprising results. In *mos*<sup>m188</sup> mutant embryos the *foxD3* expression in premigratory neural crest cells and in the floor plate is completely abolished (Figure 16B,D,F) while the expression in the tail bud is greatly reduced. Interestingly, at 14 hpf *foxD3* expression in the somites is not affected (Figure 16F) and early expression at the shield stage (gastrulation) is also normal (data not shown).

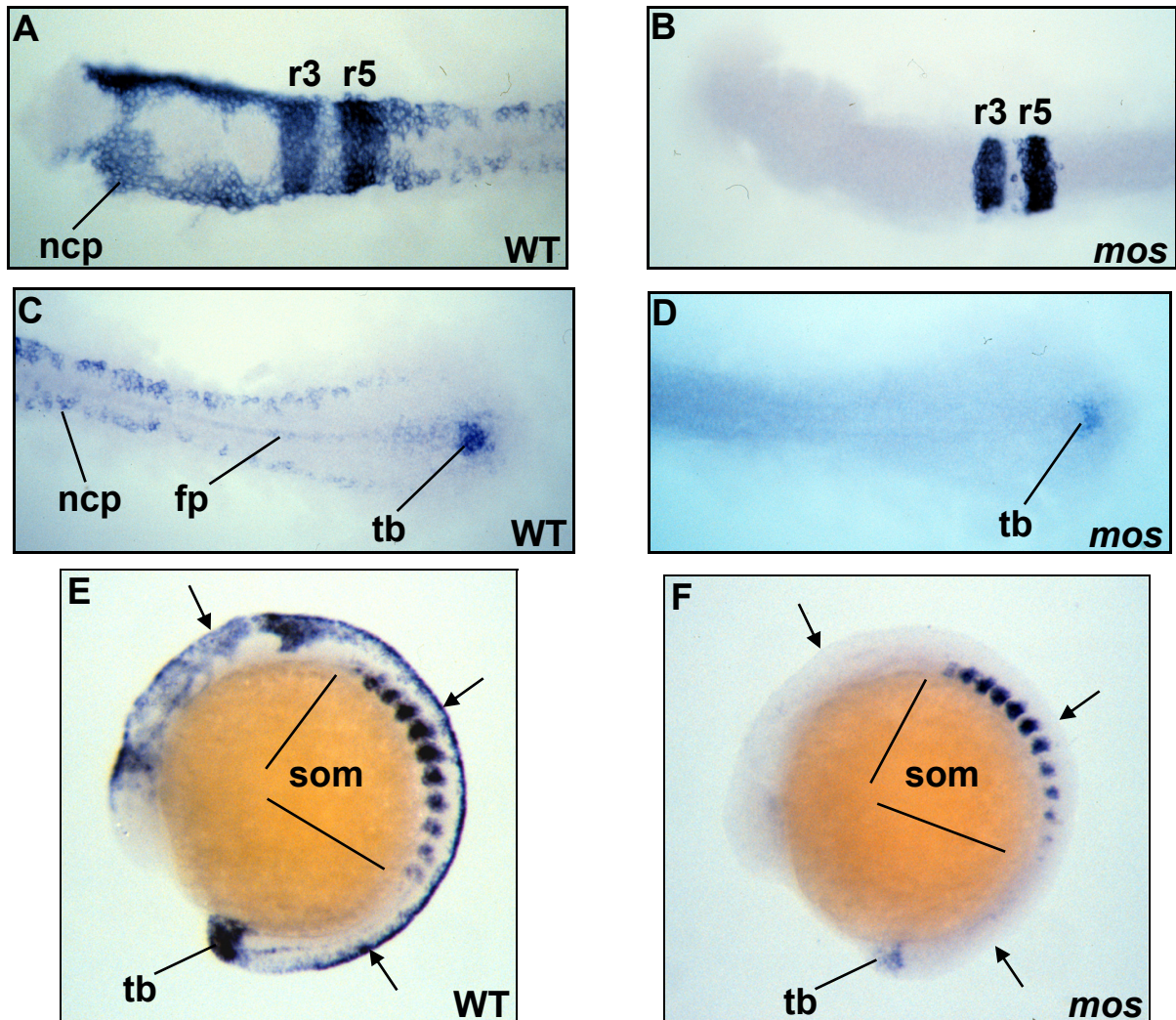


**Figure 16.** Early expression of *foxD3* in zebrafish wild-type (A,C,E) and homozygous *mos*<sup>m188</sup> (B,D,F) embryos. (A-D) *foxD3/krox-20* expression in flat-mounted 12 hpf embryos in the head region (A,B) and in the tail region (C,D). Dorsal views. *krox-20* demarcates the rhombomeres 3 and 5 (r3, r5). *foxD3* is expressed in wild-type neural crest precursors (ncp), the floor plate (fp) and in the tailbud (tb). In homozygous *mos*<sup>m188</sup> embryos *foxD3* expression in neural crest precursors and in the floor plate is abolished, whereas tailbud expression is reduced (B,D). (E,F) *foxD3* expression in 14 hpf embryos. Lateral views. In homozygous *mos*<sup>m188</sup> embryos (F) *foxD3* expression is completely downregulated in premigratory neural crest cells (arrows) and reduced in the tailbud (tb). *foxD3* somite (som) expression is normal in *mos*<sup>m188</sup> mutant embryos. Anterior is to the left.

In the course of the detailed analysis of early *foxD3* expression in premigratory neural crest cells it became clear that there is a clear gene dosage effect. In a clutch of embryos (n=40) obtained from a cross of two heterozygous fish for the *mos*<sup>m188</sup> mutation we have found that at 12 hpf a quarter did not express *foxD3* at all, a quarter showed a normal level of expression and two quarters of embryos displayed an intermediate level of *foxD3* expression. Moreover, we have genotyped these three groups of embryos with a RFLP linked very closely to the *mos*<sup>m188</sup> mutation (Haell-380-foxd3; for details see chapter 5.2.10) and found that the embryos without *foxD3*

expression were homozygous  $-/-$  for that RFLP, the embryos with medium levels of *foxD3* expression were heterozygous  $+/-$  whereas the ones with the normal *foxD3* expression level were homozygous  $+/+$  for that RFLP (Figure 17).

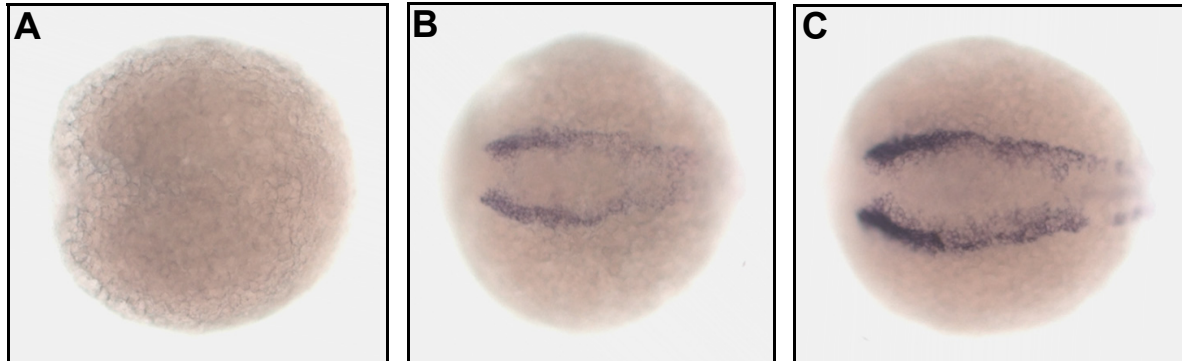


**Figure 17.** Cranial neural crest progenitors display genotype-dependent *foxD3* expression levels at 12 hpf. (A) Homozygous *mos*<sup>m188</sup> embryo. (B) Heterozygous wild-type embryo. (C) Homozygous wild-type embryo. Homozygous *mos*<sup>m188</sup> ( $-/-$ ) embryos lack *foxD3* expression completely. Heterozygous wild-type ( $+/-$ ) embryos have lower levels of *foxD3* expression than homozygous wild-type ( $+/+$ ) embryos. The genotyping has been performed based on the Haell RFLP present at position 380 in the *foxD3* gene. Dorsal views. Anterior is to the left.

### 5.2.9 *foxD3* transcripts are maternally deposited

To test whether there is a maternal deposition of *foxD3* transcripts in zebrafish embryos, I performed RT-PCR analyses with early embryo-derived RNA. The zebrafish midblastula transition (MBT) that marks the onset of zygotic transcription begins at 3 hpf. I isolated total RNA from 8-16 cell stage embryos (1), 64 cell stage embryos (2), 2.5 hpf embryos (3) and 2 dpf embryos (4) and used it as template for RT-PCR reactions, the latter representing the control for the detection of zygotic transcripts. The early stages should be equivalent to each other with respect to mRNA composition since there is no zygotic transcription occurring prior to MBT. The gene *one-eyed pinhead* (*oep*) is well known to be maternally deposited in the zebrafish oocyte and therefore has been chosen as a positive control (Zhang et al. 1998). Nested primers have been used in nested RT-PCR reactions for both *foxD3* and *oep*. Because the *oep* forward and reverse primers are in exon 3 and exon 4, respectively, and are thus spanning the third intron, only reverse transcribed mRNA can serve as template in the PCR reaction and yield a fragment of the expected size. The expected sizes of the first round PCR products are 266 bp (*foxD3*) and 246 bp (*oep*), while in the second round they are 150 bp (*foxD3*) and 180 bp (*oep*). The

results show that maternal deposits of *foxD3* mRNA are present in zebrafish embryos before MBT (Figure 18A). After the first round of PCR, only the product generated from the 2 dpf RNA template can be visualized (*foxD3* and *oep*). The nested PCR (template: 2  $\mu$ l first round product in 50  $\mu$ l total reaction volume) yields products of the expected sizes in all reactions (*foxD3* and *oep*; Figure 18A,B). In the nested PCR reactions with 2 dpf RNA as starting template by-products of unknown origin are produced (*foxD3* and *oep*).

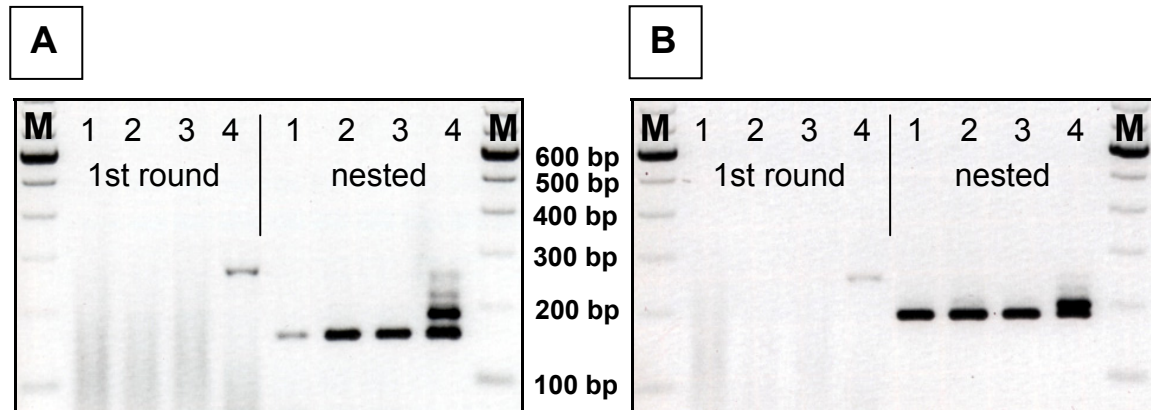


**Figure 18.** Maternal deposition of *foxD3* and *oep* in zebrafish embryos. (A) Nested RT-PCR expression analysis of *foxD3*. (B) Nested RT-PCR expression analysis of *oep*. Lane 1: 8-16 cell stage. Lane 2: 64 cell stage. Lane 3: 2.5 hpf. Lane 4: 2 dpf. Size marker (M): 100 bp ladder. The nested RT-PCR analysis detects maternally deposited transcripts of both *foxD3* and *oep* in early zebrafish embryos.



### 5.2.10 Genetic mapping of the *mos*<sup>m188</sup> locus

The *mos*<sup>m188</sup> locus was mapped using a two-generation intercross between the mutation carrying AB line and the highly polymorphic wild-type TL strain. A total genome scan using SSLP markers placed the *mos*<sup>m188</sup> locus proximal to the centromere of linkage group 6 (Figure 19; most of the mapping and cloning analysis was conducted by a postdoctoral fellow Sherri W. Sachdev). High resolution mapping using 3134 meioses defined a critical interval of 2.43cM flanked by the markers Z12094 and Z10183. Further analysis refined the genetic interval to a 0.63cM region flanked by the EST fa04h11 and the marker Z15259. This small genetic interval was examined for suitable positional candidate genes. *FoxD3* appeared as a convincing candidate gene since it was shown to be one of the early factors controlling neural crest progenitor development. Genetic mapping of an SSCP marker in the *foxD3* gene placed it at 0.03cM distance (1 recombinant in 3134 meioses) from the *mos*<sup>m188</sup> mutation (Figure 19).

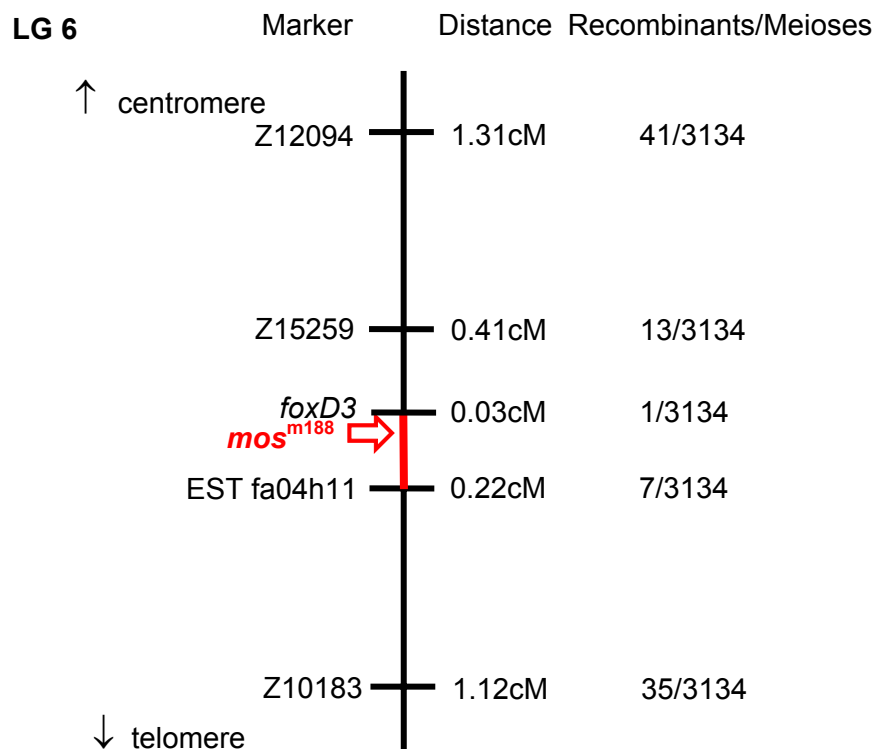


**Figure 19.** Genetic map of the *mos*<sup>m188</sup> mutation on LG 6. The arrow indicates the map position of the *mos*<sup>m188</sup> locus. The number of recombinants, the number of meioses tested and the resulting genetic distance from the mutated locus are indicated for each genetic marker.

Zebrafish *foxD3* is a 1782 bp intronless gene encoding a 371 amino acid winged helix transcription factor. The *foxD3* protein contains a conserved *fork head* DNA-binding domain, a transactivation domain near the C-terminus and an acidic domain close to the N-terminus (Odenthal and Nusslein-Volhard 1998). The *foxD3* SSCP marker reveals an interesting SNP (single nucleotide polymorphism) in the coding region of the gene. Sequencing of the PCR product revealed a single A→T polymorphism at nucleotide position 380 (coding position 184) that leads to a substitution of serine 62 for a cysteine when homozygote for T. A change like this would be typical for an ENU-induced mutation (Knapik 2000) and would affect the acidic domain of the protein, the function of which is largely unknown. The additional cysteine residue might interfere with proper disulfide bond formation between the four constitutively present cysteine residues in the FoxD3 protein. There are numerous examples of serine to cysteine mutations or polymorphisms that have been shown to disrupt protein function or have been linked to a disease phenotype (Chen et al. 2001; Xing et al. 2001). The A→T transversion in the *foxD3* coding sequence creates a new HaeIII restriction site that allows RFLP genotyping of embryos without sequencing. At this point it is unclear if this is the mutation induced by ENU and responsible for the *mos*<sup>m188</sup> phenotype, or rather it is a simple SNP without bearing on the phenotype. Further analysis is conducted in the laboratory to solve this question.

The close physical location of the *foxD3* gene to the *mos*<sup>m188</sup> locus and the results of the phenotypic analysis indicating that the mutation disrupts a gene critical for neural crest specification, prompted us to test whether knockdown of the *foxD3* gene could phenocopy the *mos*<sup>m188</sup> mutant phenotype.

### 5.2.11 Knockdown of *foxD3* function phenocopies many aspects of the *mos*<sup>m188</sup> mutation

To test whether loss of *foxD3* function can phenocopy the *mos*<sup>m188</sup> mutation I have used morpholino labeled antisense oligonucleotides directed against *foxD3* message. I used two anti-*foxD3* morpholinos: MO-1 is targeted against the first 25 coding bases (starting with the ATG) and MO-2 is targeted against the 25 bases immediately upstream of the ATG (last 25 bases of the 5'UTR).

The injection of either MO-1 or MO-2 (2 ng) into wild-type embryos ablates *val* and *krox-20* (Figure 20A,B) expression in migratory neural crest cells of the postotic stream at 15 hpf in a fashion very similar to *mos*<sup>m188</sup> mutant embryos.

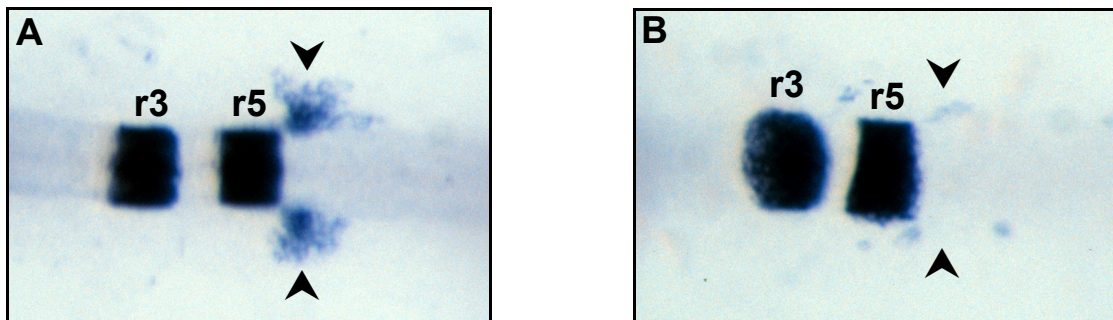


**Figure 20.** Anti-*foxD3* morpholino injection results in loss of the postotic neural crest stream expression domain of *krox-20* at 15 hpf. (A) *krox-20* expression in uninjected control embryo. (B) *krox-20* expression in embryo injected with 2 ng MO-1. The anti-*foxD3* morpholino injected embryo lacks *krox-20*-expressing postotic migratory neural crest cells (arrowheads). *krox-20* expression in the hindbrain is unperturbed (r3/r5, rhombomeres 3+5). Dorsal views. Anterior is to the left.

At this concentration (2 ng/nl) MO-1 failed to have an effect on the development of the iridophore pattern (data not shown). On the contrary, MO-2 injection at the same concentration showed a weak effect on iridophore formation, yet this effect was much stronger when 4 ng/nl or 6 ng/nl of MO-2 were injected. MO-2 also had a stronger effect on the formation of enteric neurons and dorsal root ganglia. When injected at 4 ng/nl, MO-1 affected the enteric neurons and/or the DRGs in 72% of the embryos, whereas 100% of the MO-2 injected embryos were affected in these neural crest derivatives. Injection of 6 ng/nl MO-2 resulted in cartilage phenotypes strongly reminiscent of the *mos*<sup>m188</sup> mutant phenotype (Table 13 and Figure 21).

**Table 13.** Frequencies of craniofacial cartilage phenotypes resulting from injection of anti-*foxD3* morpholino MO-2 (6 ng).

WT craniofacial cartilages	21%
Ceratohyal bent; branchial arches $\pm$ normal	10%
Unilateral absence of some or all branchial arch cartilage elements	8%
Absence of some branchial arch cartilage elements	33%
Complete absence of branchial arches 1-4 (number 5 often present)	28%

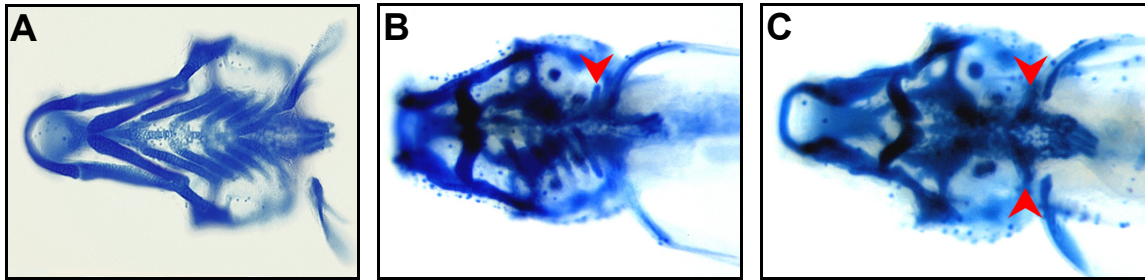


**Figure 21.** Anti-*foxD3* morpholino injection results in craniofacial cartilage defects visualized by Alcian Blue analysis of 5 dpf embryos. Ventral views. Anterior is to the left. (A) Uninjected control embryo. (B,C) Embryos injected with anti-*foxD3* morpholino MO-2 (6 ng). (B) MO-2 injected embryo with unilateral impairment of posterior arch cartilage formation. On the affected side of the embryo, all but the last (arrowhead) branchial arch cartilage elements are absent. (C) MO-2 injected embryo displaying abolishment of branchial arches 1-4. The 5th branchial arch cartilage elements are present (arrowheads).

The co-injection of MO-1 and MO-2 resulted in a stronger phenotype as compared to any single morpholino injection. The co-injected morpholinos (4 ng of each morpholino) effectively reduced the number of migratory cells in the third neural crest stream as shown by *dlx2* expression at 24 hpf (Figure 22B-D). Additionally, the first and the second neural crest streams were fused in many of the co-injected embryos (Figure 22D). These very specific phenotypes were accompanied by an unspecific reduction of the body size in co-injected embryos.

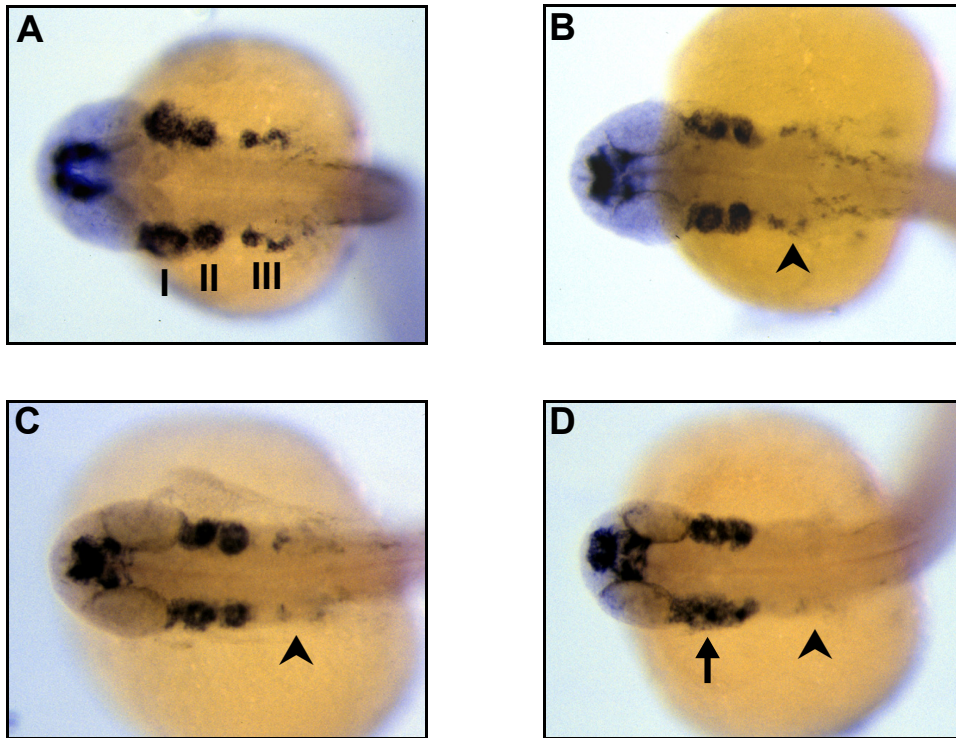


**Figure 22.** Double anti-*foxD3* morpholino injected zebrafish embryos assayed for *dlx2* expression at 24 hpf. Dorsal views. Anterior to the left. (A) Uninjected control embryo. *dlx2* expression marks the migratory neural crest cells of the three cranial neural crest streams (I+II+III). (B-D) Embryos co-injected with MO-1 and MO-2 (4 ng each). (B,C) Co-injected embryos displaying a severe reduction in the number of postotic migratory neural crest cells (arrowhead). (D) Co-injected embryo displaying fusion of the anterior neural crest streams (arrow) and almost complete abolishment of the third (postotic) stream (arrowhead).

### 5.3 Analysis of the cartilage differentiation mutations *round* ( $rnd^{m211, m641, m713, m715}$ ) and *crusher* ( $cru^{m299}$ )

#### 5.3.1 Comparative phenotypic characterization of the *round*<sup>m211</sup> and *crusher*<sup>m299</sup> mutations

The ENU-induced mutations *round*<sup>m211</sup> and *crusher*<sup>m299</sup> were recovered during the screen for embryonic lethal mutations based on their visible phenotype. One allele of the *crusher* locus ( $cru^{m299}$ ) and four independent alleles of the *round* locus were isolated,  $rnd^{m211}$ ,  $rnd^{m641}$ ,  $rnd^{m713}$  and  $rnd^{m715}$ . All *round* alleles give rise to the same mutant phenotype. I will henceforth mention only the allele(s) that were used in the experiments leading to the presented results. Both the  $rnd^{m211}$  and  $cru^{m299}$  mutations display similar phenotypes characterized by reduced body length, shorter heads and kinked pectoral fins (Figure 23C-F).

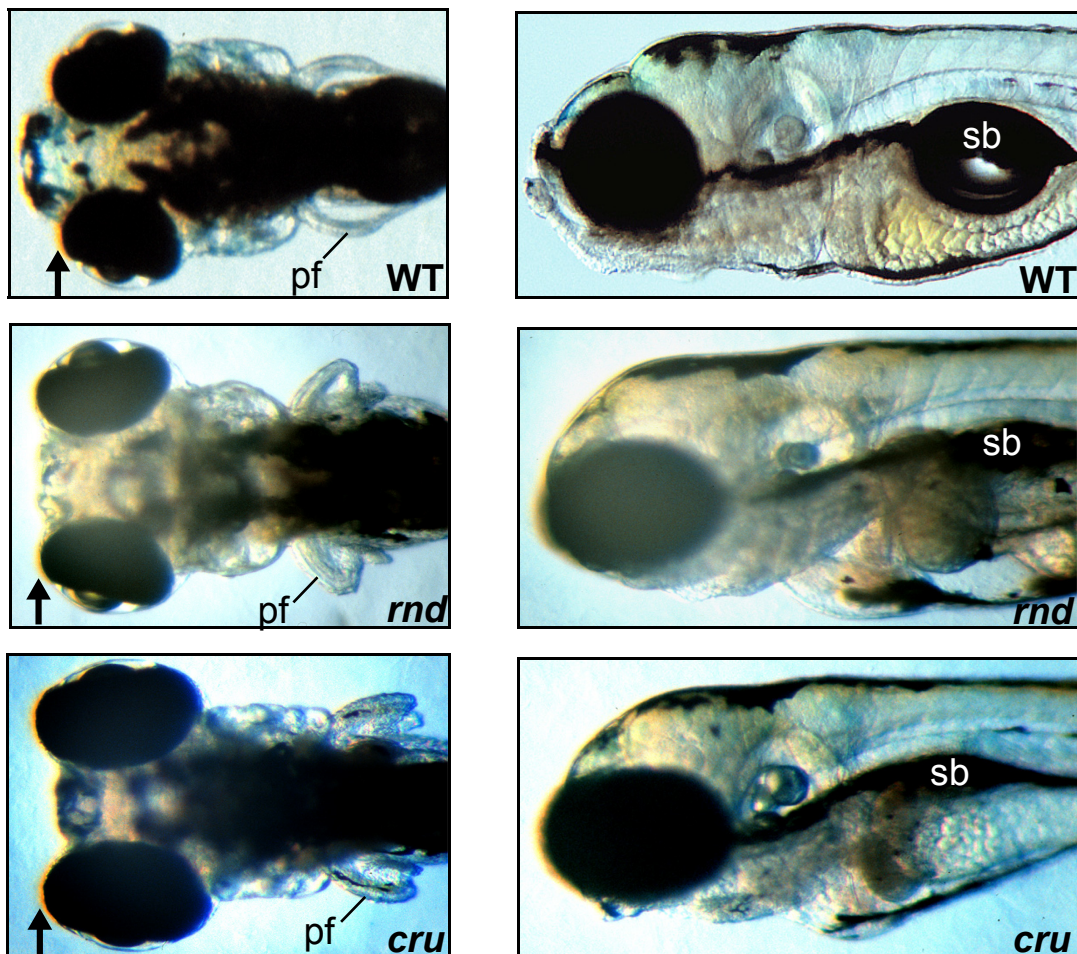


**Figure 23.** Phenotype of 5 dpf live wild-type (AB), homozygous *round*<sup>m211</sup> (CD) and homozygous *crusher*<sup>m299</sup> (EF) mutant embryos. (A,C,E) Dorsal views. There is no tissue protruding anteriorly to the eyes in the *round*<sup>m211</sup> and *crusher*<sup>m299</sup> mutant embryos (arrow). The pectoral fins (pf) are kinked in the mutant embryos. (B,D,F) Lateral views. The swim bladder (sb) is not inflated in the homozygous *round*<sup>m211</sup> and *crusher*<sup>m299</sup> embryos.

The *rnd*<sup>m211</sup> and *cru*<sup>m299</sup> phenotypes can be observed starting from 72 hpf and lead to death of the homozygous embryos by 8 dpf due to the failure of the swim bladder to inflate and the embryos' inability to feed. Both *rnd*<sup>m211</sup> and *cru*<sup>m299</sup> homozygous embryos lack tissues and skeletal elements projecting past the anterior edge of the eyes (Figure 23C,E). Additionally, there is a fin fold defect with variable expressivity in the *rnd*<sup>m211</sup> mutation. The organization of the collagenous fibers (actinotrichia) of the tail fin fold is disrupted giving rise to an abnormal fin fold morphology (Figure 24B).

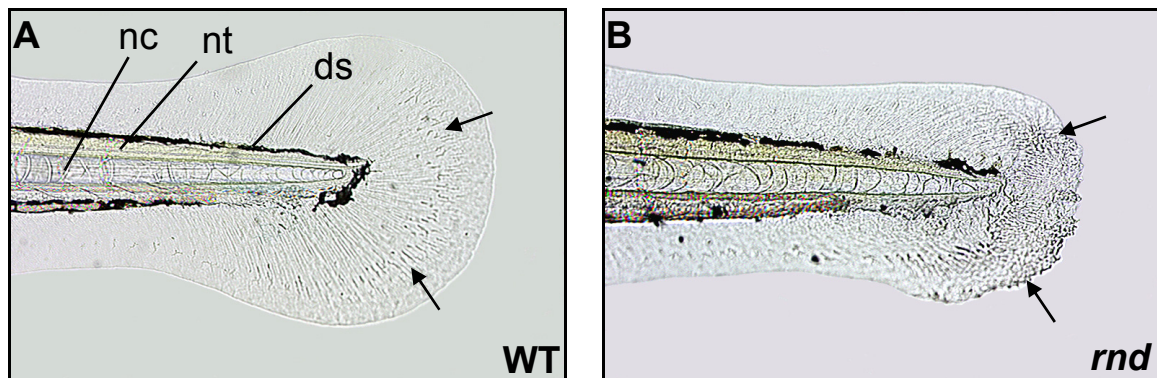


**Figure 24.** Fin fold defect in *rnd*<sup>m211</sup> mutant embryos. (A) 5 dpf wild-type embryo tail fin fold. (B) 5 dpf homozygous *rnd*<sup>m211</sup> mutant embryo tail fin fold. The wild-type pattern of actinotrichia running from the base to the tip of the fin is disrupted in homozygous *rnd*<sup>m211</sup> mutant embryos (arrows). Lateral views. ds, dorsal melanophore stripe; nc, notochord; nt, neural tube.

To gain insight into the arrangement of the craniofacial skeletal elements in *round*<sup>m211</sup> and *crusher*<sup>m299</sup> mutants, I conducted comparative analyses of Alcian Blue stained head skeletons of 5 dpf embryos. The cartilage elements of both the *rnd*<sup>m211</sup> and the *cru*<sup>m299</sup> mutant embryos are poorly defined, shortened and not projecting beyond the eyes (Figure 25C-F). The ceratohyal cartilages display very specific malformations for each of the mutations. The ceratobranchial cartilages of the branchial arches are oriented perpendicularly to the embryonic anteroposterior axis and the embryonic pectoral fins are kinked (Figure 25C,E). An interesting feature of the *cru*<sup>m299</sup> mutant embryos only is the absence of the cartilaginous otic capsule (Figure 25F).

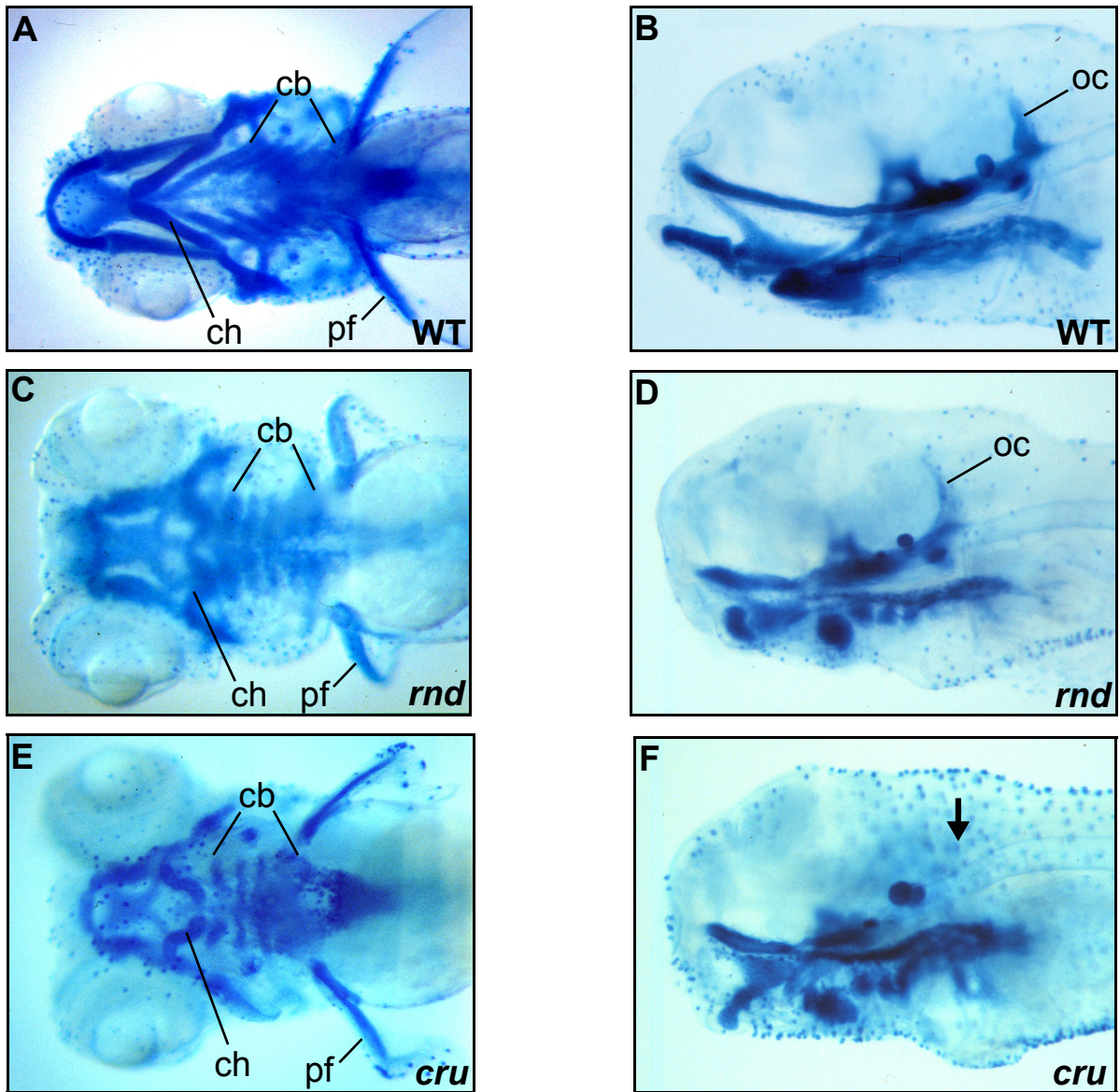


**Figure 25.** Craniofacial skeleton of 5 dpf wild-type (AB), homozygous *round*<sup>m211</sup> (CD) and homozygous *crusher*<sup>m299</sup> (EF) mutant embryos visualized by Alcian Blue staining. (A,C,E) Ventral views. In the mutant embryos, the ceratohyal (ch) cartilage elements are malformed, the ceratobranchials (cb) are oriented perpendicularly to the body length axis and the pectoral fins (pf) are kinked. (B,D,F) Lateral views. In homozygous *crusher*<sup>m299</sup> embryos the otic capsule (oc) surrounding the otic vesicle is absent (arrow).



### 5.3.2 Comparative histological characterization of the *round*<sup>m211</sup> and *crusher*<sup>m299</sup> mutations

To determine whether the gross morphological similarities of the cartilage differentiation mutations are maintained at a cellular level, I performed extensive histological analyses. For this purpose, 5 dpf wild-type, homozygous *round*<sup>m211</sup> and *crusher*<sup>m299</sup> embryos were embedded in JB-4 resin, sectioned at 5  $\mu$ m thickness and stained with Toluidine Blue (Figures 26-30).

The histological analysis revealed that the *rnd*<sup>m211</sup> mutants have a severely abnormal chondrocyte morphology accompanied by an overproduction of extracellular matrix (ECM). The mutant chondrocytes are bigger when compared to the wild-type chondrocytes and the chondrocyte nuclei are pushed to the cell periphery (Figure 26B, 27B). The chondrocyte morphology in the *cru*<sup>m299</sup> mutant embryos is also altered with respect to the wild-type embryos, and at the same time it differs greatly from the *rnd*<sup>m211</sup> histological phenotype. The *cru*<sup>m299</sup> mutant chondrocytes are smaller than in wild-type embryos and the increased synthesis of extracellular matrix is less dramatic than in *rnd*<sup>m211</sup> mutant embryos (Figure 27B,C; 28B,C).

The neurocranium of mutant *cru*<sup>m299</sup> embryos lacks the posterior parachordal and otic capsule cartilage elements which most likely are of mesodermal origin. Interestingly, the posterior parachordals in the *rnd*<sup>m211</sup> mutants display a normal wild-type chondrocyte morphology (Figure 29B,C). The semicircular canals of the otic vesicle form correctly in the *cru*<sup>m299</sup> mutant embryos. In contrast, in *rnd*<sup>m211</sup> mutant embryos the epithelial projections fail to grow out of the otocyst walls (Figure 29B,C).

The histological analysis of the pectoral fins demonstrates that the chondrocytes appear almost normal in *cru*<sup>m299</sup> mutant embryos, while the *rnd*<sup>m211</sup> pectoral fin chondrocytes display the typical abnormal *rnd*<sup>m211</sup> morphology described above (Figure 30B,C).

In summary, despite clear similarities between the *rnd*<sup>m211</sup> and *cru*<sup>m299</sup> phenotypes, both mutations exhibit important differences. The *rnd*<sup>m211</sup> mutation leads to the formation of larger chondrocytes that are overloaded with extracellular matrix components. This is accompanied by abnormal morphogenesis in the cartilage elements of the craniofacial skeleton and pectoral fins, with the exception of the

posterior parachordal cartilages that develop normally. The *cru*<sup>m299</sup> mutant embryos have smaller than normal chondrocytes displaying defects in the deposition of extracellular matrix material in the pericellular space. The fin chondrocyte morphology appears normal, but the posterior parachordal and otic capsule cartilages fail to form in *cru*<sup>m299</sup> mutant embryos. Thus, the *rnd*<sup>m211</sup> and *cru*<sup>m299</sup> loci play important and distinctive roles in the development of different skeletal elements of the cranium and the pectoral fins.

The following abbreviations are used in the Figures 26-30: bb, basibranchial; cb, ceratobranchial; ch, ceratohyal; cho, chondrocytes; ep, ethmoid plate; hs, hyosymplectic; m, Meckel's cartilage; nc, nasal canal; op, opercle; pc, parachordal cartilage; po, posterior otolith; pq, palatoquadrate; psc, pillars of the semicircular canals.

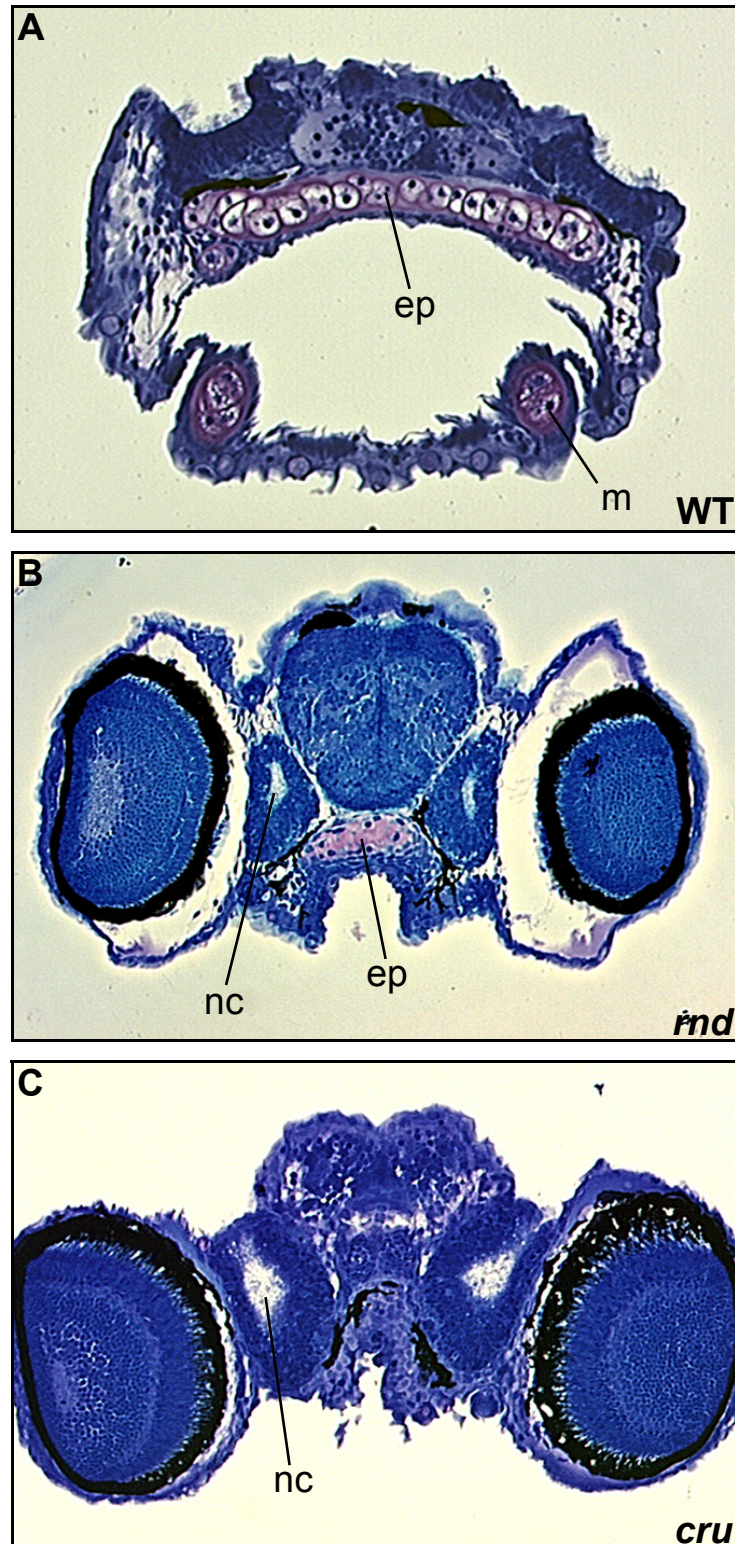


**Figure 26.** Transverse sections of 5 dpf wild-type (A), homozygous *round<sup>m211</sup>* (B) and homozygous *crusher<sup>m299</sup>* (C) mutant embryos. The WT embryo is sectioned anteriorly to the eyes, whereas the mutant embryos are cut in the anterior region of the eyes. (Both *round<sup>m211</sup>* and *crusher<sup>m299</sup>* embryos lack tissue protruding anteriorly to the eyes.) The chondrocytes of the wild-type ethmoid plate display the stack-of-coin arrangement which is typical of fully differentiated chondrocytes. The *round<sup>m211</sup>* mutant chondrocytes display an abnormal morphology characterized by an overproduction of ECM material (purple) and nuclei (blue) which are located in the chondrocyte periphery instead of the cell center. The cartilage elements of *crusher<sup>m299</sup>* mutant embryos do not extend anteriorly to the level of sectioning.

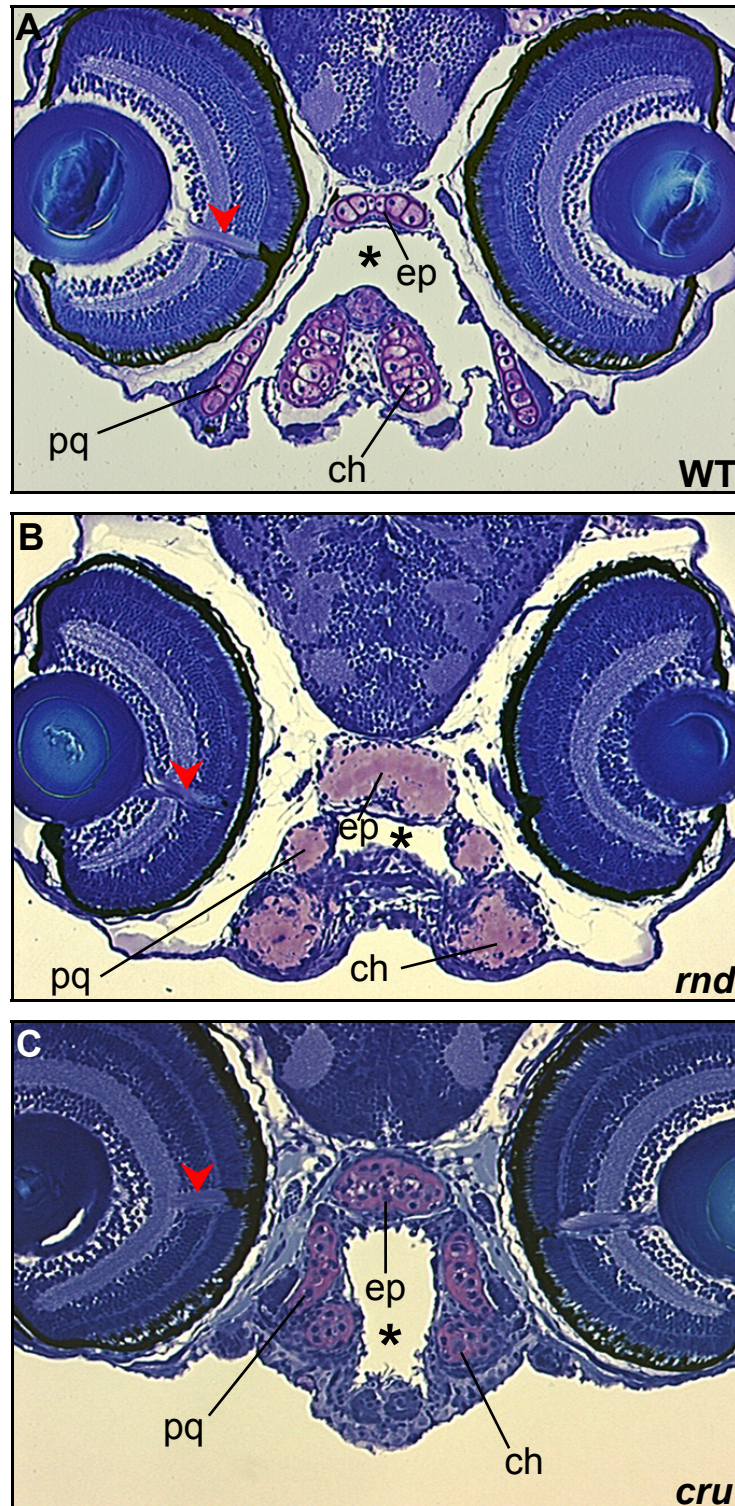


**Figure 27.** Transverse sections of 5 dpf wild-type (A), homozygous *round*<sup>m211</sup> (B) and homozygous *crusher*<sup>m299</sup> (C) mutant embryos. The embryos are sectioned at the level of the optic nerve (arrowhead). The overproduction of ECM components is more pronounced in *round*<sup>m211</sup> than in *crusher*<sup>m299</sup> mutant embryos. The shape and the spatial arrangement of the cartilage elements are altered in the homozygous mutant embryos. This results in considerable differences in the shaping of the oral cavities of the mutant and the wild-type embryos (asterisk).

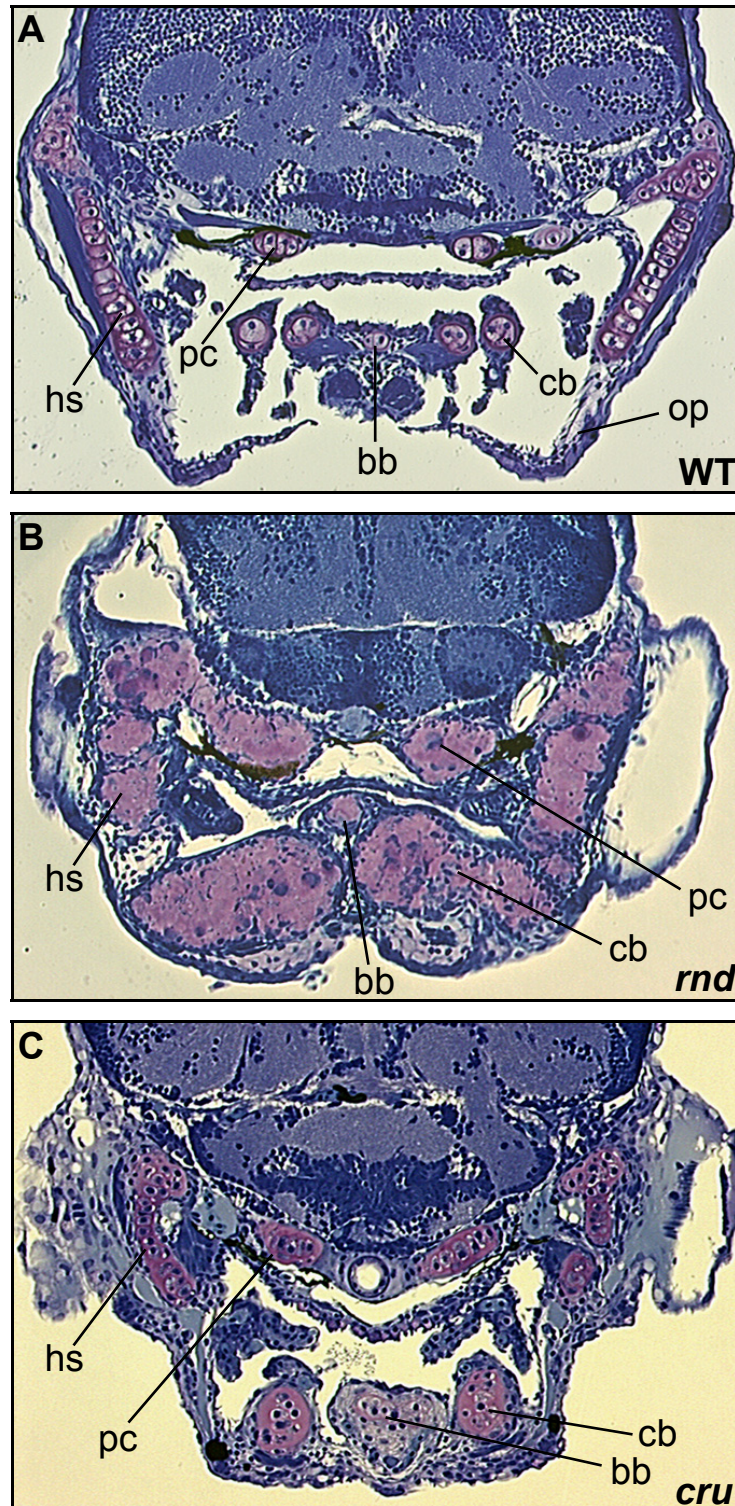


**Figure 28.** Transverse sections of 5 dpf wild-type (A), homozygous *round*<sup>m211</sup> (B) and homozygous *crusher*<sup>m299</sup> (C) mutant embryos. The embryos are sectioned at a plane between the eye and the ear. The wild-type embryo exemplifies the regular arrangement of both chondrocytes and cartilage elements. This contrasts with the perturbed cartilage differentiation which is observed in the two craniofacial mutations. For example, the ceratobranchial cartilage elements are sectioned transversely in the wild-type embryo, whereas they are sectioned longitudinally in the *round*<sup>m211</sup> mutant embryos. This is due to the ceratobranchials' orientation, which in these mutants is perpendicular to the body length axis.

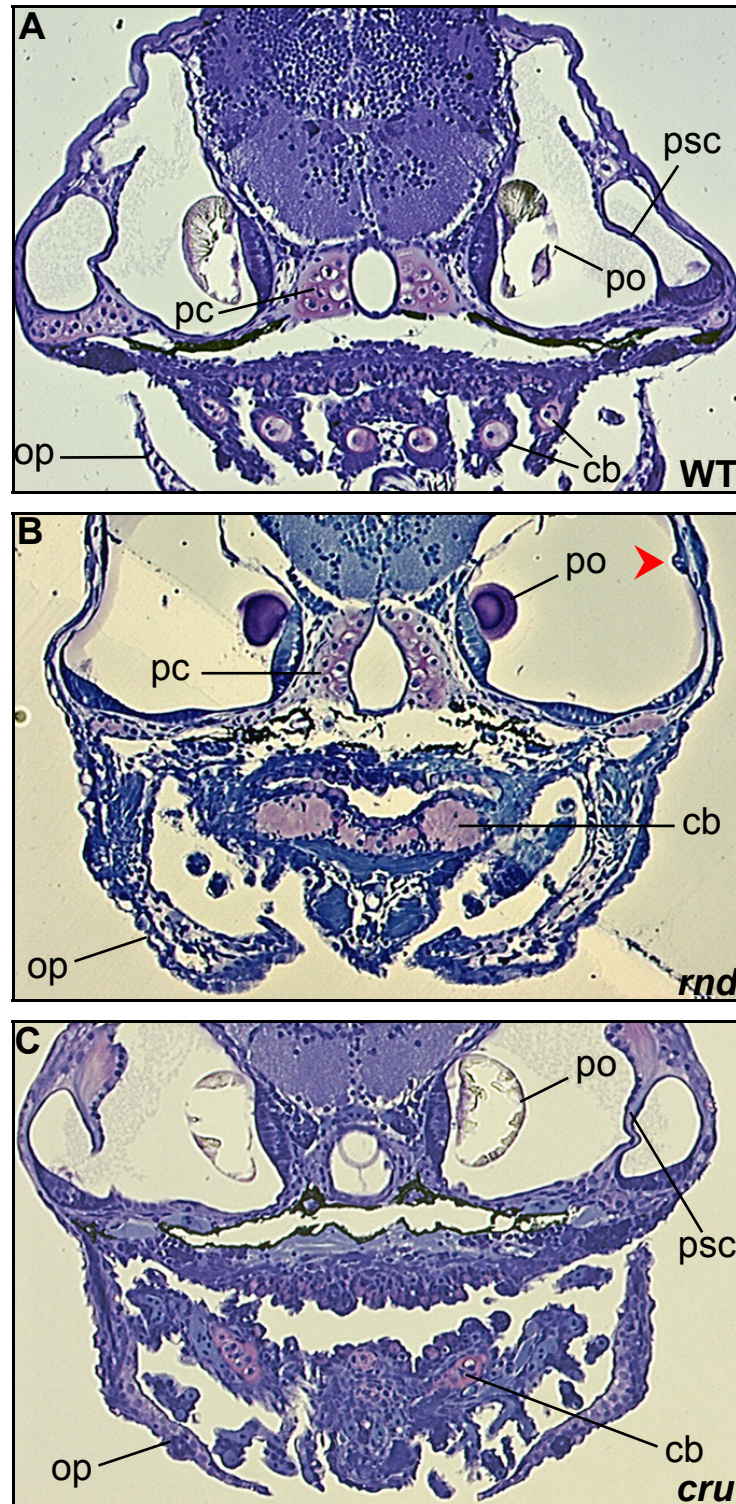


**Figure 29.** Transverse sections of 5 dpf wild-type (A), homozygous *round<sup>m211</sup>* (B) and homozygous *crusher<sup>m299</sup>* (C) mutant embryos. The embryos are sectioned at the level of the posterior otolith in the ear. The cartilage elements of the posterior neurocranium, namely the posterior parachordals and the otic capsule cartilages, most likely are of mesodermal origin. The posterior parachordals of *round<sup>m211</sup>* mutant embryos display a wild-type chondrocyte morphology, unlike all other *round<sup>m211</sup>* cartilage elements. In *crusher<sup>m299</sup>* homozygous embryos, all posterior parachordal and otic capsule cartilage elements are completely absent. The semicircular canals of the ear fail to form in *round<sup>m211</sup>* homozygous embryos (arrowhead).

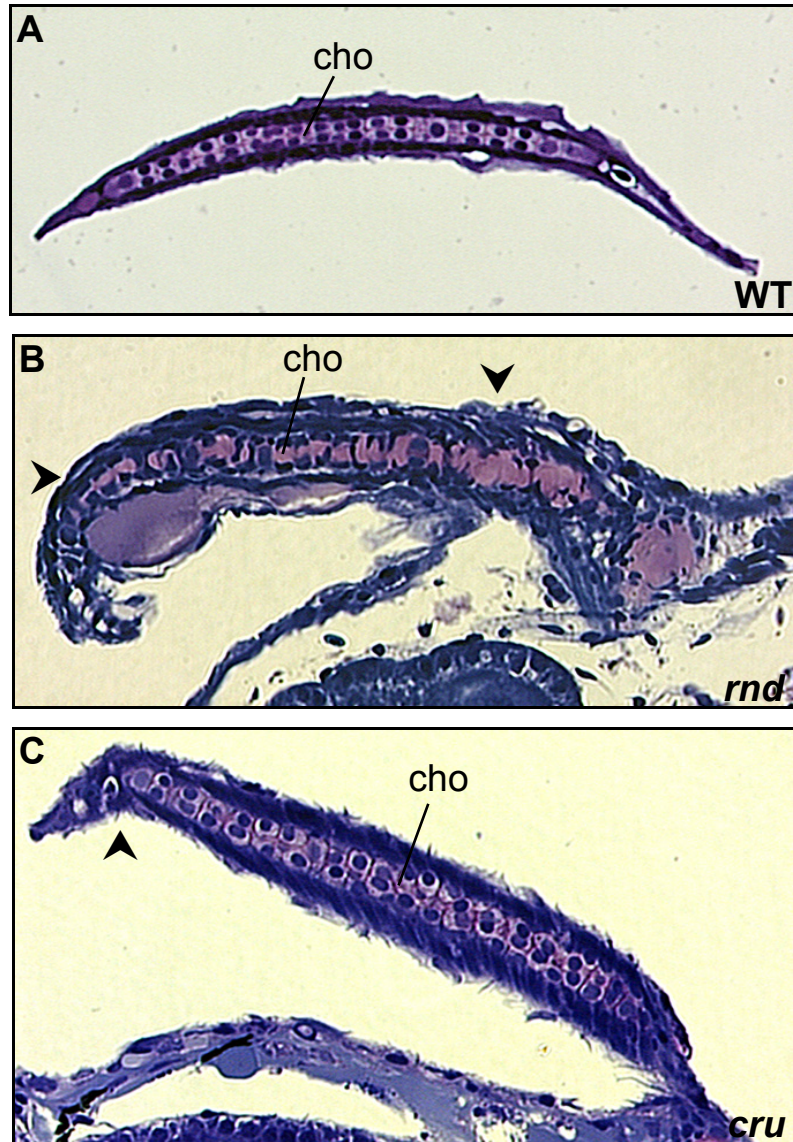


**Figure 30.** Longitudinal sections of pectoral fins in 5 dpf wild-type (A), homozygous *round*<sup>m211</sup> (B) and homozygous *crusher*<sup>m299</sup> (C) mutant embryos. The cartilage plate of wild-type pectoral fins consists of two rows of chondrocytes in a regular stack-of-coin arrangement. The pectoral fins in the *round*<sup>m211</sup> mutant embryos are kinked (arrowheads) and the fin chondrocytes are overloaded with extracellular matrix. In *crusher*<sup>m299</sup> mutant embryos the pectoral fins are also kinked (arrowhead) but exhibit an almost normal chondrocyte morphology.

### 5.3.3 Mapping of the *round*<sup>m211, m641, m715</sup> and *crusher*<sup>m299</sup> mutations

To map the *round*<sup>m211, m641, m715</sup> and *crusher*<sup>m299</sup> mutations I have taken a genetic mapping approach using PCR genotyping of F2 intercrosses with microsatellite markers. I have mapped the loci to small chromosomal intervals, providing the basis for future positional candidate gene cloning attempts. The completion of the zebrafish genome sequencing project will greatly facilitate positional cloning of these genes.

#### 5.3.3.1 The *round*<sup>m211, m641, m715</sup> mutation maps to linkage group 21

The total genome scan for the *round*<sup>m211, m641, m715</sup> mutation provided evidence that the marker Z11574 on LG 21 is linked to the mutation (Figure 31A). Genotyping of single embryos with various microsatellite markers confirmed this chromosomal location (e.g. marker Z22852; Figure 31B).

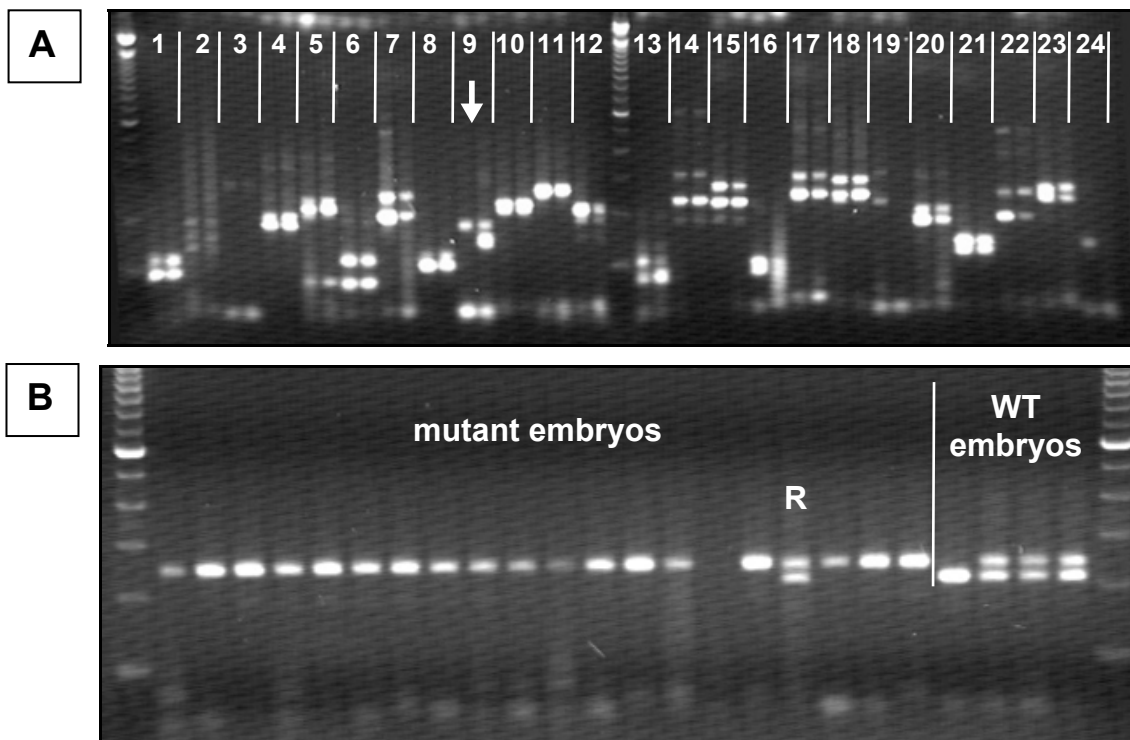


**Figure 31.** Genetic mapping of the *rnd*<sup>m211, m641, m715</sup> mutation. (A) The total genome scan was performed with 144 SSLP markers spaced evenly across the 25 zebrafish linkage groups. The numbers 1-24 represent 24 of these 144 SSLP markers which were tested for linkage to the *rnd*<sup>m211, m641, m715</sup> mutation. Each marker was tested on mutant DNA (left lane) and on wild-type DNA (right lane). The marker number 9 on this gel yields a banding pattern which strongly suggests linkage to the mutation (arrow). This marker Z11574 was subsequently tested on single embryo DNA and shown to be linked to the *rnd*<sup>m211, m641, m715</sup> mutation. (B) Genotyping of single embryos with the SSLP marker Z22852, which is located in close proximity to the *rnd*<sup>m211, m641, m715</sup> mutation. 18 from 20 mutant embryos are non-recombinants (only upper band), 1 mutant embryo is a recombinant (R, recombinant; two bands) and one PCR reaction did not work. From the four control wild-type (WT) embryos, one is a homozygote (only lower band) and three are heterozygotes (two bands).



Genotyping established that the marker Z11574 resides in a genetic distance of 1.12cM to the *round*<sup>m211, m641, m715</sup> locus (nine recombinations in 800 meioses). The critical genetic interval for the *round*<sup>m211, m641, m715</sup> locus is flanked by the microsatellite markers Z67493 and Z22852 and is located near the telomeric region of LG 21 (Figure 32). Genotyping revealed that Z22852 is separated by four recombinations in 800 meioses from the *round*<sup>m211, m641, m715</sup> mutation and is thus the closest available genetic marker, located 0.5cM off the *round*<sup>m211, m641, m715</sup> locus (Figure 31B,32).

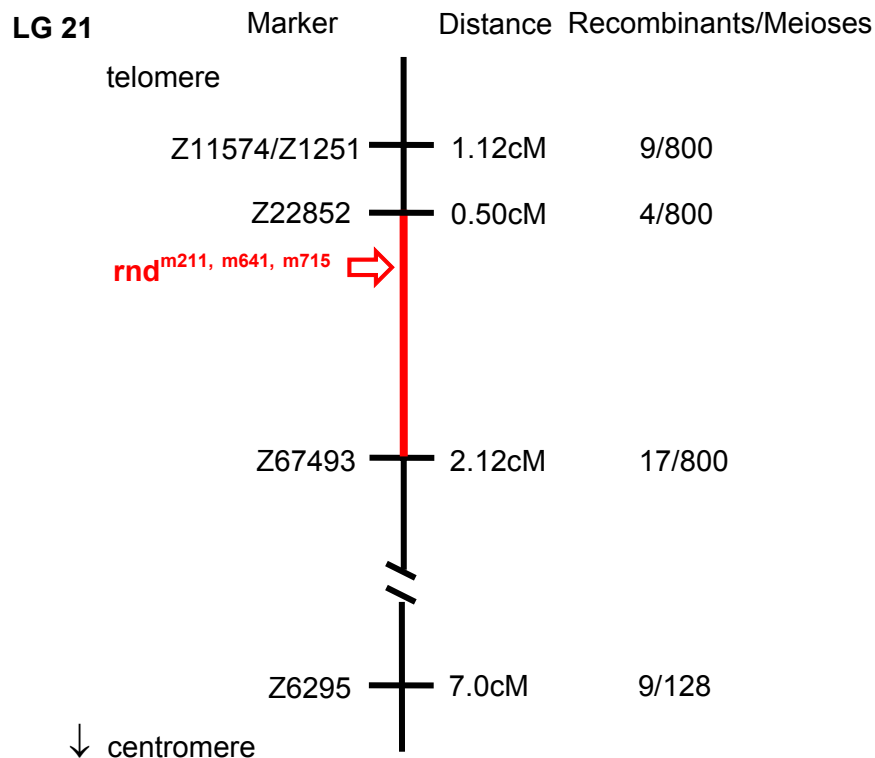


**Figure 32.** Genetic map of the *rnd*<sup>m211, m641, m715</sup> locus on LG 21. The arrow indicates the map position of the *rnd*<sup>m211, m641, m715</sup> locus. The number of recombinants, the number of meioses tested and the resulting genetic distance from the mutated locus are indicated for each genetic marker.

Many microsatellite markers from the region of LG 21 that were tested were not polymorphic in the genetic background of the *round*<sup>m211, m641, m715</sup> F2 intercrosses. This reduced the number of informative markers and hampered the fine mapping process. Moreover, the suppression of recombination events in telomeric chromosomal regions makes positional cloning of mutated loci in these areas difficult; this is because genetic distances obtained based on genetic mapping data translate into larger physical distances than in regions of non-suppressed recombination. Analysis of evolutionary conservation revealed that the *round*<sup>m211, m641, m715</sup> locus resides in a genomic region that does not display clear or extensive conservation of

synteny to genomic regions in the mouse and the human genomes. Thus, the current size of the *round*<sup>m211, m641, m715</sup> critical genetic interval remains at 2.62cM (Figure 32). Identification of the *round*<sup>m211, m641, m715</sup> gene will require a refinement of genetic mapping assisted by the analysis of the upcoming zebrafish genome sequence data.

### 5.3.3.2 Mapping of the *crusher*<sup>m299</sup> mutation

#### 5.3.3.2.1 Genetic mapping of the *crusher*<sup>m299</sup> mutation to linkage group 17

The total genome scan for the *crusher*<sup>m299</sup> mutation yielded the marker Z9831 on LG 17 as a very good candidate. The linkage to this marker was then confirmed by single embryo genotyping experiments. I built a high resolution genetic map of the *cru*<sup>m299</sup> locus, i.e. a map consisting of data based on the analysis of the large number of approximately 1950 meioses. The critical genetic interval for the *cru*<sup>m299</sup> mutation is flanked by the markers Z48508 and Z24082 and has a size of 0.72cM (Figure 33).

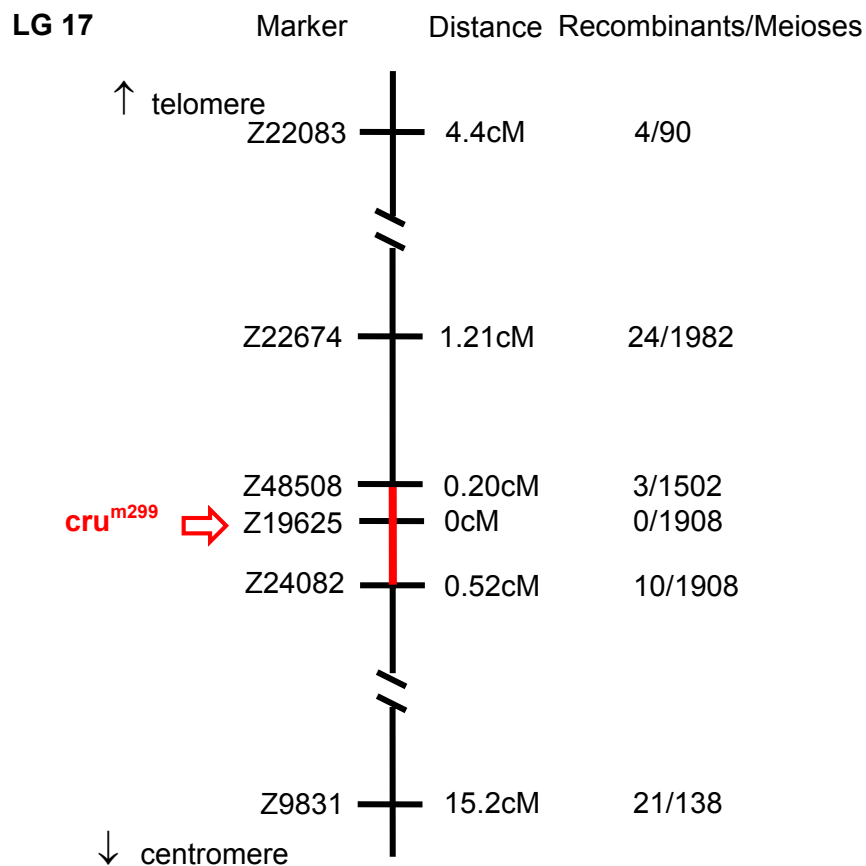


**Figure 33.** Genetic map of the *cru*<sup>m299</sup> mutation on LG 17. The arrow indicates the map position of the *cru*<sup>m299</sup> locus. The number of recombinants, the number of meioses tested and the resulting genetic distance from the mutated locus are indicated for each genetic marker.

The small genetic *cru*<sup>m299</sup> interval on LG 17 is situated in a region of non-suppressed recombination far off the telomere and the centromere and is therefore very well suited for positional cloning experiments. The markers Z22674 and Z24082 yielded 24 plus 10 recombinants in approximately 1950 meioses, respectively. These 34

recombinant embryos were subsequently genotyped with the marker Z19625 in order to determine this marker's relative map position to the *cru*<sup>m299</sup> locus. None of the 34 recombinations from the outer markers separates the marker Z19625 from the *cru*<sup>m299</sup> locus (Figure 33, 34A), showing that this marker is located in very close proximity to the mutated gene. This provided the starting point for physical mapping of the *cru*<sup>m299</sup> mutation.

#### 5.3.3.2.2 Physical mapping of the *crusher*<sup>m299</sup> mutation

Physical mapping aims at the isolation of genomic clones covering the genomic interval that has been determined by genetic mapping experiments. For the *cru*<sup>m299</sup> mutation, overlapping oligonucleotides designed from a unique non-repetitive sequence of the marker Z19625 have been used for screening the Zebrafish PAC BUSM library (RZPD number 706) and the Zebrafish BAC RPCI-71 library (RZPD number 728). Seven clones were identified in a filter hybridization and obtained from the RZPD Resource Center. Only the two clones (BAC RPCIB 728 E0536 and PAC BUSMP 706 L0137) which yielded the strongest hybridization signals could be confirmed by PCR with the marker Z19625 (short designation henceforth: BAC 728 and PAC 706). These two clones were PCR positive for Z19625 and for ESTs which encompass the entire non-repetitive part of this marker. They did not, however, contain any of the other microsatellite markers in this region. End-sequencing of these two clones and PCR amplification of these end sequences on mapcross DNAs were performed to generate new genetic markers for fine mapping. The ends of the PAC 706 clone and one end of the BAC 728 clone were determined to be non-polymorphic between the strains used in the map crosses, but the other BAC 728 end was polymorphic and could be used as a new genetic marker. SSCP analysis with this marker showed that this BAC 728 end shows no recombinations for all the 34 recombinants of the outer microsatellite markers Z22674 and Z24082. Thus, both the marker Z19625 and this BAC 728 STS (sequence tagged site) show no recombinations for the *cru*<sup>m299</sup> mutation in almost 2000 meioses and are very closely linked to the mutation (Figure 34).

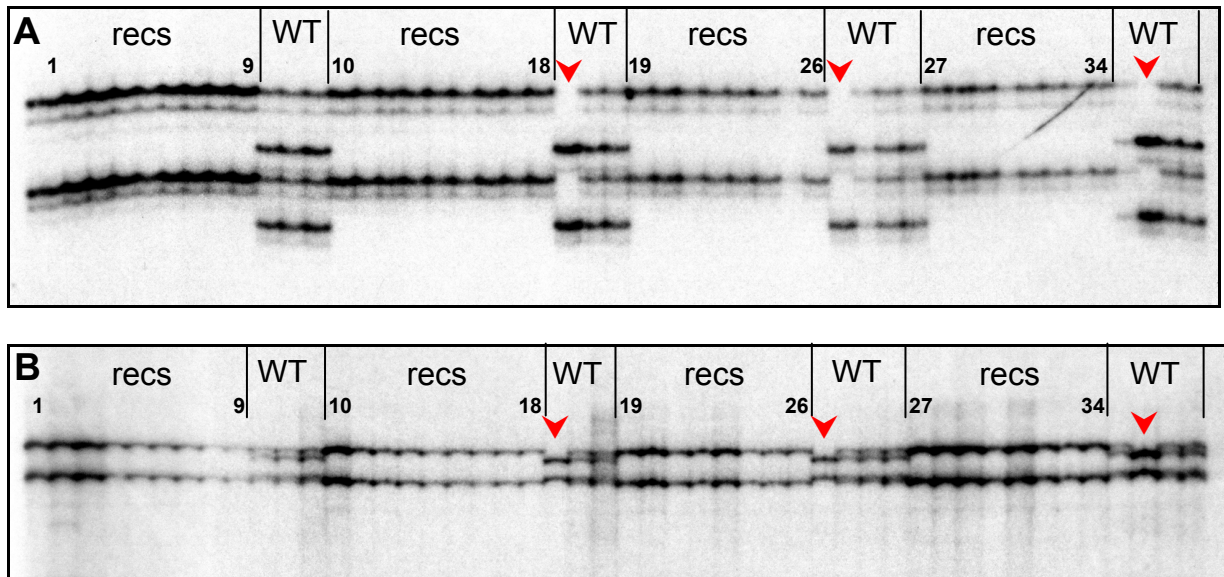


**Figure 34.** Fine mapping of the *cru*<sup>m299</sup> mutation. SSCP analysis of the 34 recombinant animals (recombinants; numbered from 1 to 34) from the flanking markers Z22674 and Z24082. (A) SSCP marker Z19625. (B) BAC 728 STS marker. Both the SSCP marker Z19625 and the BAC 728 STS show no recombination in the 34 recombinants. This is evidenced by the amplification of only the mutant specific allele. The wild-type (WT) specific allele is marked by an arrowhead in the three homozygous wild-type controls. The other wild-type controls are heterozygotes (mutant plus wild-type alleles present).

#### 5.3.3.2.3 The *sec23a* gene is likely to be disrupted by the *crusher*<sup>m299</sup> mutation

The small genetic interval where the *crusher*<sup>m299</sup> mutation was mapped and a partial sequence of the region provided by the Zebrafish Sequencing Project (Sanger Center, UK) were ideally suited for an analysis of evolutionary conservation (synteny) between the zebrafish and other – already sequenced – genomes. Gene order comparison revealed a high degree of synteny to the human genomic region 14q12-q32. I used the non-repetitive sequence of the marker Z19625 to anchor the exact position of the *cru*<sup>m299</sup> mutation. This sequence is similar to the coding sequence of the human signal recognition particle 54kDa (SRP54), that is located at 14q13.1 in the human genome. Several zebrafish ESTs mapped close to Z19625/SRP54 have their orthologues in this genomic region on human chromosome 14 (Table 14).

**Table 14.** ESTs in the *crusher*<sup>m299</sup> critical interval.

Zebrafish EST / <b>SSLP</b> marker	Human orthologous protein	Human map position
<b>Z22674</b>		
fk70a07	Dynein, cytoplasmic, heavy chain 1	14q32
fi34e04	Bromodomain adjacent to zinc finger domain	14q12-q13
<b>Z19625</b>	Signal recognition particle 54kDa SRP54	14q13.1
fi15g03	<b>SEC23 (<i>S. cerevisiae</i>) homolog A; COPII protein</b>	14q13
fc51c09	Heterogeneous nuclear ribonucleoprotein U	1q44
fc43f03+ fi11g07	Retinoblastoma binding protein 1	14q22.1-q22.3
fb07f12	PRELP (proline-arginine-rich end leucine-rich repeat protein)	1q32
<b>Z24082</b>		

Careful consideration of the genes in this region and their potential function directed my attention to the *sec23a* gene (blue font in Table 14). Sec23 is a component of coat protein II (COPII)-coated vesicles that mediate protein transport from the endoplasmic reticulum to the Golgi complex (Hicke and Schekman 1989). This transport mechanism is a prerequisite for the normal deposition of extracellular matrix components that appears to be perturbed in homozygous *cru*<sup>m299</sup> embryos. For this reason, I extracted total RNA from *cru*<sup>m299</sup> mutant embryos and wild-type siblings for further experiments. Sequencing of RT-PCR products from the *cru*<sup>m299</sup> mutant embryos revealed a single nucleotide change predicted to result in a premature stop codon in the *sec23a* gene. The precise structure of the zebrafish *sec23a* gene and the Sec23a protein are not yet known. Thus, comparison to the yeast and human orthologues is necessary to infer the structural and functional consequences of a premature stop codon. Sequence alignments between zebrafish and human sequences yield a 76% identity at the coding sequence level. Sec23 belongs to the Sec23 subfamily within the Sec23/Sec24 protein family. In humans, there are two isoforms, SEC23A and SEC23B (Paccaud et al. 1996). While SEC23A has been shown to be the functional human counterpart of the yeast COPII subunit Sec23p, the function of SEC23B is still unknown. The human SEC23A protein consists of 765 amino acids and contains five domains: An amino-terminal  $\beta$ -barrel, a zinc finger, an  $\alpha/\beta$  trunk domain, an  $\alpha$ -helical region and a carboxy-terminal gelsolin domain (Barlowe 2002; Haucke 2003). The premature stop codon found in the zebrafish *crusher*<sup>m299</sup> *sec23a* coding sequence leads to a truncated Sec23a protein. Alignment

of zebrafish partial coding sequences (including the putative mutation site) and the human full coding sequence revealed that the truncation occurs at a position which corresponds to amino acid number 402 in the human SEC23A protein. The resulting zebrafish *crusher*<sup>m299</sup> mutant protein would lack two domains, the  $\alpha$ -helical domain and the gelsolin domain. It is very well conceivable that the impairment of ER to Golgi vesicle trafficking in zebrafish *crusher*<sup>m299</sup> embryos ultimately results in perturbed cartilage differentiation and morphogenesis processes as are observed in *crusher*<sup>m299</sup> homozygous embryos. I will continue with the verification of the current result that the *crusher*<sup>m299</sup> mutation disrupts the *sec23a* gene and with the cloning of the full length cDNA of the *sec23a* gene.

## 6 Discussion

### 6.1 Zebrafish mutations as models for genetic disorders affecting neural crest and craniofacial development

The work on craniofacial development in vertebrate animal model organisms provides the basis for a better understanding of the pathogenesis of human congenital skeletal diseases. Craniofacial abnormalities comprise a large and heterogeneous group of disorders (Wilkie and Morriss-Kay 2001). Of the approximately 5,000 known human inherited conditions, over 700 lead to craniofacial abnormalities. Zebrafish share a similar neural crest organization with other vertebrate groups, suggesting that they could serve as a good model system for neural crest-related diseases in humans (Schilling 1997).

Characterization of zebrafish mutations affecting pigment cell development has led to the revelation of conserved gene functions throughout evolution. Zebrafish homozygous mutants for the various ENU-induced/spontaneous alleles of the *rose* mutation have a normal embryonic pigment pattern but display a disrupted adult melanophore and iridophore pigment pattern. The *rose* alleles have been shown to disrupt the *endothelin receptor b1* gene (Parichy et al. 2000). The *sox10/courless* gene is required for the specification of the entirety of non-ectomesenchymal neural crest derivatives, including pigment cells, neurons and glial cells (Dutton et al. 2001; Kelsh and Eisen 2000). *colourless* as well as *rose* mutants thus represent zebrafish models for the human congenital disorders Waardenburg-Shah syndrome and Hirschsprung disease. Waardenburg-Shah syndrome combines a reduced enteric nervous system which is the characteristic feature of Hirschsprung disease with reduced pigment cell numbers in skin, hair and iris. These disorders have been shown to be caused by mutations either in the *endothelin-B receptor* gene (*EDNRB*), in the gene for its ligand, *endothelin-3* (*EDN3*), or in the *SOX10* gene (Attie et al. 1995; Edery et al. 1996; Hofstra et al. 1996; Pingault et al. 1998; Puffenberger et al. 1994).

Neural crest gives rise to a very diverse set of derivatives. For this reason, defects in neural crest cell development can also have heterogeneous biological effects as illustrated by DiGeorge (= CATCH 22) syndrome, which encompasses cardiac,



craniofacial and thymus defects, among others (Scambler 2000). It is becoming clear that a large number of genes are involved in neural crest cell development and many of these genes have not yet been identified. In order to diagnose, treat, and prevent neural crest-related diseases, a further understanding of the molecular mechanisms that control neural crest cell development will be necessary. In this regard animal models for specific neural crest associated diseases provide powerful research tools.

## 6.2 Mutations affecting cartilage differentiation:

### *round*<sup>m211, m641, m713, m715</sup> and *crusher*<sup>m299</sup>

The mutations *round*<sup>m211, m641, m713, m715</sup> (henceforth: *round*<sup>m211</sup>) and *crusher*<sup>m299</sup> affect the differentiation and morphogenesis of craniofacial cartilage elements. All neural crest-derived head cartilage elements are present and appropriately positioned. Hence, the *round*<sup>m211</sup> and *crusher*<sup>m299</sup> loci act at later stages than does the *sox9a* gene, which has been shown to be disrupted by the zebrafish ENU-induced mutation *jellyfish* as well as a retroviral insertional *jellyfish* allele (Yan et al. 2002). *jellyfish* mutants fail to produce cartilage elements of the neurocranium, the pharyngeal arches and the pectoral fin skeleton. This phenotype is reminiscent of the human congenital disorder campomelic dysplasia, which is caused by mutations in the human SOX9 gene (Foster et al. 1994; Wagner et al. 1994). Zebrafish Sox9a function is not required for the specification or migration of cranial neural crest cells as evidenced by normal expression patterns of neural crest markers. Prechondrogenic condensations form in *jellyfish* mutants, but the subsequent steps, cartilage differentiation and morphogenesis, fail to occur and thus require functional Sox9a protein. In contrast, the phenotype of *round*<sup>m211</sup> and *crusher*<sup>m299</sup> homozygous embryos is milder than in *jellyfish* homozygous embryos: Chondrocyte differentiation and cartilage morphogenesis take place yet are severely perturbed. In addition, *round*<sup>m211</sup> mutant embryos display defects in pectoral fin cartilage differentiation, otic vesicle morphology and in tail fin fold formation

The pharyngeal skeleton in *round*<sup>m211</sup> and *crusher*<sup>m299</sup> mutants is reduced to a similar extent as in *jekyll* mutants. Embryos homozygous for the ENU-induced *jekyll* mutation are characterized by very weak or absent Alcian blue staining. Histological sections revealed that the cartilaginous pharyngeal arches are present but smaller and lack the metachromatic purple staining surrounding the chondrocytes when

---

stained with Toluidine Blue or its homologue Methylene Blue. This is indicative of a loss of sulfated glycosaminoglycans. *jekyll* is the only zebrafish mutation affecting cartilage differentiation which has been cloned until now. The *jekyll* mutation disrupts a homolog of *Drosophila Sugarless*, a UDP-glucose dehydrogenase (*ugdh*) gene encoding the enzyme required for the conversion of UDP-glucose into UDP-glucuronic acid (Walsh and Stainier 2001). UDP-glucuronic acid is an essential component of the disaccharide units of many glycosaminoglycans such as heparan sulfate, chondroitin sulfate and hyaluronic acid. Glycosaminoglycans are integral constituents of proteoglycans of the extracellular matrix and the *jekyll* mutation interferes with glycosaminoglycan biosynthesis, thus disrupting the production and deposition of normal cartilage matrix proteoglycans.

Although Alcian Blue staining shows poorly defined cartilage rods in *cru*<sup>m299</sup> and *rnd*<sup>m211</sup> mutant embryos, Toluidine Blue staining of histological sections reveals that mutant chondrocytes display an overproduction of extracellular matrix components rich in sulfated glycosaminoglycans. This matrix overproduction is especially pronounced in *round*<sup>m211</sup> mutant chondrocytes where the matrix components accumulate in the cytoplasm. The defects in the *round*<sup>m211</sup> mutation might thus be attributed to perturbations in the control of the biosynthesis of matrix components such as proteoglycans or in mechanisms involved in the export of matrix components.

The cranial neural crest derived cartilage elements of the pharyngeal arches and the anterior neurocranium are present but exhibit defects in cartilage differentiation in *crusher*<sup>m299</sup> homozygous embryos. In contrast, *crusher*<sup>m299</sup> mutant embryos lack the entire posterior parachordal and otic capsule cartilages, which represent the paraxial mesoderm-derived posterior part of the neurocranium (Chibon 1967; Langille and Hall 1986; Le Lievre 1978). Interestingly, these cartilage elements that are absent in the *cru*<sup>m299</sup> mutants are not only present in *rnd*<sup>m211</sup> homozygous embryos but even consist of apparently normal chondrocytes displaying an unaffected morphology. This suggests the presence of different chondrocyte specification/differentiation processes in neural crest-derived and in paraxial mesoderm-derived cartilages. Moreover, the pectoral fin chondrocytes in *cru*<sup>m299</sup> homozygous embryos display an almost normal morphology compared to *rnd*<sup>m211</sup> pectoral fin chondrocytes that exhibit severe

differentiation defects. This argues for the existence of different chondrocyte maturation mechanisms in pectoral fin chondrocytes and chondrocytes of the craniofacial skeleton.

### 6.3 Genetic mapping and cloning of the *round*<sup>m211, m641, m715</sup> and *crusher*<sup>m299</sup> mutations

The *round*<sup>m211, m641, m715</sup> and *crusher*<sup>m299</sup> mutations have been mapped to genetic intervals of 2.62cM (*rnd*<sup>m211, m641, m715</sup>; LG 21) and 0.72cM (*cru*<sup>m299</sup>; LG 17), respectively. The critical interval determined for the *round*<sup>m211, m641, m715</sup> mutation is not syntenic to single blocks in either the mouse or the human genome. This complicates the identification of good candidate genes. Completion of the Zebrafish Genome Sequencing Project will significantly facilitate the identification of the gene that is disrupted by the *round*<sup>m211, m641, m715</sup> mutation.

An excellent candidate gene for the *crusher*<sup>m299</sup> mutation is *sec23a*. ESTs for this gene have been mapped to the *crusher*<sup>m299</sup> critical interval, the human and mouse syntenic regions contain this gene in a comparable location and sequencing revealed a single nucleotide change in the coding sequence of homozygous *crusher*<sup>m299</sup> mutant embryos, predicted to result in a premature stop codon. In yeast (*Saccharomyces cerevisiae*), Sec23 is a component of coat protein II (COPII)-coated vesicles (Hicke and Schekman 1989). COPII-coated vesicles bud from the endoplasmic reticulum (ER) to export newly synthesized proteins to the Golgi complex. A set of three cytosolic components containing five proteins is sufficient to reconstitute the process of ER vesicle formation (Matsuoka et al. 1998). This COPII coat multi-protein complex consists of the small GTPase Sar1p, the Sec23-Sec24 complex and the Sec13-Sec31 complex. GTPase Sar1p recruits the heterodimeric Sec23-Sec24 complex in a first step to generate a Sec23/24-Sar1 prebudding complex. The recruitment of the Sec13-Sec31 heterodimeric complex subsequently leads to vesicle budding. Sec23 and Sec24 proteins comprise five distinct domains: a  $\beta$ -barrel, a zinc finger, an  $\alpha/\beta$  trunk domain forming the heterodimer interface, an  $\alpha$ -helical region and a carboxy-terminal gelsolin module (Barlowe 2002; Haucke 2003). The gelsolin domain is the only domain that does not contribute to the inner surface of the Sec23/24-Sar1 prebudding complex and is thus likely to interact with the Sec13-Sec31 complex (Bi et al. 2002). The truncated protein predicted to result from

the *crusher*<sup>m299</sup> mutation lacks both the  $\alpha$ -helical region and this carboxy-terminal gelsolin domain. Thus it is conceivable that the *crusher*<sup>m299</sup> mutation acts by disruption of COPII-coated vesicle trafficking. Vesicle transport pathways have been shown to be highly conserved from yeast to humans (Mellman and Warren 2000). Nevertheless, although the structure and function of COPII components have been well characterized in terms of biochemistry and genetics in yeast (Kaiser and Schekman 1990; Ramirez et al. 1983), animal models might still reveal unexpected changes in vesicle trafficking mechanisms. Genome and gene duplication events in the vertebrate lineage provided the basis for the appearance of new gene copies with many potential “fates”. For example, vertebrate *Sec23a* and *Sec23b* genes seem to have arisen from an ancestral *Sec23* gene (Paccaud et al. 1996). The new copy might act redundantly to the ancient gene, it might be co-opted by different developmental pathways and hence diverge significantly from the ancestral gene or it might become a non-functional pseudogene. As no metazoan models for impaired COPII-coated vesicle trafficking have been reported, the *crusher*<sup>m299</sup> mutation might represent the first model allowing the dissection of the role of *sec23a* in development. Additional experiments have to be performed in order to verify the preliminary results pointing at *sec23a* representing the *crusher*<sup>m299</sup> gene. These include sequencing of grandparental (GO) strains, of F1 heterozygotes and of F2 progeny in order to confirm the Mendelian segregation of the ENU-induced mutation.

## 6.4 The role of the *mother superior*<sup>m188</sup> gene in neural crest development

To put the findings on the role of the *mos*<sup>m188</sup> mutation in neural crest development in perspective it is indispensable to consider what is already known from the study of additional zebrafish mutations affecting similar neural crest derivatives. I will focus here on the neural crest mutations that have been cloned in the zebrafish and point out important implications and conclusions regarding the function of the *mos*<sup>m188</sup> gene.

The ENU-induced *sucker* mutation specifically affects the development of the lower jaw and other ventral pharyngeal arch cartilage elements. *sucker* corresponds to *endothelin-1*, which encodes a secreted peptide and is expressed in ventral compartments of pharyngeal arch primordia (Miller et al. 2000). Interestingly, the expression is confined to pharyngeal endoderm, surface ectoderm and arch paraxial mesoderm and excludes cranial skeletogenic neural crest. This is in accordance with *endothelin-1* acting as a morphogen along the dorsoventral axis, which is required in the environment of neural crest cells (Kimmel et al. 2003). Different *endothelin-1* levels induce skeletogenic neural crest cells to form the appropriate cartilage elements with respect to position, size and shape. One key downstream target of Endothelin-1 in mediating dorsoventral arch patterning is the bHLH transcription factor *Hand2* (Miller et al. 2003). Expression of both *endothelin-1* and *hand2* will be tested in the future in *mos*<sup>m188</sup> mutant embryos. This might be informative with regard to the fusion of palatoquadrate and hyosymplectic and with regard to the absence of the ceratohyal in *mos*<sup>m188</sup> mutants.

Retinoic acid is involved in many developmental processes and consequently, depriving vertebrate embryos of retinoic acid causes a variety of developmental defects, among them neural crest cell death, the absence of limb buds and posterior branchial arches, abnormalities of facial structures, small somites and hindbrain segmentation defects, which collectively are known as the vitamin A-deficient syndrome (Dickman et al. 1997; Maden et al. 1996; Maden et al. 2000). The effects of retinoic acid are exerted through nuclear receptors which act as ligand-activated transcriptional regulators and have been shown to directly regulate several *Hox* genes (Mangelsdorf et al. 1995). Two zebrafish mutations affecting retinoic acid

biosynthesis recapitulate many aspects of the vitamin A-deficient syndrome. These ENU-induced mutations, *neckless* and *no-fin*, disrupt the gene *raldh2*, encoding the retinaldehyde dehydrogenase 2 that converts retinal to retinoic acid (Begemann et al. 2001; Grandel et al. 2002). The *neckless* and *no-fin* mutants lack the pectoral fins and almost all branchial arch cartilages. Consistent with a phenotype caused by impaired retinoic acid signaling, the two mutations exhibit caudal hindbrain patterning defects and exogenous application of retinoic acid rescues certain aspects of the mutant phenotypes. In both *neckless* and *no-fin*, *dlx2* expression is disrupted specifically in the third (postotic) cranial neural crest stream that will form the branchial cartilages whereas the expression of premigratory neural crest markers such as *snail2* was shown not to be altered. Thus, despite the perturbation of early hindbrain patterning, the onset of defects in neural crest development in *neckless* and *no-fin* mutants appears to be substantially later than in *mos*<sup>m188</sup> mutants which display strongly reduced expression of the neural crest progenitor marker genes *sox9b*, *snail2* and *crestin*. Moreover, *foxD3* expression in *mos*<sup>m188</sup> mutant neural crest progenitor cells is completely abolished whereas the somite expression domain is unaffected, revealing distinct tissue-specific regulation mechanisms. *Pax3* has been shown to act upstream of *FoxD3* in mice and *pax3* expression is unaffected by the *mos*<sup>m188</sup> mutation. These data strongly suggest that the *mos*<sup>m188</sup> gene acts downstream of *pax3* and upstream of *foxD3*, *sox9b* and *snail2*.

A recent study investigated the developmental functions of the zebrafish *bcox* gene encoding the  $\beta,\beta$ -carotene-15,15'-oxygenase, which catalyzes the cleavage of provitamin A to produce retinal, the retinoic acid precursor (Lampert et al. 2003). Morpholino-mediated knockdown of *bcox* function leads to an almost complete absence of branchial arch cartilages whereas pectoral fin cartilage development is only slightly impaired. In situ analysis of *bcox* morphants revealed a mild caudal hindbrain patterning defect, reduced *ap-2 $\alpha$*  expression in cranial neural crest cells and reduced *dlx2* expression in the posterior branchial arch primordia. A common feature of *bcox* morphants and *mos*<sup>m188</sup> mutants is the impairment of an additional neural crest derivative: *bcox* morphants lack iridophores completely, whilst they are significantly reduced in *mos*<sup>m188</sup> mutants. One major difference between the early *bcox* morphants/*neckless/no-fin* and the *mos*<sup>m188</sup> mutant phenotypes is that the *dlx2* expression in *mos*<sup>m188</sup> mutant embryos is altered in all three cranial neural crest

streams whereas in the *bcox* morphants/*neckless/no-fin* the effect is restricted to the postotic stream. However, in *mos*<sup>m188</sup> mutant embryos the postotic stream is affected most severely, resulting in a craniofacial phenotype similar to the mutants and morphants with impaired retinoic acid signaling. In addition, the *mos*<sup>m188</sup> mutation disrupts the appropriate formation of second (hyoid) arch cartilages, whereas first (mandibular) arch derivatives are largely unaffected. This suggests that there are different partially redundant mechanisms controlling the specification of mandibular, hyoid and branchial arch cartilage elements, respectively. Interestingly, the posteriormost branchial arch cartilage elements are present in many *mos*<sup>m188</sup> mutant embryos indicating additional differences in terms of specification among the branchial arches. The *mos*<sup>m188</sup> gene appears to be pivotal for the specification and/or maintenance of skeletogenic neural crest cells of the pharyngeal arches 2-6.

*mos*<sup>m188</sup> mutant embryos exhibit perturbed development of both neural crest derivatives and ectodermal placode derivatives. This is also true for several mutations that disrupt the forkhead gene *foxi1*, affecting the formation of the otic placode, the epibranchial placodes and the pharyngeal arches. These are the spontaneous mutation *hearsay* (Solomon et al. 2003), four *foxi1* alleles (*foo*) generated via retroviral insertional mutagenesis (Nissen et al. 2003) as well as the ENU-induced mutation *no soul* (Lee et al. 2003). The otic placode in mutant embryos is either absent or reduced in size and often it is split into two or more even smaller placodes. In addition, the pharyngeal arches 2, 3 and 4 are affected in the mutants, but the severity differs greatly between the different mutations, corresponding to major differences in *dlx2* expression at the pharyngula stage. The *foxi1* mutant phenotype implies an analogy to the *mos*<sup>m188</sup> mutant phenotype because it encompasses defects in both neural crest and placodal derivatives. Moreover, the postotic cranial neural crest cells migrate adjacent to the otic placode and appropriate migration thus might depend on signals from the otic placode.

The posterior lateral line of *mos*<sup>m188</sup> mutant embryos exhibits supernumerary neuromasts. It is possible that the *mos*<sup>m188</sup> gene independently interferes with neural crest and lateral line placode development. It is conceivable, however, that the neural crest and the placodal derivative defects have a common causative origin. Both neural crest progenitors and cranial ectodermal placodes arise at the neural plate border in immediate vicinity (Baker and Bronner-Fraser 2001). This also holds true for postotic cranial neural crest precursors and the cells of the posterior lateral line

primordium, that are located posterior to the otic placode prior to the onset of migration. Early neural crest marker expression revealed a strong reduction of premigratory and migratory postotic cranial neural crest cells in *mos*<sup>m188</sup> mutant embryos, suggesting defects in either specification or maintenance/survival. It is conceivable that these cells are mis-specified as lateral line primordium cells. This could account for excess cells in the lateral line placode and for the deposition of supernumerary neuromast organs. In-depth analysis of lateral line placode development in *mos*<sup>m188</sup> mutant embryos is required to verify this hypothesis. Furthermore, a detailed analysis of cell death as well as cell lineage tracing experiments employing laser-mediated uncaging of previously injected caged tracer molecules should help to clarify the fate of the cells that fail to be specified as caudal cranial neural crest in *mos*<sup>m188</sup> mutant embryos.

## 6.5 The role of the *foxD3* gene in neural crest development

The winged helix transcription factor FoxD3 has been shown to be involved in neural crest development in a number of species. Misexpression of *FoxD3* in the chicken neural tube leads to a promotion of neural crest cell fate versus neuroepithelial fate (Dottori et al. 2001; Kos et al. 2001). Moreover, *FoxD3* misexpression causes a suppression of interneuron differentiation and a repression of melanoblast development. Studies in *Xenopus* yielded conflicting results. *FoxD3* overexpression leads to an induction of neural crest marker expression and neural crest differentiation in one study (Sasai et al. 2001), whereas it has been shown to prevent neural crest formation in another one (Pohl and Knochel 2001). *FoxD3* overexpressing cells do not migrate or differentiate according to the latter study, whilst in the chick *Foxd3* overexpressing cells emigrate from the neural tube and display a neural crest-like phenotype (Dottori et al. 2001). These results might reflect differences in experimental design as well as interspecies differences in the roles of *FoxD3* in neural crest development. Moreover, they suggest that fine tuning of both the spatial and temporal *FoxD3* expression pattern is crucial for neural crest formation and not yet sufficiently understood.

The *foxD3* gene is an excellent candidate gene for the *mos*<sup>m188</sup> mutation. *FoxD3* expression in zebrafish *mos*<sup>m188</sup> mutant embryos is intriguing, displaying complete



abolishment of *foxD3* transcripts exclusively in all neural crest progenitor cells and in floor plate cells, while the expression in the somites is not affected. The level of *foxD3* expression in neural crest progenitors is genotype-dependent, suggesting that in these cells the *foxD3* gene is subject to autoregulation, requiring its own functional gene product for transcription. Sequence analyses of F2 *mos*<sup>m188</sup> siblings revealed a potential mutation A→T within the coding sequence of *foxD3*, leading to a substitution of serine 62 for cysteine in the acidic domain of the foxD3 protein. This region was sequenced in 10 homozygous *mos*<sup>m188</sup> embryos and in 10 wild-type embryos and the results were fully consistent with this A→T transversion representing the *mos*<sup>m188</sup> mutation disrupting the function of the *foxD3* gene. Genetic mapping, however, placed the *foxD3* gene in a distance of 0.03cM to the *mos*<sup>m188</sup> gene (1 recombinant in 3134 meioses). Hence, if the polymorphic A/T site represents a SNP that cosegregates with the *mos*<sup>m188</sup> mutation, extensive sequencing of F2 *mos*<sup>m188</sup> sibling animals might fail to distinguish between an ENU-induced mutation and a SNP.

Additionally we have to take into account the possibility of a cis-regulatory mutation in *foxD3* that would also comply with the genotype-dependent *foxD3* expression levels. The A/T polymorphism cosegregating with the *mos*<sup>m188</sup> mutation allows to perform an experiment which will distinguish between the two hypotheses of the *mos*<sup>m188</sup> mutation representing a cis-regulatory mutation in *foxD3* versus the *mos*<sup>m188</sup> mutation disrupting the coding sequence of *foxD3* or a gene upstream of *foxD3*. This experiment consists of surveying which of the polymorphic alleles are expressed in *mos*<sup>m188</sup> heterozygous embryos. If the *mos*<sup>m188</sup> mutation is in a cis-regulatory region of *foxD3*, then the expression of the cosegregating T allele is shut down and only the A allele is expressed. If the *mos*<sup>m188</sup> mutation is not in a cis-regulatory region of *foxD3*, then in heterozygotes both alleles will be expressed at lower levels than in wild-type homozygotes.

Targeted knockdown of *foxD3* function with morpholino antisense oligonucleotides generates a phenocopy of the main aspects of the *mos*<sup>m188</sup> phenotype. These experiments revealed that *foxD3* morphants fail to appropriately form neural crest derivatives such as branchial arch cartilages, iridophores, enteric neurons and dorsal root ganglia. The derivatives of the postotic cranial neural crest stream were affected

in a manner equivalent to the *mos*<sup>m188</sup> mutation whereas the second stream derivatives of the second pharyngeal arch were only mildly affected. In compliance with this, *foxD3* morphants display severe perturbation of the postotic cranial neural crest expression domains of the neural crest specific genes *val*, *krox-20* and *dlx2*, while the anterior cranial neural crest streams are only slightly impaired. Hence, it is beyond question that the zebrafish *foxD3* gene plays a pivotal role in neural crest cell specification or maintenance. If not disrupted by the *mos*<sup>m188</sup> mutation, *foxD3* acts in a pathway downstream of the *mos*<sup>m188</sup> gene and may well be the principal mediator of *mos*<sup>m188</sup> gene function in neural crest progenitor cells.

In the mouse *FoxD3* has been shown to be required for the maintenance of pluripotent embryonic progenitor cells (Hanna et al. 2002). *FoxD3* *-/-* mouse embryos die shortly after implantation. Thus, conditional knockout approaches will be necessary to address the roles of *FoxD3* in mammalian neural crest development. Since neural crest cells comprise a population of pluripotent progenitor cells, it is conceivable that *FoxD3* performs similar tasks in neural crest development and in early mammalian development. The zebrafish *mos*<sup>m188</sup> mutation represents a model system that allows to study neural crest development in the complete absence of *foxD3* gene expression. The results suggest that zebrafish *foxD3* indeed is required for the specification and/or maintenance of subsets of neural crest progenitor cells that give rise to both ectomesenchymal (craniofacial cartilage) and non-ectomesenchymal (pigment cells, enteric neurons, dorsal root ganglia) derivatives.

## 7 Summary

The mechanisms of neural crest specification and cartilage differentiation are not well understood. To address these issues, molecular and functional characterizations of four ENU-induced zebrafish mutations affecting craniofacial development - *brk* (*brk*<sup>m452</sup>), *mother superior* (*mos*<sup>m188</sup>), *round* (*rnd*<sup>m211, m641, m713, m715</sup>) and *crusher* (*cru*<sup>m299</sup>) - have been conducted. The mutations *rnd*<sup>m211</sup> and *cru*<sup>m299</sup> affect differentiation and morphogenesis of craniofacial cartilages. Extensive histological analyses revealed that the chondrocytes in *rnd*<sup>m211</sup> and *cru*<sup>m299</sup> homozygous mutants share an increase in the synthesis of extracellular matrix components but display a quite different cell morphology. Using a bulked segregant genetic mapping approach, I mapped the *rnd*<sup>m211, m641, m715</sup>, *cru*<sup>m299</sup> and *brk*<sup>m452</sup> mutations to small genetic intervals on the zebrafish linkage groups 21, 17 and 14, respectively. This provides the basis for future positional candidate cloning of the underlying loci. Preliminary evidence suggests that the *crusher*<sup>m299</sup> mutation disrupts the *sec23a* gene encoding a subunit of coat protein II (COPII)-coated vesicles. COPII-coated vesicles mediate trafficking of newly synthesized proteins from the endoplasmic reticulum to the Golgi complex. The *mos*<sup>m188</sup> mutation causes an extensive loss of craniofacial cartilages of the pharyngeal arches. Here, I demonstrate that several additional neural crest derivatives are affected by the *mos*<sup>m188</sup> mutation. These comprise pigment cells (mainly iridophores), enteric neurons and dorsal root ganglia. Moreover, lateral line placode development is impaired, leading to the presence of supernumerary neuromast organs in *mos*<sup>m188</sup> homozygous embryos. Gene expression analyses revealed that the formation of cranial neural crest streams is severely perturbed in *mos*<sup>m188</sup> mutant embryos and is preceded by diminished expression of key genes in neural crest progenitor cells. Interestingly, the expression of the transcription factor *foxD3* in cranial and trunk neural crest progenitors is completely abolished in *mos*<sup>m188</sup> mutant embryos. Furthermore, targeted gene knockdown of *foxD3* using morpholino antisense oligonucleotides resulted in a phenocopy of many aspects of the *mos*<sup>m188</sup> mutation. Genetic fine mapping placed the *foxD3* gene in a distance of only 0.03cM to the *mos*<sup>m188</sup> mutation. Taken together, these data provide strong evidence that the *mos*<sup>m188</sup> gene and *foxD3* are required for the specification and/or maintenance of subsets of ectomesenchymal and non-ectomesenchymal neural crest progenitors.

## 8 Bibliography

- Akimenko, M. A., Ekker, M., Wegner, J., Lin, W. and Westerfield, M. (1994). "Combinatorial expression of three zebrafish genes related to distal-less: part of a homeobox gene code for the head." *J Neurosci* **14**(6): 3475-86.
- Andermann, P., Ungos, J. and Raible, D. W. (2002). "Neurogenin1 defines zebrafish cranial sensory ganglia precursors." *Dev Biol* **251**(1): 45-58.
- Arikawa-Hirasawa, E., Watanabe, H., Takami, H., Hassell, J. R. and Yamada, Y. (1999). "Perlecan is essential for cartilage and cephalic development." *Nat Genet* **23**(3): 354-8.
- Arikawa-Hirasawa, E., Wilcox, W. R., Le, A. H., Silverman, N., Govindraj, P., Hassell, J. R. and Yamada, Y. (2001). "Dyssegmental dysplasia, Silverman-Handmaker type, is caused by functional null mutations of the perlecan gene." *Nat Genet* **27**(4): 431-4.
- Attie, T., Till, M., Pelet, A., Amiel, J., Edery, P., Boutrand, L., Munnich, A. and Lyonnet, S. (1995). "Mutation of the endothelin-receptor B gene in Waardenburg-Hirschsprung disease." *Hum Mol Genet* **4**(12): 2407-9.
- Baker, C. V. and Bronner-Fraser, M. (2001). "Vertebrate cranial placodes I. Embryonic induction." *Dev Biol* **232**(1): 1-61.
- Barlowe, C. (2002). "Three-dimensional structure of a COPII prebudding complex." *Dev Cell* **3**(4): 467-8.
- Begbie, J., Brunet, J. F., Rubenstein, J. L. and Graham, A. (1999). "Induction of the epibranchial placodes." *Development* **126**(5): 895-902.
- Begemann, G., Schilling, T. F., Rauch, G. J., Geisler, R. and Ingham, P. W. (2001). "The zebrafish neckless mutation reveals a requirement for raldh2 in mesodermal signals that pattern the hindbrain." *Development* **128**(16): 3081-94.
- Bi, X., Corpina, R. A. and Goldberg, J. (2002). "Structure of the Sec23/24-Sar1 prebudding complex of the COPII vesicle coat." *Nature* **419**(6904): 271-7.
- Cano, A., Perez-Moreno, M. A., Rodrigo, I., Locascio, A., Blanco, M. J., del Barrio, M. G., Portillo, F. and Nieto, M. A. (2000). "The transcription factor snail controls epithelial-mesenchymal transitions by repressing E-cadherin expression." *Nat Cell Biol* **2**(2): 76-83.
- Chen, L., Li, C., Qiao, W., Xu, X. and Deng, C. (2001). "A Ser(365)-->Cys mutation of fibroblast growth factor receptor 3 in mouse downregulates Ihh/PTHrP signals and causes severe achondroplasia." *Hum Mol Genet* **10**(5): 457-65.
- Chibon, P. (1967). "[Nuclear labelling by tritiated thymidine of neural crest derivatives in the amphibian Urodele *Pleurodeles waltlii* Michah]." *J Embryol Exp Morphol* **18**(3): 343-58.
- Cooke, J., Moens, C., Roth, L., Durbin, L., Shiomi, K., Brennan, C., Kimmel, C., Wilson, S. and Holder, N. (2001). "Eph signalling functions downstream of Val to regulate cell sorting and boundary formation in the caudal hindbrain." *Development* **128**(4): 571-80.
- Cornell, R. A. and Eisen, J. S. (2000). "Delta signaling mediates segregation of neural crest and spinal sensory neurons from zebrafish lateral neural plate." *Development* **127**(13): 2873-82.
- Couly, G. F., Coltey, P. M. and Le Douarin, N. M. (1993). "The triple origin of skull in higher vertebrates: a study in quail-chick chimeras." *Development* **117**(2): 409-29.

- David, N. B., Saint-Etienne, L., Tsang, M., Schilling, T. F. and Rosa, F. M. (2002). "Requirement for endoderm and FGF3 in ventral head skeleton formation." Development **129**(19): 4457-68.
- DeLise, A. M., Fischer, L. and Tuan, R. S. (2000). "Cellular interactions and signaling in cartilage development." Osteoarthritis Cartilage **8**(5): 309-34.
- Dickman, E. D., Thaller, C. and Smith, S. M. (1997). "Temporally-regulated retinoic acid depletion produces specific neural crest, ocular and nervous system defects." Development **124**(16): 3111-21.
- Dottori, M., Gross, M. K., Labosky, P. and Goulding, M. (2001). "The winged-helix transcription factor Foxd3 suppresses interneuron differentiation and promotes neural crest cell fate." Development **128**(21): 4127-38.
- Driever, W., Solnica-Krezel, L., Schier, A. F., Neuhauss, S. C., Malicki, J., Stemple, D. L., Stainier, D. Y., Zwartkruis, F., Abdelilah, S., Rangini, Z., Belak, J. and Boggs, C. (1996). "A genetic screen for mutations affecting embryogenesis in zebrafish." Development **123**: 37-46.
- Dutton, K. A., Pauliny, A., Lopes, S. S., Elworthy, S., Carney, T. J., Rauch, J., Geisler, R., Haffter, P. and Kelsh, R. N. (2001). "Zebrafish colourless encodes sox10 and specifies non-ectomesenchymal neural crest fates." Development **128**(21): 4113-25.
- Edey, P., Attie, T., Amiel, J., Pelet, A., Eng, C., Hofstra, R. M., Martelli, H., Bidaud, C., Munnich, A. and Lyonnet, S. (1996). "Mutation of the endothelin-3 gene in the Waardenburg-Hirschsprung disease (Shah-Waardenburg syndrome)." Nat Genet **12**(4): 442-4.
- Favor, J. (1999). "Mechanisms of mutation induction in germ cells of the mouse as assessed by the specific locus test." Mutat Res **428**(1-2): 227-36.
- Foster, J. W., Dominguez-Steglich, M. A., Guioli, S., Kowk, G., Weller, P. A., Stevanovic, M., Weissenbach, J., Mansour, S., Young, I. D., Goodfellow, P. N. and et al. (1994). "Campomelic dysplasia and autosomal sex reversal caused by mutations in an SRY-related gene." Nature **372**(6506): 525-30.
- Gendron-Maguire, M., Mallo, M., Zhang, M. and Gridley, T. (1993). "Hoxa-2 mutant mice exhibit homeotic transformation of skeletal elements derived from cranial neural crest." Cell **75**(7): 1317-31.
- Gilmour, D. T., Maischein, H. M. and Nusslein-Volhard, C. (2002). "Migration and function of a glial subtype in the vertebrate peripheral nervous system." Neuron **34**(4): 577-88.
- Gompel, N., Cubedo, N., Thisse, C., Thisse, B., Dambly-Chaudiere, C. and Ghysen, A. (2001). "Pattern formation in the lateral line of zebrafish." Mech Dev **105**(1-2): 69-77.
- Graham, A., Heyman, I. and Lumsden, A. (1993). "Even-numbered rhombomeres control the apoptotic elimination of neural crest cells from odd-numbered rhombomeres in the chick hindbrain." Development **119**(1): 233-45.
- Graham, A. and Smith, A. (2001). "Patterning the pharyngeal arches." Bioessays **23**(1): 54-61.
- Grandel, H., Lun, K., Rauch, G. J., Rhinn, M., Piotrowski, T., Houart, C., Sordino, P., Kuchler, A. M., Schulte-Merker, S., Geisler, R., Holder, N., Wilson, S. W. and Brand, M. (2002). "Retinoic acid signalling in the zebrafish embryo is necessary during pre-segmentation stages to pattern the anterior-posterior axis of the CNS and to induce a pectoral fin bud." Development **129**(12): 2851-65.
- Haffter, P., Granato, M., Brand, M., Mullins, M. C., Hammerschmidt, M., Kane, D. A., Odenthal, J., van Eeden, F. J., Jiang, Y. J., Heisenberg, C. P., Kelsh, R. N.,

- Furutani-Seiki, M., Vogelsang, E., Beuchle, D., Schach, U., Fabian, C. and Nusslein-Volhard, C. (1996). "The identification of genes with unique and essential functions in the development of the zebrafish, *Danio rerio*." Development **123**: 1-36.
- Hall, B. K. and Miyake, T. (2000). "All for one and one for all: condensations and the initiation of skeletal development." Bioessays **22**(2): 138-47.
- Hanna, L. A., Foreman, R. K., Tarasenko, I. A., Kessler, D. S. and Labosky, P. A. (2002). "Requirement for *Foxd3* in maintaining pluripotent cells of the early mouse embryo." Genes Dev **16**(20): 2650-61.
- Haucke, V. (2003). "Vesicle budding: a coat for the COPs." Trends Cell Biol **13**(2): 59-60.
- Hicke, L. and Schekman, R. (1989). "Yeast *Sec23p* acts in the cytoplasm to promote protein transport from the endoplasmic reticulum to the Golgi complex in vivo and in vitro." Embo J **8**(6): 1677-84.
- Hofstra, R. M., Osinga, J., Tan-Sindhunata, G., Wu, Y., Kamsteeg, E. J., Stulp, R. P., van Ravenswaaij-Arts, C., Majoor-Krakauer, D., Angrist, M., Chakravarti, A., Meijers, C. and Buys, C. H. (1996). "A homozygous mutation in the endothelin-3 gene associated with a combined Waardenburg type 2 and Hirschsprung phenotype (Shah-Waardenburg syndrome)." Nat Genet **12**(4): 445-7.
- Holland, L. Z. and Holland, N. D. (1996). "Expression of *AmphiHox-1* and *AmphiPax-1* in amphioxus embryos treated with retinoic acid: insights into evolution and patterning of the chordate nerve cord and pharynx." Development **122**(6): 1829-38.
- Hunt, P., Gulisano, M., Cook, M., Sham, M. H., Faiella, A., Wilkinson, D., Boncinelli, E. and Krumlauf, R. (1991). "A distinct *Hox* code for the branchial region of the vertebrate head." Nature **353**(6347): 861-4.
- Hunter, M. P. and Prince, V. E. (2002). "Zebrafish *hox* paralogue group 2 genes function redundantly as selector genes to pattern the second pharyngeal arch." Dev Biol **247**(2): 367-89.
- Kaiser, C. A. and Schekman, R. (1990). "Distinct sets of *SEC* genes govern transport vesicle formation and fusion early in the secretory pathway." Cell **61**(4): 723-33.
- Kelsh, R. N. and Eisen, J. S. (2000). "The zebrafish colourless gene regulates development of non-ectomesenchymal neural crest derivatives." Development **127**(3): 515-25.
- Kelsh, R. N., Schmid, B. and Eisen, J. S. (2000). "Genetic analysis of melanophore development in zebrafish embryos." Dev Biol **225**(2): 277-93.
- Kimmel, C. B., Miller, C. T., Kruze, G., Ullmann, B., BreMiller, R. A., Larison, K. D. and Snyder, H. C. (1998). "The shaping of pharyngeal cartilages during early development of the zebrafish." Dev Biol **203**(2): 245-63.
- Kimmel, C. B., Miller, C. T. and Moens, C. B. (2001). "Specification and morphogenesis of the zebrafish larval head skeleton." Dev Biol **233**(2): 239-57.
- Kimmel, C. B., Ullmann, B., Walker, M., Miller, C. T. and Crump, J. G. (2003). "Endothelin 1-mediated regulation of pharyngeal bone development in zebrafish." Development **130**(7): 1339-51.
- Knapik, E. W. (2000). "ENU mutagenesis in zebrafish--from genes to complex diseases." Mamm Genome **11**(7): 511-9.
- Knapik, E. W., Goodman, A., Atkinson, O. S., Roberts, C. T., Shiozawa, M., Sim, C. U., Weksler-Zangen, S., Trolliet, M. R., Futrell, C., Innes, B. A., Koike, G.,

- McLaughlin, M. G., Pierre, L., Simon, J. S., Vilallonga, E., Roy, M., Chiang, P. W., Fishman, M. C., Driever, W. and Jacob, H. J. (1996). "A reference cross DNA panel for zebrafish (*Danio rerio*) anchored with simple sequence length polymorphisms." Development **123**: 451-60.
- Knapik, E. W., Goodman, A., Ekker, M., Chevrette, M., Delgado, J., Neuhaus, S., Shimoda, N., Driever, W., Fishman, M. C. and Jacob, H. J. (1998). "A microsatellite genetic linkage map for zebrafish (*Danio rerio*)." Nat Genet **18**(4): 338-43.
- Knecht, A. K. and Bronner-Fraser, M. (2002). "Induction of the neural crest: a multigene process." Nat Rev Genet **3**(6): 453-61.
- Knudson, C. B. and Knudson, W. (2001). "Cartilage proteoglycans." Semin Cell Dev Biol **12**(2): 69-78.
- Kos, R., Reedy, M. V., Johnson, R. L. and Erickson, C. A. (2001). "The winged-helix transcription factor FoxD3 is important for establishing the neural crest lineage and repressing melanogenesis in avian embryos." Development **128**(8): 1467-79.
- Kuratani, S. (1997). "Spatial distribution of postotic crest cells defines the head/trunk interface of the vertebrate body: embryological interpretation of peripheral nerve morphology and evolution of the vertebrate head." Anat Embryol (Berl) **195**(1): 1-13.
- Lampert, J. M., Holzschuh, J., Hessel, S., Driever, W., Vogt, K. and Von Lintig, J. (2003). "Provitamin A conversion to retinal via the beta,beta-carotene-15,15'-oxygenase (bcox) is essential for pattern formation and differentiation during zebrafish embryogenesis." Development **130**(10): 2173-86.
- Lander, A. D. and Selleck, S. B. (2000). "The elusive functions of proteoglycans: in vivo veritas." J Cell Biol **148**(2): 227-32.
- Langille, R. M. and Hall, B. K. (1986). "Evidence of cranial neural crest contribution to the skeleton of the sea lamprey, *Petromyzon marinus*." Prog Clin Biol Res **217B**: 263-6.
- Le Lievre, C. S. (1978). "Participation of neural crest-derived cells in the genesis of the skull in birds." J Embryol Exp Morphol **47**: 17-37.
- Lee, S. A., Shen, E. L., Fiser, A., Sali, A. and Guo, S. (2003). "The zebrafish forkhead transcription factor Foxi1 specifies epibranchial placode-derived sensory neurons." Development **130**(12): 2669-2679.
- Li, M., Zhao, C., Wang, Y., Zhao, Z. and Meng, A. (2002). "Zebrafish sox9b is an early neural crest marker." Dev Genes Evol **212**(4): 203-6.
- Li, Y. X., Zdanowicz, M., Young, L., Kumiski, D., Leatherbury, L. and Kirby, M. L. (2003). "Cardiac neural crest in zebrafish embryos contributes to myocardial cell lineage and early heart function." Dev Dyn **226**(3): 540-50.
- Lister, J. A., Robertson, C. P., Lepage, T., Johnson, S. L. and Raible, D. W. (1999). "nacre encodes a zebrafish microphthalmia-related protein that regulates neural-crest-derived pigment cell fate." Development **126**(17): 3757-67.
- Liu, J. P. and Jessell, T. M. (1998). "A role for rhoB in the delamination of neural crest cells from the dorsal neural tube." Development **125**(24): 5055-67.
- Liu, T. X., Zhou, Y., Kanki, J. P., Deng, M., Rhodes, J., Yang, H. W., Sheng, X. M., Zon, L. I. and Look, A. T. (2002). "Evolutionary conservation of zebrafish linkage group 14 with frequently deleted regions of human chromosome 5 in myeloid malignancies." Proc Natl Acad Sci U S A **99**(9): 6136-41.
- Lumsden, A. and Keynes, R. (1989). "Segmental patterns of neuronal development in the chick hindbrain." Nature **337**(6206): 424-8.

- Lumsden, A., Sprawson, N. and Graham, A. (1991). "Segmental origin and migration of neural crest cells in the hindbrain region of the chick embryo." Development **113**(4): 1281-91.
- Luo, R., An, M., Arduini, B. L. and Henion, P. D. (2001). "Specific pan-neural crest expression of zebrafish Crestin throughout embryonic development." Dev Dyn **220**(2): 169-74.
- Ma, L., Golden, S., Wu, L. and Maxson, R. (1996). "The molecular basis of Boston-type craniosynostosis: the Pro148-->His mutation in the N-terminal arm of the MSX2 homeodomain stabilizes DNA binding without altering nucleotide sequence preferences." Hum Mol Genet **5**(12): 1915-20.
- Maconochie, M., Krishnamurthy, R., Nonchev, S., Meier, P., Manzanares, M., Mitchell, P. J. and Krumlauf, R. (1999). "Regulation of Hoxa2 in cranial neural crest cells involves members of the AP-2 family." Development **126**(7): 1483-94.
- Maden, M., Gale, E., Kostetskii, I. and Zile, M. (1996). "Vitamin A-deficient quail embryos have half a hindbrain and other neural defects." Curr Biol **6**(4): 417-26.
- Maden, M., Graham, A., Zile, M. and Gale, E. (2000). "Abnormalities of somite development in the absence of retinoic acid." Int J Dev Biol **44**(1 Spec No): 151-9.
- Mangelsdorf, D. J., Thummel, C., Beato, M., Herrlich, P., Schutz, G., Umesono, K., Blumberg, B., Kastner, P., Mark, M., Chambon, P. and et al. (1995). "The nuclear receptor superfamily: the second decade." Cell **83**(6): 835-9.
- Matsuoka, K., Orci, L., Amherdt, M., Bednarek, S. Y., Hamamoto, S., Schekman, R. and Yeung, T. (1998). "COPII-coated vesicle formation reconstituted with purified coat proteins and chemically defined liposomes." Cell **93**(2): 263-75.
- McGinnis, W. and Krumlauf, R. (1992). "Homeobox genes and axial patterning." Cell **68**(2): 283-302.
- Mellman, I. and Warren, G. (2000). "The road taken: past and future foundations of membrane traffic." Cell **100**(1): 99-112.
- Michelmore, R. W., Paran, I. and Kesseli, R. V. (1991). "Identification of markers linked to disease-resistance genes by bulked segregant analysis: a rapid method to detect markers in specific genomic regions by using segregating populations." Proc Natl Acad Sci U S A **88**(21): 9828-32.
- Miller, C. T., Schilling, T. F., Lee, K., Parker, J. and Kimmel, C. B. (2000). "sucker encodes a zebrafish Endothelin-1 required for ventral pharyngeal arch development." Development **127**(17): 3815-28.
- Miller, C. T., Yelon, D., Stainier, D. Y. and Kimmel, C. B. (2003). "Two endothelin 1 effectors, hand2 and bapx1, pattern ventral pharyngeal cartilage and the jaw joint." Development **130**(7): 1353-65.
- Moens, C. B., Cordes, S. P., Giorgianni, M. W., Barsh, G. S. and Kimmel, C. B. (1998). "Equivalence in the genetic control of hindbrain segmentation in fish and mouse." Development **125**(3): 381-91.
- Moens, C. B., Yan, Y. L., Appel, B., Force, A. G. and Kimmel, C. B. (1996). "valentino: a zebrafish gene required for normal hindbrain segmentation." Development **122**(12): 3981-90.
- Mullins, M. C., Hammerschmidt, M., Haffter, P. and Nusslein-Volhard, C. (1994). "Large-scale mutagenesis in the zebrafish: in search of genes controlling development in a vertebrate." Curr Biol **4**(3): 189-202.
- Nasevicius, A. and Ekker, S. C. (2000). "Effective targeted gene 'knockdown' in zebrafish." Nat Genet **26**(2): 216-20.



- Neuhauss, S. C., Solnica-Krezel, L., Schier, A. F., Zwartkruis, F., Stemple, D. L., Malicki, J., Abdelilah, S., Stainier, D. Y. and Driever, W. (1996). "Mutations affecting craniofacial development in zebrafish." Development **123**: 357-67.
- Nissen, R. M., Yan, J., Amsterdam, A., Hopkins, N. and Burgess, S. M. (2003). "Zebrafish foxi one modulates cellular responses to Fgf signaling required for the integrity of ear and jaw patterning." Development **130**(11): 2543-54.
- Noden, D. M. (1988). "Interactions and fates of avian craniofacial mesenchyme." Development **103**(Suppl): 121-40.
- Odenthal, J. and Nusslein-Volhard, C. (1998). "fork head domain genes in zebrafish." Dev Genes Evol **208**(5): 245-58.
- Paccaud, J. P., Reith, W., Carpentier, J. L., Ravazzola, M., Amherdt, M., Schekman, R. and Orci, L. (1996). "Cloning and functional characterization of mammalian homologues of the COPII component Sec23." Mol Biol Cell **7**(10): 1535-46.
- Parichy, D. M., Mellgren, E. M., Rawls, J. F., Lopes, S. S., Kelsh, R. N. and Johnson, S. L. (2000). "Mutational analysis of endothelin receptor b1 (rose) during neural crest and pigment pattern development in the zebrafish *Danio rerio*." Dev Biol **227**(2): 294-306.
- Parichy, D. M., Rawls, J. F., Pratt, S. J., Whitfield, T. T. and Johnson, S. L. (1999). "Zebrafish sparse corresponds to an orthologue of c-kit and is required for the morphogenesis of a subpopulation of melanocytes, but is not essential for hematopoiesis or primordial germ cell development." Development **126**(15): 3425-36.
- Pasqualetti, M., Ori, M., Nardi, I. and Rijli, F. M. (2000). "Ectopic Hoxa2 induction after neural crest migration results in homeosis of jaw elements in *Xenopus*." Development **127**(24): 5367-78.
- Pingault, V., Bondurand, N., Kuhlbrodt, K., Goerich, D. E., Prehu, M. O., Puliti, A., Herbarth, B., Hermans-Borgmeyer, I., Legius, E., Matthijs, G., Amiel, J., Lyonnet, S., Ceccherini, I., Romeo, G., Smith, J. C., Read, A. P., Wegner, M. and Goossens, M. (1998). "SOX10 mutations in patients with Waardenburg-Hirschsprung disease." Nat Genet **18**(2): 171-3.
- Piotrowski, T., Schilling, T. F., Brand, M., Jiang, Y. J., Heisenberg, C. P., Beuchle, D., Grandel, H., van Eeden, F. J., Furutani-Seiki, M., Granato, M., Haffter, P., Hammerschmidt, M., Kane, D. A., Kelsh, R. N., Mullins, M. C., Odenthal, J., Warga, R. M. and Nusslein-Volhard, C. (1996). "Jaw and branchial arch mutants in zebrafish II: anterior arches and cartilage differentiation." Development **123**: 345-56.
- Pizette, S. and Niswander, L. (2000). "BMPs are required at two steps of limb chondrogenesis: formation of prechondrogenic condensations and their differentiation into chondrocytes." Dev Biol **219**(2): 237-49.
- Pohl, B. S. and Knochel, W. (2001). "Overexpression of the transcriptional repressor FoxD3 prevents neural crest formation in *Xenopus* embryos." Mech Dev **103**(1-2): 93-106.
- Prince, V. and Lumsden, A. (1994). "Hoxa-2 expression in normal and transposed rhombomeres: independent regulation in the neural tube and neural crest." Development **120**(4): 911-23.
- Prince, V. E., Moens, C. B., Kimmel, C. B. and Ho, R. K. (1998). "Zebrafish hox genes: expression in the hindbrain region of wild-type and mutants of the segmentation gene, valentino." Development **125**(3): 393-406.
- Puffenberger, E. G., Hosoda, K., Washington, S. S., Nakao, K., deWit, D., Yanagisawa, M. and Chakravart, A. (1994). "A missense mutation of the

- endothelin-B receptor gene in multigenic Hirschsprung's disease." Cell **79**(7): 1257-66.
- Ramirez, R. M., Ishida-Schick, T., Krilowicz, B. L., Leish, B. A. and Atkinson, K. D. (1983). "Plasma membrane expansion terminates in *Saccharomyces cerevisiae* secretion-defective mutants while phospholipid synthesis continues." J Bacteriol **154**(3): 1276-83.
- Russell, W. L., Kelly, E. M., Hunsicker, P. R., Bangham, J. W., Maddux, S. C. and Phipps, E. L. (1979). "Specific-locus test shows ethylnitrosourea to be the most potent mutagen in the mouse." Proc Natl Acad Sci U S A **76**(11): 5818-9.
- Sasai, N., Mizuseki, K. and Sasai, Y. (2001). "Requirement of FoxD3-class signaling for neural crest determination in *Xenopus*." Development **128**(13): 2525-36.
- Sato, M. and Yost, H. J. (2003). "Cardiac neural crest contributes to cardiomyogenesis in zebrafish." Dev Biol **257**(1): 127-39.
- Scambler, P. J. (2000). "The 22q11 deletion syndromes." Hum Mol Genet **9**(16): 2421-6.
- Schilling, T. F. (1997). "Genetic analysis of craniofacial development in the vertebrate embryo." Bioessays **19**(6): 459-68.
- Schilling, T. F. and Kimmel, C. B. (1994). "Segment and cell type lineage restrictions during pharyngeal arch development in the zebrafish embryo." Development **120**(3): 483-94.
- Schilling, T. F., Piotrowski, T., Grandel, H., Brand, M., Heisenberg, C. P., Jiang, Y. J., Beuchle, D., Hammerschmidt, M., Kane, D. A., Mullins, M. C., van Eeden, F. J., Kelsh, R. N., Furutani-Seiki, M., Granato, M., Haffter, P., Odenthal, J., Warga, R. M., Trowe, T. and Nusslein-Volhard, C. (1996). "Jaw and branchial arch mutants in zebrafish I: branchial arches." Development **123**: 329-44.
- Schilling, T. F., Prince, V. and Ingham, P. W. (2001). "Plasticity in zebrafish hox expression in the hindbrain and cranial neural crest." Dev Biol **231**(1): 201-16.
- Schwartz, N. (2000). "Biosynthesis and regulation of expression of proteoglycans." Front Biosci **5**: D649-55.
- Shibuya, T. and Morimoto, K. (1993). "A review of the genotoxicity of 1-ethyl-1-nitrosourea." Mutat Res **297**(1): 3-38.
- Shimeld, S. M. and Holland, P. W. (2000). "Vertebrate innovations." Proc Natl Acad Sci U S A **97**(9): 4449-52.
- Shimoda, N., Knapik, E. W., Ziniti, J., Sim, C., Yamada, E., Kaplan, S., Jackson, D., de Sauvage, F., Jacob, H. and Fishman, M. C. (1999). "Zebrafish genetic map with 2000 microsatellite markers." Genomics **58**(3): 219-32.
- Shum, L. and Nuckolls, G. (2002). "The life cycle of chondrocytes in the developing skeleton." Arthritis Res **4**(2): 94-106.
- Solomon, K. S., Kudoh, T., Dawid, I. B. and Fritz, A. (2003). "Zebrafish foxi1 mediates otic placode formation and jaw development." Development **130**(5): 929-40.
- Thisse, C., Thisse, B. and Postlethwait, J. H. (1995). "Expression of snail2, a second member of the zebrafish snail family, in cephalic mesendoderm and presumptive neural crest of wild-type and spadetail mutant embryos." Dev Biol **172**(1): 86-99.
- Topczewski, J., Sepich, D. S., Myers, D. C., Walker, C., Amores, A., Lele, Z., Hammerschmidt, M., Postlethwait, J. and Solnica-Krezel, L. (2001). "The zebrafish glypican knypek controls cell polarity during gastrulation movements of convergent extension." Dev Cell **1**(2): 251-64.
- Tosney, K. W. (1982). "The segregation and early migration of cranial neural crest cells in the avian embryo." Dev Biol **89**(1): 13-24.

- Veitch, E., Begbie, J., Schilling, T. F., Smith, M. M. and Graham, A. (1999). "Pharyngeal arch patterning in the absence of neural crest." Curr Biol **9**(24): 1481-4.
- Wagner, T., Wirth, J., Meyer, J., Zabel, B., Held, M., Zimmer, J., Pasantes, J., Bricarelli, F. D., Keutel, J., Hustert, E. and et al. (1994). "Autosomal sex reversal and campomelic dysplasia are caused by mutations in and around the SRY-related gene SOX9." Cell **79**(6): 1111-20.
- Walsh, E. C. and Stainier, D. Y. (2001). "UDP-glucose dehydrogenase required for cardiac valve formation in zebrafish." Science **293**(5535): 1670-3.
- Wilkie, A. O. and Morriss-Kay, G. M. (2001). "Genetics of craniofacial development and malformation." Nat Rev Genet **2**(6): 458-68.
- Xing, D. Y., Tan, W., Song, N. and Lin, D. X. (2001). "Ser326Cys polymorphism in hOGG1 gene and risk of esophageal cancer in a Chinese population." Int J Cancer **95**(3): 140-3.
- Yan, Y. L., Miller, C. T., Nissen, R. M., Singer, A., Liu, D., Kirn, A., Draper, B., Willoughby, J., Morcos, P. A., Amsterdam, A., Chung, B. C., Westerfield, M., Haffter, P., Hopkins, N., Kimmel, C., Postlethwait, J. H. and Nissen, R. (2002). "A zebrafish sox9 gene required for cartilage morphogenesis." Development **129**(21): 5065-79.
- Zhang, J., Talbot, W. S. and Schier, A. F. (1998). "Positional cloning identifies zebrafish one-eyed pinhead as a permissive EGF-related ligand required during gastrulation." Cell **92**(2): 241-51.
- Zou, H. and Niswander, L. (1996). "Requirement for BMP signaling in interdigital apoptosis and scale formation." Science **272**(5262): 738-41.

## 9 Acknowledgements

I am particularly indebted to Dr. Ela Knapik, Prof. Dr. Rudolf Grosschedl and Prof. Dr. Friederike Eckardt-Schupp, who supervised this Ph.D. thesis project. I would like to thank all the members of the Zebrafish Genetics Laboratory in the Institute of Developmental Genetics at the GSF National Research Center for Environment and Health for creating a pleasant working environment. These are Petra Hammerl, Sherri Sachdev, Alejandro Barrallo, Mercedes Montero, Georg Schmidt, Junichi Honda, Christiane Knappmeyer and the animal caretakers Heike Grunewald and Vera Brätschkus.

Special thanks to the following students who did great jobs in supporting the mapping process of the *crusher*<sup>m299</sup> and *brak*<sup>m452</sup> mutations: Jan Havel, Kristina Haage and Caroline Kumsta. I am indebted to Dr. Ilse-Dore Adler and Dr. Jack Favor for critical reading of the manuscript.

Most importantly, this thesis would be incomplete without a mention of the immeasurable continuous support from my parents.

## 10 Curriculum Vitae

**Name:** Michael Rainer Lang

**Date and Place of Birth:** November 12, 1973; Münster-Hiltrup, Germany

**Citizenship:** German

### Education:

- 2000 – 2003 Doctorate, Ludwig Maximilians University Munich, Germany  
PhD thesis: Towards Genetic Dissection of Neural Crest Specification and Cartilage Differentiation in Zebrafish (*Danio rerio*)  
Immediate thesis advisor: Dr. Ela Knapik, GSF National Research Center for Environment and Health, Neuherberg, Germany  
Principal thesis advisor: Prof. Dr. Rudolf Grosschedl, Ludwig Maximilians University, Munich, Germany
- 1999 Diploma in Biology, Free University of Berlin, Germany  
Diploma thesis title: Isolation and Molecular Genetic Characterization of the Mouse gamma2-COP Gene  
Thesis advisor: Prof. Dr. Hans-Hilger Ropers, Max-Planck-Institute of Molecular Genetics (MPIMG), Berlin, Germany
- 1993 – 1999 Study of Biology, Free University of Berlin, Germany

### Courses:

- 2002 EMBO Practical Course “Molecular and Genetic Tools for the analysis of Medaka and Zebrafish Development” at EMBL Heidelberg, Germany
- 2000 Biological Safety Course (Kurs zur Erlangung der Sachkunde nach Gentechnik-Sicherheitsverordnung für Projektleiter und Beauftragte für die Biologische Sicherheit) at GSF Research Center, Neuherberg, Germany
- 2000 Radiation Safety Course (Grundkurs im Strahlenschutz im nichtmedizinischen Bereich) at GSF Research Center, Neuherberg, Germany

### Teaching experience:

- 2000 – 2003 Supervision of undergraduate students in genetics projects at the Technical University of Munich, Germany
- 1997 – 1998 Tutor in courses and seminars at the Institute of Zoology of the Free University of Berlin, Germany

### Duties:

- 2001 – 2003 Deputy Radiation Safety Officer for the Departments of Developmental Genetics and Experimental Genetics at GSF Research Center, Neuherberg, Germany
- 2000 – 2003 First Aid Officer for the Department of Developmental Genetics at GSF Research Center, Neuherberg, Germany

### Volunteer position:

- 1993 – 2000 Active member of the German Red Cross in the disaster preparedness unit

**Publications:**

Sachdev S.W., Dietz U.H., Oshima Y., **Lang M.R.**, Knapik E.W., Hiraki Y. and Shukunami C. (2001): Sequence analysis of zebrafish *chondromodulin-1* and expression profile in the notochord and chondrogenic regions during cartilage morphogenesis. *Mech. Dev.* 105, 157-162.

**Meeting presentations:**

Sachdev S.W., **Lang M.R.** and Knapik E.W.: Specification of the neural crest stem cells by the *mother superior* gene. Fifth International Conference on Zebrafish Development & Genetics, Madison, USA, June 12-16, 2002.

Sachdev S.W., **Lang M.R.**, Barrallo A. and Knapik E.W.: Genetic Control of Neural Crest Specification and Development in Zebrafish. Evolution of Developmental Diversity, Cold Spring Harbor Laboratory, NY, USA, April 17-21, 2002.

Sachdev S.W., Barrallo A., **Lang M.R.** and Knapik E.W.: Characterization of ENU-induced craniofacial mutations in zebrafish (*Danio rerio*). 14<sup>th</sup> International Congress of Developmental Biology, Kyoto, Japan, July 8-12, 2001.

**Lang M.R.** and Knapik E.W.: Characterization of Zebrafish Mutations Affecting Cartilage Differentiation. Second European Conference on Zebrafish Genetics and Development, London, UK, April 19-22, 2001.